ABSTRACT

DU, JINMEI. Distribution of Liquid Drops on Solid Surfaces between Flat Surface and Fibers. (Under the direction of Dr. Stephen Michielsen and Dr. Hoon Joo Lee).

Understanding the ability of a liquid to transfer from a flat surface to fibers can provide basic information enabling the design and preparation of superoleophobic or oil self-cleaning materials. Based on the literature review, a Laplace pressure difference will change the shape of droplet and even move it when the force caused by this pressure difference overcomes the resistive forces such as gravitational and viscosity forces. The final shape and location of droplets on different materials or different geometrical structures are determined by the system free energy. Based on experimental observations and the predictions of the ability of a liquid to transfer, it is found that the theory can be used to predict and explain low surface tension liquid (oil) transfer and the final location of the liquid. It is also found that the height of a fiber which is vertically attached on a flat surface should be longer than the length of the drop on the fiber to prevent the drop wetting the flat surface; if a low surface tension liquid on a flat surface touches a cylindrical fiber resting on the flat surface and normal to it, the drop should move such that it lies on both the flat surface and the fiber. However, the liquid does not climb the cylindrical fiber or transfer to its tip. If subsequently the fiber is raised, then the droplet may remain with the flat surface, transfer to the fiber tip, or transfer to the tip and the body of fiber. The theoretical equations derived from Carroll's equation and our experimental observations prove that droplets do move along a conical fiber. However, the critical relationships between liquid motion and droplet size, surface tension, conical fiber geometry should be obtained to provide information on liquid transferring ability.

Distribution of Liquid Drops on Solid Surfaces between Flat Surface and Fibers

by
Jinmei Du

A dissertation submitted to the Graduate Faculty of
North Carolina State University
in partial fulfillment of the
requirements for the degree of
Doctor of Philosophy

Fiber and Polymer Science

Raleigh, North Carolina

2010

APPROVED BY:

Dr. Stephen Michielsen (Co-Chair of Advisory Committee)	Dr. Hoon Joo Lee (Co-Chair of Advisory Committee)
Dr. Keith Beck	Dr. Jan Genzer
Dr. Orlando Rojas	

DEDICATION

To

My Parents

and

My Whole Family

BIOGRAPHY

Jinmei Du was born in Shandong, China. She attended Qingdao University in Textile Chemistry department in 1998 and received her Bachelor degree in 2002. After that she completed her study for Master degree in the same department in 2005. Jinmei continued her education as a doctoral student in Fiber and Polymer Science under the direction of Drs. Stephen Michielsen and Hoon Joo Lee in the College of Textiles at North Carolina State University in 2007.

On July 2004, Jinmei married Changhai Xu who received his Ph.D degree in Fiber and Polymer Science in the College of Textiles at North Carolina State University in 2009.

ACKNOWLEDGMENTS

I would like to express my sincerest thanks to my advisors Drs. Stephen Michielsen and Hoon Joo Lee, who persevered with me throughout my educational experience and research work as a student in the Fiber and Polymer Science program. I am also most appreciative of the other members of my advisory committee, Dr. Keith Beck, Dr. Jan Ganzer and Dr. Orlando Rojas, whose knowledge and expertise contributed to the completion of this dissertation.

I would like to say thanks to my lovely husband Changhai Xu for everything. Without your love, affection, constant support, and willingness to sacrifice, this goal could not have been achieved. I love you with all of my heart. I am deeply grateful for parents whose early instruction, love, support, and continued sacrifices have laid the foundation for all my successes in life.

I would like to acknowledge my gratitude to my friends, who encouraged me during this difficult process. Thank you so much for your time, your support, your well wishes, and your friendship.

TABLE OF CONTENTS

LIST OF TABLES

LIST OF FIGURES

Chapter 1 Introduction

A surface having a water contact angle greater than 150^{o} and a very low roll-off angle is called a superhydrophobic surface.[1, 2] High contact angles can be obtained by combined treatments with low surface tension chemical agents and increasing surface roughness. The roll-off angle depends on the drop size[3] and the contact angle hysteresis, which is the difference between the advancing and receding contact angles.[4] Self-cleaning is so termed as water easily rolls off a superhydrophobic surface taking away dirt. It would be beneficial if similar "superoleophobic" materials existed. Compared with water, oils, such as vegetable oil and most machine oils, have lower surface tension and more easily wet solid surfaces. Superoleophobicity is commonly desired for clothing and carpets, which are easily contaminated by oil but are not easy to clean.

The idea of superhydrophobicity was introduced six decades ago by A. Cassie working for the British Council of the Wool Industries.[5] Since then superhydrophobic treatments have been studied in both academia and industry. Among these studies, mimics of the superhydrophobic plant leaves have recently received more attention. There are two different types of water-repellent plant leaves exemplified by: Lotus leaves and Lady's Mantle leaves. Lotus leaves have hydrophobic cuticles and protuberances which provide high surface roughness, while Lady's Mantle leaves have hydrophilic hairs on their less hydrophilic surface. The term "Lotus effect" is used for surfaces which have water repellency via either mechanism.

Compared with reports of superhydrophobic surfaces, reports of superoleophobic surfaces are extremely rare. However, Lady's Mantle leaves provide a clue for designing a superoleophobic surface using oleophilic fibers and a less oleophilic surface since the leaves are superhydrophobic although covered by hydrophilic hairs.

It is known that a liquid droplet resting on a solid surface has a Laplace pressure, which is the pressure difference caused by the interfacial surface tension between the liquid and vapor. For a static droplet, the Laplace pressure should be the same at each point of the liquid-vapor interface; otherwise the pressure difference will change the shape of the drop or even move it when the force caused by Laplace pressure difference can overcome resistive forces. On a cylindrical fiber, the Laplace pressure is constant within the drop based on Carroll's equations[6], but decreases with increasing fiber radius[7]. This suggests that a droplet will have a decreasing Laplace pressure on a conical fiber as the fiber radius increases. The difference of the Laplace pressure varied by the change of fiber radius may provide a force which drives the droplet to move along the fiber.

The background for this research includes the wetting behavior of liquids on solid surfaces, e.g. smooth flat surface, rough surfaces and fibers; the influence of fiber surface morphology in liquid spreading; the Laplace pressure and the system free energy of droplets on solid surfaces; and the motion of liquid on fibers.

The objectives of this study are threefold:

1) investigate conditions required for liquids transferring between a flat smooth surface and fibers;
2) explore prerequisites for spontaneous movement of liquids along fibers; and
3) provide theoretical and experimental analysis of wetting a single fiber as a model superoleophobic surfaces.

Chapter 2 Literature Review

2.1. Introduction

Superhydrophobic treatments have been studied in both academia and industry due to their water repellency. Lotus leaves have hydrophobic cuticles and protuberances which provide high surface roughness as shown in Figure 2.1.a. Nakajima et al. obtained superhydrophobic films by coating a fluoroalkyl silane on a substrate.[8] Michielsen and Lee designed and prepared superhydrophobic surfaces using woven structures and flocked surfaces.[9, 10] Zhu et al. prepared a superhydrophobic surface by electrospinning a hydrophilic material, poly(hydroxybutyrate-co-hydroxyvalerate).[11] Zhai et al. found that superhydrophobic behavior of the lotus leaf structure can be achieved by creating a semifluorinated silane coated polyelectrolyte multilayer surface.[12]

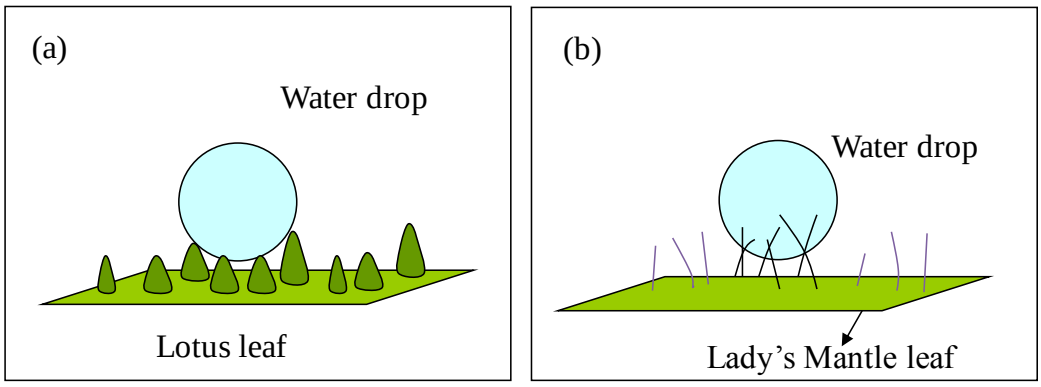

Figure 2.1. Schematics of a water drop on (a) Lotus leaf, and (b) Lady's Mantle leaf.[14]

Lady's Mantle leaves have hydrophilic hairs on their less hydrophilic surface shown in Figure 2.1.b, which is very different from Lotus leaves. Ulrike et al. reported a method of

mimicking the structure of Lady's Mantle leaves.[13] However, experiments have not successfully mimicked the Lady's Mantle leaves to produce superhydrophobic surfaces. Production of superoleophobic surfaces resisting wetting with oil, which has much lower surface tension, are extremely rare. Research to provide theoretical and experimental evidence for model superoleophobic surfaces is needed.

Research review

Tuteja, Zimmermann, and Cao created superoleophobic surfaces by combining chemical composition, roughened texture and surface curvature.[15-17] Cohen et al. pointed out that materials could be oil repellent with proper combination of re-entrant curvature and suitable alteration of the surface energy.[15, 18] Brewer et al. suggested that fluoropolymer fiber coated materials could provide low surface tension liquid repellent properties to textiles.[19] Cao et al. demonstrated that porous Si films fabricated by a convenient gold assisted electrodeless etching process would produce a superoleophobic surface on an intrinsically oleophilic self-assembled monolayer coated Si surface.[20] Steele et al. obtained a superoleophobic surface on large and flexible surfaces, by spraying an emulsion of ZnO nanoparticles and waterborne perfluoroacrylic polymer.[21] Yan et al. created a surface on which salad oil exhibited a 130° contact angle by coating fluorinated alkylsilane on a needle-like surface of polyalkyppyrrole films. The geometrical factor of the film did not change during coating.[22] Hsieh et al. found that rough surfaces coated with titanium dioxide nanoparticles and perfluoroalkyl methacrylic copolymer could achieve contact angles as high as 144° for ethylene glycol.[23] However, surfaces which can resist low surface tension liquid such as

dodecane (γ_{LV} = 25 mN/m) wetting are rare.

Patent review

Reihs et al. invented a method for producing a superoleophobic surface on an aluminum base by anodized/anodic oxidation. They created a superoleophobic surface which had high liquid contact angle and low roll-off angle by combining this treatment with low surface tension chemical application. [24] They also developed water-repellent and oil-repellent surfaces using an ultraviolet laser to obtain very high number of pores per surface area. First they coated surface with an oil-repellent agent which was dissolved and freely moveable, and then coated a the material with a second cover (outer surface). Through the pores created by ultraviolet illumination the oil-repellent agents could diffuse to the outer surface to create an outer coating which had an n-decane contact angle larger than 90°.[25] Lamon et al. presented an invention to obtain an oleophobic filtration medium including polymeric membranes and other substrates that are coated with polymerized substituted or unsubstituted para-xylene.[26] Yamaguchi et al. invented a method of preparing a water and oil repellent treatment of textiles. The water and oil repellent agent comprises at least one fluorine-containing compound and it also has a cationic emulsifier and a salt.[27]

Understanding wetting behavior is helpful to mimic the Lotus effect, because the mechanisms and technology can be applied to approach superhydrophobic and superoleophobic surface. In this chapter, contact angle and wetting behavior of liquid on smooth and rough flat surface are compared, the differences of these two factors on a flat

surface and fibers are introduced, and the possibility of droplet spontaneously moving from one place to another is discussed.

2.2. Contact angle and wetting behavior

The characterization of surface tensions between the interacting solid and liquid is the key to understanding the wetting behaviors of solid materials.[15, 18] It is difficult to directly measure the surface energy of solids but easy to obtain the contact angles of liquid on solid surfaces. Therefore, contact angles between liquid with a known surface tension and a solid are measured for the evaluation of surface characteristics such as surface energy and wetting behavior. The relationship between the surface tensions and contact angle is given by Young's equation:[28]

$$\frac{\gamma_{SV} - \gamma_{SL}}{\gamma_{LV}} = \cos\theta_e \tag{2.1}$$

where γ_{SV}, γ_{SL}, and γ_{LV} are the interfacial surface tension between solid-vapor, solid-liquid and liquid-vapor, respectively (Figure 2.2). Young's equation is only applicable to flat smooth surfaces, and the system should be at equilibrium. When θ_e for a test liquid is larger than 20°, it is assumed that $\gamma_{SV} = \gamma_S$ and $\gamma_{LV} = \gamma_L$.[29] Equation (2.1) can be reformulated as:

$$\frac{\gamma_S - \gamma_{SL}}{\gamma_L} = \cos\theta_e \tag{2.2}$$

According to Fowkes[30] and Lee[31], when only dispersion interactions are present the interface tension between solid and liquid is given by the following equation:

$$\gamma_{SL}^{LW} = (\sqrt{\gamma_S^{LW}} - \sqrt{\gamma_L^{LW}})^2 \quad (2.3)$$

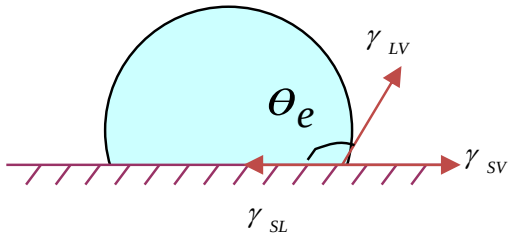

Figure 2.2. Liquid droplet on flat surface.

Wetting behavior and apparent contact angle are related with surface structure.[32] Since Young's equation is only appropriate for a flat smooth surface, other approaches are proposed to express the contact angle of liquid on a rough surface.[33, 34] There are two popular models when the surface is roughened: Wenzel model and Cassie-Baxter model.

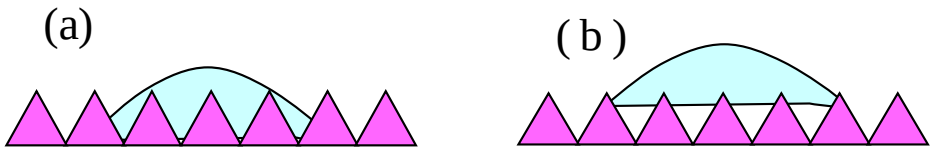

Figure 2.3. Liquid droplet on a rough surface: (a) Wenzel model, and (b) Cassie-Baxter model.

In 1936, Wenzel showed how a rough surface can influence apparent contact angle and presented a definition for surface roughness, *r*, through which an apparent contact angle can

be calculated.[35] According to Wenzel theory, if liquid completely wets a solid rough surface (Figure 2.3.a) the apparent contact angle (θ_r^W) between liquid and the rough surface can be described as follows:

$$\cos\ \theta_r^W = r \cos\ \theta_e \tag{2.4}$$

where r is the ratio of the total true wetted area of a rough surface to the area beneath the drop obtained by projecting the drop onto a plane, and θ_e is the equilibrium Young contact angle on a smooth surface of the same material. r is greater than or equal to 1, because the total area of a rough surface must be greater than or equal to the projected area beneath it. The Wenzel model describes two different behaviors: in the case of $\theta_e < 90°$, liquid sinks into and contacts with the rough surface $\theta_r^W \sim 0$; in the other case of $\theta_e > 90°$, $cos\theta_r^W$ goes toward -1 and θ_r^W approaches 180°. The behaviors suggest that with increasing roughness of a hydrophilic surface ($\theta_e < 90°$) its hydrophilicity improves; while the hydrophobicity becomes better when the roughness of hydrophobic surface ($\theta_e > 90°$) increased.

Cassie and Baxter extended the Wenzel model to porous surfaces (Figure 2.3.b). In the Cassie-Baxter model, liquid sits on top of a composite surface consisting of solid surface and air, and it does not fill the cavities. Cassie and Baxter suggested the following equation in 1944[36]

$$\cos\ \theta_r^{CB} = f_1 \cos\ \theta_e - f_2 \tag{2.5}$$

where $f_1 = \dfrac{\text{area in contact with liquid}}{\text{projected area}}$, $f_2 = \dfrac{\text{area in contact with air}}{\text{projected area}}$,

here, the *projected area* is the sum of the apparent areas of solid and air, which directly

contact with a liquid.

The original Cassie-Baxter equation is often approximated by the following equation.[37, 38]

$$\cos\ \theta_r^{CB} = \phi_S\left(\cos\ \theta_e + 1\right) - 1 \qquad (2.6)$$

where ϕ_S is the ratio of the rough surface area in contact with liquid to the projected area covered by the liquid. Since $\phi_S \leq 1$, $cos\theta_r^{CB}$ is less than or equal to $\cos\theta_e$, which means θ_r^{CB} is always greater than or equal to θ_e. Even though Equation (2.6) is used today, it is only valid when liquid is in contact with a flat, porous surface. For most rough surfaces, the original form, Equation (2.5), should be applied instead.[9]

Based on Equations (2.1 – 2.6) it is clear that a water or oil repellent surface which is roughened and has low surface energy could be produced through the process of chemical and physical treatments, and this is consistent with the mechanism of Lotus leaves.

2.3. Liquid on solid surface

Whether liquid wets a flat solid surface or not depends on the spreading coefficient S which is described as $S = \gamma_{SV} - \gamma_{SL} - \gamma_{LV}$. The increased liquid-vapor surface energy should be balanced by a gain of interfacial energy at the solid-liquid and solid-vapor surfaces if liquid spreads spontaneously along solid surface.

2.3.1. Liquid connected with reservoir on a solid surface

On a flat surface

As shown in Figure 2.4.a, the original position of a liquid on a flat surface is O. If the liquid can spread it will pass position B. The free energy of a liquid on area A_{OB} is G_1 before spreading and G_2 after spreading. The energy difference of area OB before and after spreading is $\Delta G = G_2 - G_1$.

$$G_1 = \gamma_{SV} A_{OB} \tag{2.7}$$

$$G_2 = \gamma_{LV} A_{OB} + \gamma_{SL} A_{OB} \tag{2.8}$$

$$\Delta G = (\gamma_{LV} + \gamma_{SL} - \gamma_{SV}) A_{OB} = -SA_{OB} \tag{2.9}$$

It is well known that a system always prefers the lower energy state. Therefore, whether the liquid can spontaneously spread on a flat surface or not depends on state of the interfacial free energy. According to Equation (2.9) if $S < 0$, ΔG is positive and the liquid cannot spread on the solid surface; and if $S > 0$, the liquid will spread on the surface.

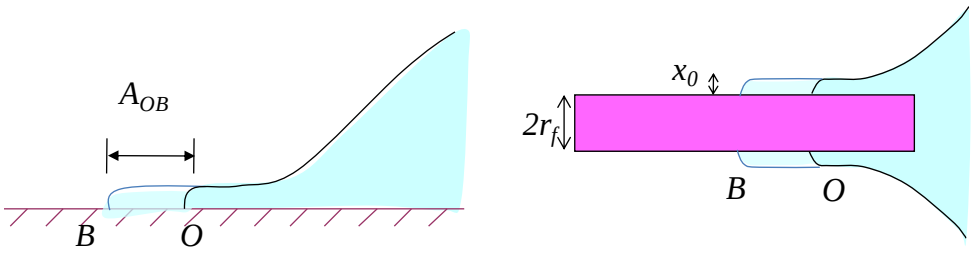

(a) (b)

Figure 2.4. Schematics of spreading of a liquid contacted with a huge reservoir: (a) on a flat smooth surface, and (b) on a cylinder. x_0 is the liquid film thickness on cylinder. *O* and *B* are the positions before and after spreading, respectively.

On a cylinder

The spreading of liquid on a smooth cylinder is different from a flat surface as shown in Figure 2.4.b. Interfacial free energy before spreading G_1 and after spreading G_2 for unit spreading length can be represented as:

$$G_1 = \gamma_{SV} \pi r_f^2 \tag{2.10}$$

$$G_2 = \gamma_{SL} \pi r_f^2 + \gamma_{LV} \pi (r_f + x_0)^2 \tag{2.11}$$

Because the increased liquid-vapor interfacial surface area (radius $r_f + x_0$) is larger than those of solid-liquid (radius r_f) for liquid spreading on cylinder surface, the energy difference of liquid before and after spreading on cylinder, $\Delta G = G_2 - G_1$, will be negative only when the spreading coefficient S is larger than a positive critical S_C rather than just greater than zero. When $S < S_C$, liquid will not spread on cylinder even though the spreading coefficient is positive. Brochard, de Gennes, and Neimark showed how to analyze the critical S_C.[39-41] The

free energy of the thin liquid film on fiber G is given as:

$$G = G_1 + G_2 + G_3 \tag{2.12}$$

where G_1 is the excess liquid air interfacial energy per unit volume due to cylindrical geometry, G_2 is the energy due to the spreading term, G_3 is caused by long range forces, and these three energies can be given as:

$$G_1 = \frac{2\gamma_{LV}}{x_0 + 2r_f} \tag{2.13}$$

$$G_2 = -\frac{2Sr_f}{x_0^2 + 2x_0 r_f} \tag{2.14}$$

$$G_3 = \frac{\gamma_{LV} a^2 r_f}{x_0^2 (x_0^2 + 2x_0 r_f)} \tag{2.15}$$

where x_0 is the equilibrium film thickness, a is a molecular size and r_f is the cylinder radius.

The critical spreading S_C is derived from two conditions: the equality of free energy between a uniform thin liquid film and a droplet ($G = 0$) and the minimum of free energy of a thin liquid film ($dG / dx_0 = 0$). Therefore, based on Equations (2.12) – (2.15), S_C can be derived as following:

$$S_C = \frac{3}{2}\gamma_{LV}\left(\frac{a}{r_f}\right)^{2/3} \tag{2.16}$$

2.3.2. Finite liquid droplet on a solid surface

On a flat surface

As shown in Figure 2.5 A_S is the total flat surface area and G_1 and G_2 are the free energies of

spherical cap and flat uniform film forms, respectively. The relationship between free energy, surface tension and interfacial surface area can be expressed as:

$$G_1 = \gamma_{LV} A_{LV} + \gamma_{SL} A_{SL} + \gamma_{SV} (A_S - A_{SL}) \tag{2.17}$$

$$G_2 = \gamma_{LV} A_S + \gamma_{SL} A_S \tag{2.18}$$

where A_{LV} and A_{SL} are interfacial surface areas between the liquid and the vapor and the solid and the liquid, respectively. The liquid-vapor and solid-liquid interfacial surface areas are equal when the liquid exists in the form of a film and both are expressed with solid surface area A_S. Based on Equations (2.17) and (2.18), the energy difference ΔG between the liquid drop G_1 and the film G_2 is

$$\Delta G = G_2 - G_1 = \gamma_{LV} (A_S - A_{LV}) + (\gamma_{SL} - \gamma_{SV})(A_S - A_{SL}) \tag{2.19}$$

In the case of a spherical cap, the entire solid surface area A_S is much larger than the solid-liquid interfacial surface area A_{LV}, (A_S - $A_{LV} \approx A_S$), and A_S is also much larger than the liquid-vapor interfacial surface area A_{SL} (A_S - $A_{SL} \approx A_S$); therefore Equation (2.19) can be simplified to

$$\Delta G = (\gamma_{LV} + \gamma_{SL} - \gamma_{SV}) A_S = -SA_S \tag{2.20}$$

The final form taken by a liquid on a solid depends on spreading coefficient S. Liquid cannot spread on the solid surface when S is negative, but it can spread on the solid surface as long as the spreading coefficient S is positive.

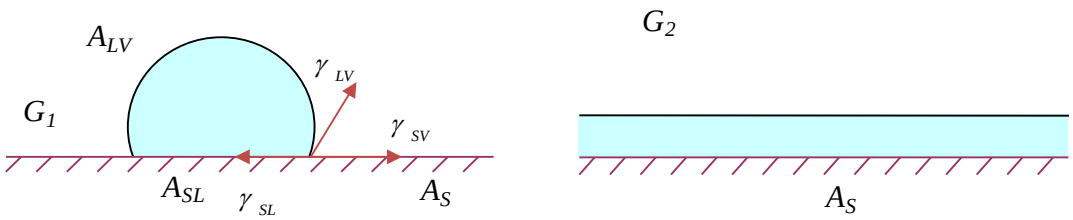

(a) (b)

Figure 2.5. Schematics of a liquid drop on a flat smooth solid surface: (a) before spreading-spherical cap, and (b) after spreading-flat uniform film. The total flat surface areas A_S in (a) and (b) are same.

On a cylinder

Figure 2.6 presents the forms of liquid drops before and after spreading on a cylinder in which A_S is the total cylinder surface area, and A_{LV} and A_{SL} are liquid-vapor interfacial contact area and solid-liquid interfacial contact area. Subscripts *1* and *2* represent the states of the liquid just after dropping it on the cylinder and after forming undulating drop, respectively. As always G_1 and G_2 are the total free energy before and after spreading. They can be written:

$$G_1 = \gamma_{LV} A_{LV-1} + \gamma_{SL} A_{SL-1} + \gamma_{SV} (A_S - A_{SL-1}) \tag{2.21}$$

$$G_2 = \gamma_{LV} A_{LV-2} + \gamma_{SL} A_{SL-2} + \gamma_{SV} (A_S - A_{SL-2}) \tag{2.22}$$

Therefore the interfacial free energy difference ΔG between state (Figure 2.6.a) and (Figure 2.6.b) is

$$\Delta G = G_2 - G_1 = \gamma_{LV} (A_{LV-2} - A_{LV-1}) + (\gamma_{SL} - \gamma_{SV})(A_{SL-2} - A_{SL-1}) \tag{2.23}$$

Since $cos\theta_e = (\gamma_{SV} - \gamma_{SL}) / \gamma_{LV}$, Equation (2.23) can be rewritten as

$$\Delta G = \gamma_{LV} [(A_{LV-2} - A_{LV-1}) - (A_{SL-2} - A_{SL-1}) \cos \theta_e] \quad (2.24)$$

A_{LV-2} is greater than A_{LV-1} because a sphere has the smallest surface area among all shapes. Since liquid is spreading along the cylinder to form an unduloid shape, the solid-liquid contact area will increase for a drop transforming its shape from a spherical shape to undulating shape ($A_{LV-2} > A_{LV-1}$). According to Equation (2.24), when $cos\theta_e = (A_{LV-2} - A_{LV-1}) / (A_{SL-2} - A_{SL-1})$, ΔG is negative and a liquid drop will form an undulating shape on the cylinder. This verifies the phenomenon that liquid drop would be asymmetric on hydrophobic or oleophobic cylinder surface, because the asymmetric system has lower interfacial surface energy compared to a symmetric undulating shape. This also proves the phenomenon that liquid shape is symmetric on hydrophilic or oleophilic smooth cylinder without the influence of external forces such as gravity.

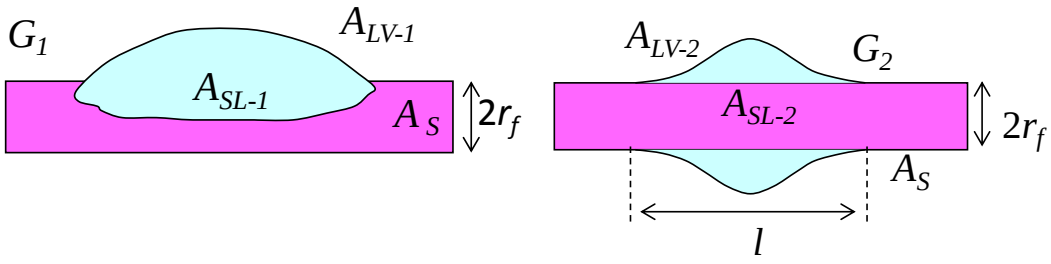

(a) (b)

Figure 2.6. Schematics of a liquid drop on a cylinder: (a) before spreading, and (b) after spreading.

No matter whether a drop on a solid surface is connected to a liquid reservoir or a liquid droplet is dropped on the surface, liquid cannot spread along the solid surface and completely wet if the spreading coefficient is negative for flat smooth surface or the coefficient is smaller than the critical value for cylinder. To avoid liquid spreading, reducing surface tension of solid surface by chemical modification is a potential solution.

2.3.3. Liquid on cylinder pulled out from reservoir

It is well known that if a cylinder is pulled out of a liquid reservoir very slowly, the only liquid transferred is a spherical drop hanging on the end of the cylinder. If the pulling out velocity is very large, there is not enough time for liquid to return to the reservoir. However, sometimes the thin film will form undulating drops. Therefore there could be two final forms for the case of quickly pulling a cylinder out of a reservoir: flat uniform film and undulating drops. The two possible forms are presented in Figure 2.7 where r_f is radius of cylinder, x_0 is liquid film thickness, x is thickness of undulating drop, and λ is wavelength of the undulation.

In Figure 2.7, G_1 and G_2 are the interfacial free energy per wavelength of liquid-vapor in the form of flat film and undulating drop, respectively. $\Delta G = G_2 - G_1$ is the free energy difference of the liquid which exists in the above two forms and they can be described as:

$$G_1 = 2\pi\left(r_f + x_0\right)\gamma_{LV}\,\lambda \tag{2.25}$$

$$G_2 = \int_0^{\lambda} 2\pi\left(r_f + x\right)\gamma_{LV}\,dy \tag{2.26}$$

$$\Delta G = \int_0^{\lambda} 2\pi\,(r_f + x)\gamma_{LV}\,dy - 2\pi\,(r_f + x_0)\gamma_{LV}\,\lambda \tag{2.27}$$

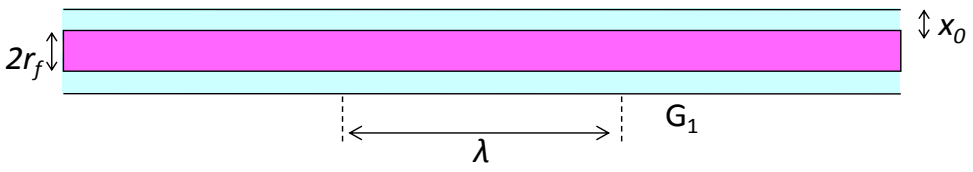

(a)

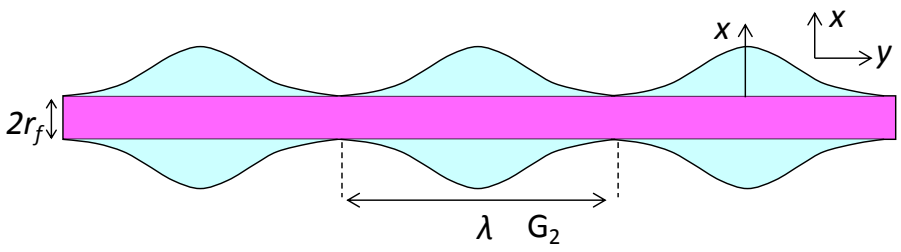

(b)

Figure 2.7. Schematics of liquid on a cylinder pulled out from a reservoir: (a) flat uniform film, and (b) undulating drop.

The surface area of undulating shape $\int_0^{\lambda} 2\pi(r_f + x)\, dy$ can be calculated according to the Rayleigh instability.[6, 42] According to Equation (2.27), ΔG is negative when λ is greater than $2\pi(r_f + x_0)$, and liquid on cylinder becomes undulating. A flat liquid film will exist when the film length is shorter than $2\pi(r_f + x_0)$, because the surface energy of the film is lower than the undulating drop at this length range. Thus for long films, the film will break up into undulating drops. The same result should occur if liquid vapor condenses on the cylinder.

2.4. Laplace pressure of liquid on solid surface

The energy analysis is used to verify which form liquid would prefer when it is on solid flat surface and cylinder. However, the shape of drop is decided by the Laplace pressure which is

the pressure difference sustained across the interface between a liquid and a vapor, and is given by the Young-Laplace Equation (2.28)

$$\Delta P = \gamma_{LV}\left(\frac{1}{R_1}+\frac{1}{R_2}\right) = K \tag{2.28}$$

where K is constant, $R_1 = x\mathrm{cosec}\phi$ and $R_2 = \mathrm{d}\phi / ds$ are the principal radii of curvature and s is the arc length of drop shape. The Laplace pressure at each point of the interface between liquid and vapor should be the same if the drop is static on a solid surface; otherwise the force caused by a difference in the Laplace pressure will change the drop shape.

2.4.1. Laplace pressure of liquid on flat surface

Liquid forms a spherical cap on a solid flat surface as shown in Figure 2.8, where R_0 is the radius of the sphere. Since the principal radii of curvature of the sphere are equal to its radius ($R_1 = R_2 = R_0$), the Young-Laplace Equation (2.28) can be transformed to:

$$\Delta P = \gamma_{LV}\left(\frac{1}{R_1}+\frac{1}{R_2}\right) = \frac{2\gamma_{LV}}{R_0} \tag{2.29}$$

$$R_0 = \left(\frac{3V_0}{\pi}\right)^{1/3}\left(2-3\cos\theta+\cos^3\theta\right)^{-1/3} \tag{2.30}$$

where $\theta = \theta_e$.

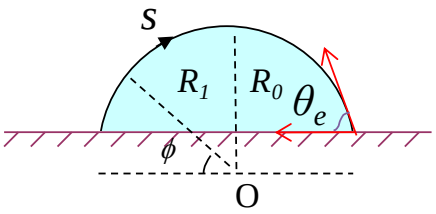

Figure 2.8. Schematics of the principal radii of curvatures of a liquid drop on a flat surface.

2.4.2. Laplace pressure of liquid on fiber tip

For liquid on a fiber tip when the liquid volume is small and the contact line is away from the edge as shown in Figure 2.9.a, the drop is a part of sphere because the drop rests on a flat surface. The Laplace pressure of this drop can be obtained by Equation (2.29) and (2.30).

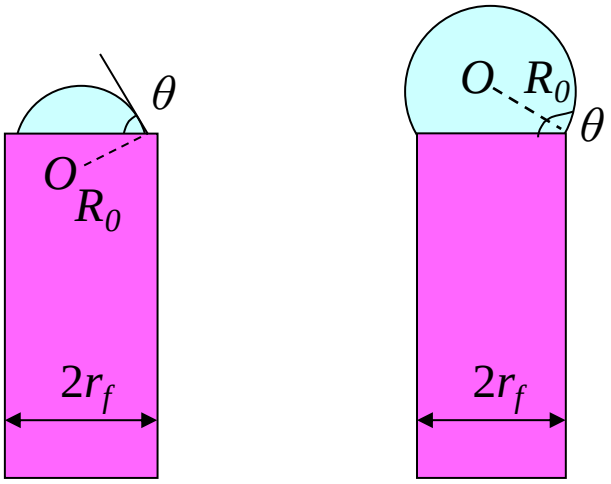

(a) (b)

Figure 2.9. Schematics of the principal radii of curvatures of a liquid drop on fiber tip: (a) drop contact line away from the edge of fiber tip, and (b) drop pinning at the edge.

As the liquid volume grows, the drop radius grows until the drop completely covers the tip of the fiber. As still more liquid is added, the apparent contact angle (θ) increases. At this point, the contact line between the drop edge and the fiber is pinned at the edge of the fiber but the drop still is a part of sphere. As the drop size continues to grow, eventually, the apparent contact angle becomes larger than the critical angle as derived by Extrand, Oliver et al. and Chang et al.[43-46] At this point, the drop has expanded to the point where it now touches the

side of the fiber, the drop collapses and encapsulates the tip. Before the collapse, the Laplace pressure of the drop can be expressed in Equation (2.29) and the principal radius of curvature R_0 is a function of drop volume V_0.

2.4.3. Laplace pressure of liquid on cylindrical fiber

A drop will show an undulating shape on a hydrophilic cylinder instead of a spherical cap shape on a flat surface due to the morphology of cylinder. It is easy to see that an undulating shape has both convex and concave parts seperated by an inflection point. The principal radius of curvature R_2 is different for the convex part of the drop than for the concave part as shown in Figure 2.10.a and 2.10.b.

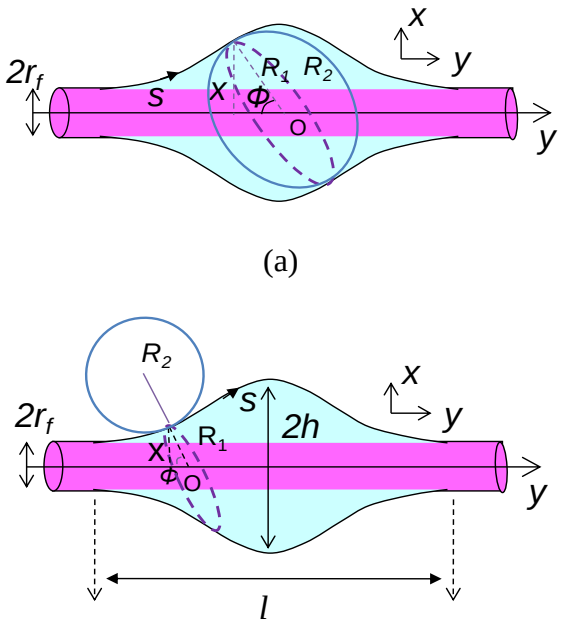

Figure 2.10. Schematics of principal radii of curvatures of a liquid drop on a cylinder: (a) on the convex part, and (b) on the concave part.

Carroll derived the Young-Laplace Equation (2.28) for an undulating drop on a cylinder in 1976:[6]

$$\Delta P = \frac{2\gamma_{LV}}{r_f}\left[\frac{n - \cos\theta_{fiber}}{n^2 - 1}\right] \tag{2.31}$$

where r_f is radius of fiber, $n = h / r_f$ and h is the maximum height of drop derived by r_f and drop volume V_0, and the subscript fiber refers to "on the fiber" as shown in Figure 2.10.b. It is easy to see that the Laplace pressure ΔP of a liquid on a cylinder is determined by the liquid surface tension, the radius of the cylinder and the liquid volume.

The liquid-vapor surface area $A_{LV\text{-}fiber}$ and solid-liquid surface area $A_{SL\text{-}fiber}$ of a droplet on the fiber body have been given by Carroll[6]

$$A_{LV-fiber} = 4\pi r_f^2 n(a + n)E(\varphi, k) \tag{2.32}$$

$$A_{SL-fiber} = 4\pi r_f^2\left[aF(\varphi, k) + nE(\varphi, k)\right] \tag{2.33}$$

where $F(\varphi, k)$ and $E(\varphi, k)$ are the elliptical integrals of the first and second kind, respectively. $a = (n\cos\theta_{fiber} - 1) / (n - \cos\theta_{fiber})$, $k^2 = 1 - a^2 / n^2$ and $\sin^2\varphi = (1 / k^2)(1\text{-}1 / n^2)$. In addition, n is constrained by the droplet volume, V_0, which for the droplet on a fiber body is given by Carroll[6] as:

$$V_0 = \frac{2\pi r_f^3}{3} n\left[(2a^2 + 3an + 2n^2)E(\varphi, k) - a^2 F(\varphi, k) + \frac{1}{n}\left(\frac{n^2 - 1}{1 - a^2}\right)^{0.5}\right] - 2\pi r_f^3\left[aF(\varphi, k) + nE(\varphi, k)\right] \tag{2.34}$$

Carroll pointed out that the drop surface area, volume, Laplace pressure and the static contact

angle θ_{fiber} could be obtained from the measurement of drop shape parameter h with the limitation that the drop should be symmetrical along the cylinder axis direction which requires $\theta_{fiber} < 60^0$. By observing the shape of a droplet on cylindrical fiber Yamaki et al. provided a method to obtain liquid contact angle on fiber, and the predicted angle was very close to the observed one.[47] Song et al. presented a method to calculate the static contact angle according to the geometry of droplet on a cylinder. The method could provide an accurate contact angle to within 5°.[48] Wagner could obtain highly accurate contact angle by calculating dimensions of droplet on fiber. [49]

2.4.4. Laplace pressure of liquid on conical fiber

Laplace pressure influences the shape of a drop and a difference in pressure creates a driving force which can change the shape and even force a drop to move. The Laplace pressure ΔP will decrease with an increase in liquid volume V_0 since the radius of the drop increases (Equations (2.29) and (2.31)). This explains why a small drop of liquid will flow into a larger one if these two drops are connected with each other. The Laplace pressure of a droplet varies on solid surfaces which have different surface tensions since the different solid-liquid surface tensions cause a difference in the contact angles and thus changes the radii of curvature. Thus, a droplet could move from lower surface tension area to a higher one, which results in the motion of a drop from hydrophobic areas to hydrophilic areas. A drop may also travel along a cylinder which has proper surface roughness caused by radius variation, because according to Equation (2.31) the Laplace pressure increases if the radius of cylinder decreases provided n remains nearly constant. Therefore, a Laplace pressure difference should exist for the case of

a liquid on a conical fiber whose radius increases from the tip to the base as shown in Figure 2.11. The Laplace pressure of a drop on the small radius section of the cone is larger than on the larger radius region according to Equation (2.31). This suggests that a drop may move along a fiber from smaller radius to a larger one, if gravity can be ignored.

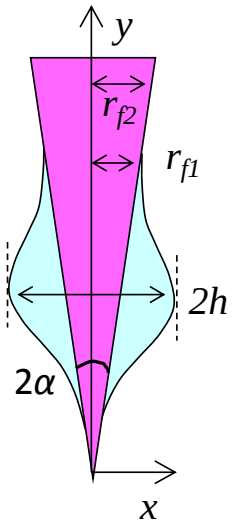

Figure 2.11. Schematic of a liquid drop on a conical fiber. Radius of the cone increases from the tip to base of the cone (marked as *y* direction), and *a* is the half-angle of the cone.

Besides showing the variation in radius, Figure 2.11 also indicates that the maximum thickness of the drop *h* changes for different locations along the cone. Based on Equation (2.31) the gradient of Laplace pressure difference of a drop on conical fiber along the cone axis (*y* direction) can be expressed as:

$$\left.\frac{d\Delta P}{dy}\right|_{V_0} = 2\gamma_{LV} \left.\frac{d\left(\frac{h - r_f \cos\theta_e}{h^2 - r_f^2}\right)}{dy}\right|_{V_0} \tag{2.35}$$

Equation (2.35) can be rewritten as:

$$\left.\frac{d\Delta P}{dy}\right|_{V_0} = -\frac{2\gamma_{LV}}{\left(h^2 - r_f^2\right)^2}\left\{\left(h^2 + r_f^2 - 2hr_f\cos\theta_e\right)\frac{dh}{dy} + \left[\left(h^2 + r_f^2\right)\cos\theta_e - 2hr_f\right]\frac{dr_f}{dy}\right\}_{V_0} \tag{2.36}$$

In the case of undulating drop on a thin hydrophilic cylinder, the maximum radius of the drop R_0 ($R_0 = h - r_f$) is much larger than r_f; therefore h can be assumed to be a constant ($h \approx R_0$) with constant liquid volume V_0. When n >> 1, $n - \cos\theta_e \approx n - 1$. Equation (2.36) can be reformulated as:

$$\left.\frac{d\Delta P}{dy}\right|_{V_0} = -\frac{2\gamma_{LV}}{\left(r_f + R_0\right)^2}\left.\frac{dr_f}{dy}\right|_{V_0} = -\left.\frac{2\gamma_{LV}\tan\alpha}{\left(r_f + R_0\right)^2}\right|_{V_0} \tag{2.37}$$

In the case of a very thin liquid film on a on a conical fiber ($r_f \approx h$), and Equation (2.36) can be written as:

$$\left.\frac{d\Delta P}{dy}\right|_{V_0} = -\left.\frac{\gamma_{LV}\tan\alpha}{r_f^2}\right|_{V_0} \tag{2.38}$$

Lorenceau[7] demonstrated that for a liquid with $\cos\theta_e \approx 1$ Carroll's Equation (2.31) can be

written as $\Delta P = 2\gamma_{LV} / (h + r_f)$ and the pressure difference along the cone in the direction of increasing radius and at constant volume changed would be given by Equations (2.37) and (2.38), respectively.

In Equation (2.37) and (2.38) α is the half-angle of the cone and the negative sign means the Laplace pressure decreases in the direction that the radius of the cone increases. The driving force caused by the pressure difference in the liquid would drive it to move if the force is large enough to overcome the resistive forces. Liu et al. also pointed out that a liquid droplet has the least potential energy on the base of a conical fiber compared to other locations on the cone, which means the liquid droplet tends to move from conical fiber tip to its base.[50]

2.5. Motion of a droplet on a conical fiber

When a drop moves on a conical fiber, there are three forces working on it: driving force F_{driv}, gravitational force F_G, and viscous force F_η. Dissipation occurs because of the friction of relative motion caused by viscosity of liquid. Since the friction between gas and liquid molecules and the friction between liquid molecules are negligible for low viscosity liquid, the dissipation mainly comes from the liquid wedge of moving drop.

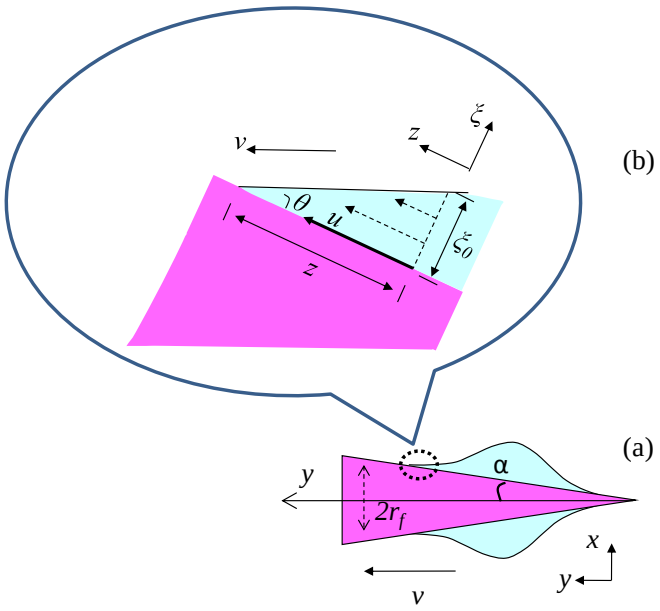

Figure 2.12. Schematics of a drop on a cone: (a) liquid moving on the cone, and (b) the magnification of liquid wedge of the moving drop. The drop moves with an average velocity v along cone axis in the direction of increasing radius (marked as y), and it moves along the cone surface with an instantaneous velocity $u(\xi)$.

Figure 2.12 presents the liquid wedge in steady state, and θ is the dynamic contact angle. The velocity $u(\xi)$ of liquid has a gradient along the liquid thickness because of viscosity of liquid. Suppose the liquid moves at an average velocity v along fiber axis (y direction). Then the relationship between the instantaneous velocity $u(\xi)$ along the cone surface and the average v along the cone axis can be written[40, 51, 52] as:

$$u(\xi) = \frac{v}{2\cos\alpha}\left[-1 + 3\left(\frac{\xi}{\xi_0} - 1\right)^2\right] \tag{2.39}$$

where ξ is the liquid thickness and ξ_0 is the thickness of the liquid layer at a level z of the

contact line between liquid and fiber in the liquid wedge ($\xi_0 = \theta z$) as shown in Figure 2.12.b. The viscous force over the wedge depth ξ_0 is $3\eta v / 2\cos\alpha$ where η is the liquid viscosity; hence, the viscous force in the liquid wedge per unit length of the contact line can be expressed as:

$$f_\eta = \int_{z_{min}}^{z_{max}} \frac{3\eta v}{2\theta z \cos\alpha} dz = \frac{3\eta v k}{2\theta \cos\alpha} \tag{2.40}$$

where $k = ln(z_{max} / z_{min})$, z_{max} and z_{min} are the maximum and minimum cutoff lengths and they are $z_{max} = (\rho g / \gamma_{LV})^{-0.5}$, and $z_{min} \sim a\theta^{-1}$ (ρ is liquid density, g is the gravitational acceleration, and a is a molecular size). Therefore, the viscous force along fiber axis, which is the opposite direction as the driving force caused by Laplace pressure gradient, is $3\eta k v / 2\theta$.The total viscous force F_η in the liquid wedge at radius r_f of cone can be written as:

$$F_\eta = 2\pi r_f f_\eta \cos\alpha = \frac{3\pi\eta r_f k v}{\theta} \tag{2.41}$$

The net driving force F_{driv} can be obtained by integrating the Laplace pressure difference times the area around the entire liquid surface.

$$F_{driv} = \int \pi (x - r_f)^2 d\Delta P \tag{2.42}$$

Based on Equation (2.37), Equation (2.42) can be reformed as:

$$F_{driv} = \int \pi (x - r_f)^2 \frac{2\gamma_{LV} \tan\alpha}{(r_f + R_0)^2} dy \tag{2.43}$$

For $r_f << R_0$, $2\gamma_{LV}\tan\alpha / (r_f + R_0)^2$ has almost no change for a very thin cone, so

$$F_{driv} = \frac{2\gamma_{LV}\tan\alpha}{(r_f + R_0)^2}\int \pi (x - r_f)^2 dy \tag{2.44}$$

According Carroll's equations, the relationship between *dy* and *dx* of a droplet on cylinder fiber can be expressed as:

$$\frac{dy}{dx} = -\frac{x^2 + ahr_f}{\sqrt{(h^2 - x^2)(x^2 - a^2 r_f^2)}} \tag{2.45}$$

where $a = (n\cos\theta_{fiber} - 1) / (n - \cos\theta_{fiber})$, θ_{fiber} is the Young contact angle of the liquid on a flat surface of the same material as the fiber.

It is well know that $\int\pi(x - r_f)^2 dy$ is the liquid drop volume V_0, so

$$F_{driv} = \frac{2\gamma_{LV}\tan\alpha}{(r_f + R_0)^2}V_0 \tag{2.46}$$

The gravitational force of liquid drop F_G is

$$F_G = \rho g V_0 \sin\beta \tag{2.47}$$

where ρ is the density of the liquid, g is the gravitational constant, β is the tilt angle with horizon direction of the cone as shown in Figure 2.13.

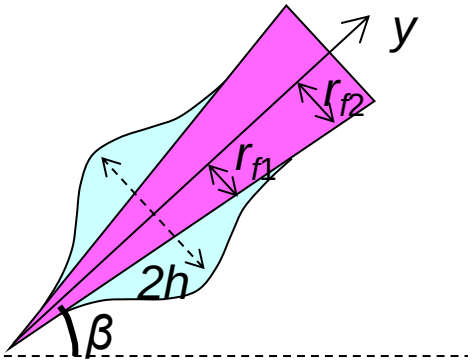

Figure 2.13. Schematic of a liquid drop on a titled conical fiber. Radius of the cone increases from the tip to base of the cone (marked as *y* direction), and the cone is tilted at an angle β with horizon direction.

For the case of drop moving spontaneously on a cone, the driving force should be equal or greater than the resistive forces (gravitational force and viscous force): $F_{driv} \geq F_G + F_\eta$; therefore based on Equation (2.41), (2.46) and (2.47) the gradient of the cone, $tan\alpha$, and the average velocity of drop v can be expressed as:

$$\tan\ \alpha\ \geq\ (\rho g V_0 \sin\ \beta\ +\ \frac{3\pi\eta\ kr_f v}{\theta})\frac{(r_f\ +\ R_0)^2}{2\gamma_{LV} V_0} \tag{2.48}$$

$$v \leq \left[\frac{2\gamma_{LV}\ \tan\ \alpha}{(r_f\ +\ R_0)^2} - \rho g \sin\ \beta\right]\frac{\theta V_0}{3\pi\eta\ kr_f} \tag{2.49}$$

To keep the drop moving with average velocity v, $tan\alpha$ should satisfy Equation (2.48). For the case of the motion of drop forming a Hoffman wedge[7, 53], in which viscous and interfacial forces are dominant, the dynamic contact angle θ can be described as $\theta = (6k\eta v/\gamma_{LV})^{1/3}$. Unlike

a drop moving on a planar surface, the drop on a fiber can sometimes form a global macroscopic wedge with a dynamic contact angle θ which is close to the Young static contact angle θ_e, instead of a local Hoffman wedge.[7] When the dissipation is global and if the motion does not affect the static shape of drop, the dynamic contact angle can be expressed with the static angle: $\theta \sim (h - r_f) / l$.[52, 54]

From Equation (2.49), it can be seen that the velocity of a drop has relationships with liquid surface tension and volume, local radius and gradient of the cone. With an increase in the gradient of a cone or in the liquid volume, the velocity of the drop should increase, and it should decrease if the radius of the cone increases.

A Laplace pressure difference could provide the driving force to drive oil from an oleophobic surface to an oleophilic surface. It also can cause liquid to move on the surface of a conical fiber once the driving force overcomes the resistive forces. Hence, if the surface is oleophobic, the cone attached to it is less oleophilic, and the gradient of the cone is large enough, it is possible that oil could transfer from the tip to the base of the cone and stay there without falling back. This may be the mechanism of Lady's Mantle leaves which is super liquid repellent.

2.6. Summary

In this chapter, the wetting behavior of flat surfaces and cylinders are introduced. The liquid static contact angle on smooth flat surfaces and the apparent contact angles on rough flat

surfaces can be described by Young, Wenzel and Cassie-Baxter Equations (2.1, 2.4, and 2.5), respectively.

Liquid spreads on flat smooth surfaces when the surface is connected with a liquid reservoir or when just a small liquid drop is dropped on it if the spreading coefficient is positive. For a cylinder, the coefficient must be greater than a critical value ($S > S_C$) for the liquid to spread. Usually either a symmetric undulating drop forms on a hydrophilic cylinder or an asymmetric shape exists if the external force is not negligible and the static contact angle is too large. The Laplace pressure of a liquid on a flat surface and on a cylinder was presented as Equations (2.29) and (2.31).

The Laplace pressure should be same throughout a static liquid drop; otherwise the pressure difference will force the drop to change shape or even move. The Laplace pressure of a drop on a cylinder varies with changes of liquid volume v_0, wetting behavior θ_e or radius r_f of the cylinder. The drop can move once the driving force overcomes the resistive force such as gravitational force and viscous force. Understanding the wetting behavior of solid surface could provide clues to obtain superhydrophobic and superoleophobic surfaces.

Even though the contact angle and wetting behavior of roughened flat surfaces and cylinders are mentioned in this chapter, what we are interested in is the motion of individual droplets on a flat smooth surface and on a cylindrical or conical fiber connected on this smooth surface. The conditions for a droplet to transfer from a flat smooth surface to a fiber, and for

a droplet to move along a fiber can be obtained according to theoretical and experimental research in this area. These conditions will provide useful information on approaching superoleophobic or oil self-cleaning materials for mimicking Lady's Mantle leaves.

Chapter 3 Experimental

3.1. Materials

Polyester (PET) film was obtained from DuPont (Wilmington, DE). Teflon® film (polytetrafluoroethylene) was obtained from SmallParts (Miramar, FL). Nylon monofilament was obtained from Pure Fishing. Inc. (Columbia, SC). Polypropylene (PP) monofilaments were obtained from Hahl. Inc. (Lexington, SC). Methanol (CH_3OH) was obtained from Sigma-Aldrich (St. Louis, MO). Ethylene glycol ($HOCH_2CH_2OH$, EG) was obtained from Fisher (Waltham, MA). Kaydol was obtained from CBM group of NC (Research Triangle Park, NC). Inc. Water used was processed by double deionized filter system (DI water). All the chemicals were used without further purification.

3.2. Cleaning of materials

All flat films and monofilaments were ultrasonic cleaned by Sonicwise SM-146H with methanol for 30 minutes at 20 °C to remove contamination on the material surfaces.

3.3. Drop transfer from one location to another

3.3.1. Drop transfer from flat surfaces to fiber tips or bodies

To determine whether a liquid drop would transfer from a flat surface to a cylinder, different diameter fibers (cylinders) were moved vertically by hand into contact with a liquid drop on a flat surface. Subsequently, the cylinder was lifted vertically to see whether the drop transferred to the cylinder.

3.3.2. Drop transfer from fiber tips to bodies

To discover if a liquid drop would prefer on fiber tip or on the tip and the body of fiber, different liquid drops were dropped on nylon fiber tip using a 2.0 μL syringe (Hamilton, #88400, Reno, NV) by hand.

3.3.3. Drop motion between flat surface and fiber

Drops of DI water, EG and Kaydol were placed on flat surfaces of Teflon® and polyester using a 10.0 μL syringe (Hamilton, #80075, Reno, NV) first, and then nylon, polypropylene and glass fibers were moved horizontally into the center of the drop by hand. Drop volumes of 2.0 and 4.0 μL were used for all liquids. Several fiber radii were used for each type of fiber. The drop-fiber-flat surface combination was photographed using a Meiji EMZ-13TR zoom stereo microscope (Meiji Techno America, Santa Clara, CA) fitted with a Canon EOS camera (Canon USA, Inc. NY). The light source was a Meiji MA964/TF LED Ring Illuminator (Meiji Techno America, Santa Clara, CA).

3.4. Characterization

3.4.1. Contact angle measurements

After gently dropping a liquid drop on sample using a 10.0 μL syringe (Hamilton, #80075, Reno, NV), the liquid contact angle on the sample was measured using a Rame-Hart contact angle goniometer and a Newport 495 series rotation stage (Newport Co., Irvine, CA) at 20°C. The volume of the applied droplets was 2.0 μL.

3.4.2. Fiber radii measurement

To obtain the average fiber radius at least five fibers were measured using a Mitutoya MDC-1" MJ digimatic micrometer (Mitutoya USA, Aurora, IL). Each fiber was placed between the micrometer tips and the micrometer closed until both tips just touched the fiber. The diameter was read directly from the micrometer.

3.4.3. Drop dimensions measurement

The drop dimensions were measured from photomicrographs by measuring the fiber radius, the length of the drop, the width of the contact spot between the drop and the flat surface, and, when possible, the widest width of the drop in number of pixels using Revolution™ v1.6.0b195 software. The fiber radius, which had been independently determined, was used to determine the length per pixel conversion factor. The dimensions measured in pixels were then converted to millimeters.

3.5. Drop dimensions prediction

The drop dimensions were predicted by Matlab R2008b based on Carroll's equations.[6]

Chapter 4 Results and Discussion

The goal of this dissertation is to provide theoretical and experimental evidence for a model of superoleophobic surfaces. As discussed in Chapter 2, we are attempting to mimic the superhydrophobic behavior of certain plant leaves which have hydrophilic hairs on their less hydrophilic surface. To understand the effect of multiple hairs on some superhydrophobic leaves, study about the wetting behavior of single hairs is necessary. The information related to liquid transferring from a flat surface to the tip of a fiber is useful to design re-entrant superoleophobic materials which prevent the wetting of the flat surface and maintain small drops climbing along the fibers. This information can be provided by Laplace pressure and free energy of the droplet on the solid surface.

4.1. Laplace pressure and free energy of liquid on solid surfaces

Again, a liquid droplet on a solid surface has a Laplace pressure (ΔP), which is the pressure difference sustained across the interface between liquid and vapor due to surface tension, and the Laplace pressure difference ($d\Delta P$) is determined by the shape of a droplet. The free energy is determined from the surface tension of solid-liquid γ_{SL}, liquid-vapor γ_{LV}, the surface energy of solid-vapor γ_{SV}, and the surface area of these interfaces. The Laplace pressure and free energy control the drop shape and location.

4.1.1. Laplace pressure and free energy of liquid on flat smooth surface

Liquid forms a spherical cap on a solid flat surface (Figure 2.8), where R_0 is the radius of the sphere. Since the principal radii of curvature of a sphere are equal to its radius ($R_1 = R_2 = R_0$), the Laplace pressure can be obtained by Equation (2.29). The free energy of a droplet on a flat smooth surface is:

$$G_{flat} = \gamma_{LV} A_{LV-flat} + \gamma_{SL-flat} A_{SL-flat} + \gamma_{SV-flat} (A_{total-flat} - A_{SL-flat}) \tag{4.1}$$

which can be rewritten using Young's equation:

$$G_{flat} = \gamma_{LV} (A_{LV-flat} - \cos\theta_{flat} A_{SL-flat}) + \gamma_{SV-flat} A_{total-flat} \tag{4.2}$$

where θ_{flat} is Young's contact angle for a liquid on a flat surface, γ is the surface tension, the subscripts *LV*, *SL*, and *SV* refer to liquid-vapor, solid-liquid, solid-vapor interfaces, respectively, A_{LV}, A_{SL} and A_{total} are the surface areas of the liquid-vapor, solid-liquid, and total solid surface, respectively, and the subscript *flat* refers to "on a flat surface."

For a droplet of volume V_0 resting on a flat smooth surface, the principle radius of the droplet, R_0, can be obtained according to Equation (2.30); the surface area of liquid-vapor $A_{LV\text{-}flat}$ and solid-liquid $A_{SL\text{-}flat}$ are:

$$A_{LV-flat} = 2\pi R_0^2 (1 - \cos\theta_{flat}) \tag{4.3}$$

$$A_{SL-flat} = \pi (R_0 \sin\theta_{flat})^2 \tag{4.4}$$

4.1.2. Laplace pressure and free energy of liquid on a fiber body

When a liquid droplet resides on the fiber body between the two ends, the Laplace pressure can be obtained by Equation (2.31) and the free energy of a droplet on the fiber is:

$$G_{fiber} = \gamma_{LV}\,(A_{LV-fiber} - \cos\theta_{fiber}\,A_{SL-fiber}) + \gamma_{SV-fiber}\,A_{total-fiber} \tag{4.5}$$

where θ_{fiber} is the Young's contact angle of liquid on a flat surface made of the same material as the fiber, γ, *LV*, *SL*, *SV*, A_{LV}, A_{SL}, A_{total} have the same meaning as the previous definitions, and subscript *fiber* refers to "on fiber body."

The surface area of liquid-vapor $A_{LV\text{-}fiber}$ and solid-liquid $A_{SL\text{-}fiber}$ of a droplet on a fiber body have been given by Carroll[6] and they are mentioned in Chapter 2 as Equation (2.32) and (2.33) :

$$A_{LV-fiber} = 4\pi r_f^2 n(a+n)E(\varphi,k) \tag{2.32}$$

$$A_{SL-fiber} = 4\pi r_f^2\left[aF(\varphi,k) + nE(\varphi,k)\right] \tag{2.33}$$

where $F(\varphi, k)$ and $E(\varphi, k)$ are the elliptical integrals of the first and second kind, respectively. $n = h / r_f$, $a = (n\cos\theta_{fiber} - 1)/(n - \cos\theta_{fiber})$, $k^2 = 1 - a^2 / n^2$ and $\sin^2\varphi = (1 / k^2)(1 - 1 / n^2)$. In addition, n is constrained by the droplet volume, V_0, which for the droplet on a fiber body is given by Carroll[6] as:

$$V_0 = \frac{2\pi r_f^3}{3} n\left[(2a^2 + 3an + 2n^2)E(\varphi,k) - a^2F(\varphi,k) + \frac{1}{n}\left(\frac{n^2-1}{1-a^2}\right)^{0.5}\right] - 2\pi r_f^3\left[aF(\varphi,k) + nE(\varphi,k)\right] \tag{2.34}$$

In Carroll's publication, drop length, interfacial surface area of liquid-vapor, and liquid

volume can be given if the contact angle and the maximum liquid thickness are provided. It is found that for drops of different volume, V_0, there is one corresponding n for each drop, and n increases with increasing V_0. Linear regression method can be used to get the n value at which the calculated liquid volume (V_0) equals to the real drop volume (V_{liquid}). The interfacial surface areas of liquid-vapor and solid-liquid are the functions of n, r_f and θ_{fiber}. Therefore, using fiber radius (r_f), liquid volume (V_{liquid}), and the liquid contact angles on a fiber (θ_{fiber}), the dimensions and interfacial surface areas of the drop (drop profile) can be obtained. The profile of a drop on the middle of a fiber can be carried out by running Matlab. The profile is required to obtain the Laplace pressure and the free energy of a drop on the fiber, which can be used to predict the motion and the final location of the drop.

4.1.3. Laplace pressure and free energy of liquid on both flat surface and fiber

For a liquid that resides on both a flat surface and a fiber, the way to calculate the Laplace pressure and the free energy is different than the ones that reside only on the flat surface or only on the fiber body. Since the real static contact angle of a liquid on a solid surface is determined by the solid-liquid, solid-vapor, and liquid-vapor surface tensions, the Young contact angle between the liquid and the flat surface should be the same as if it resides only on the flat surface. Likewise, the static contact angle of liquid on the fiber of the flat surface and fiber combined system should be the same as for the fiber alone. As shown in Figure 4.1, the water deposited on a Teflon® flat surface has the same contact angle (θ_{flat} = 115°) with that on a Teflon® flat surface after a glass fiber was horizontally moved into the water; and the water contact angle on the glass fiber is approximately 35° which is the same as we

measured when it is on a flat glass surface.

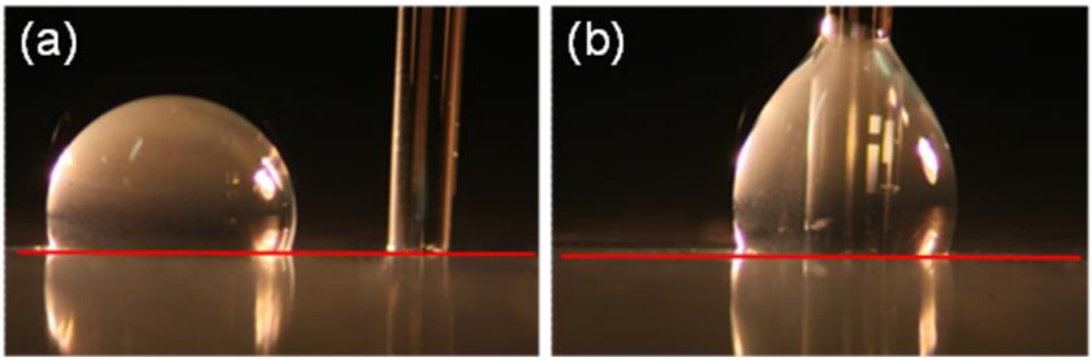

Figure 4.1. Water droplet on a Teflon® flat surface and a glass fiber: (a) on flat surface, and (b) on both flat surface and fiber.

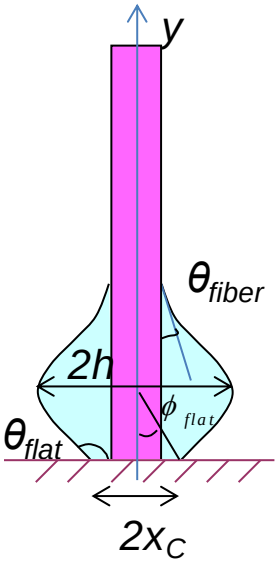

Figure 4.2. Schematic of a droplet on both flat surface and fiber.

When a liquid droplet is static, the Laplace pressure of the droplet at the interface of

liquid-vapor should be same. Therefore, it can be assumed that the droplet residing on both flat surface and fiber should have an undulating bell shape, which is the same as if the drop resides only on fiber, but is cut off by the flat plane, as shown in Figure 4.2.

In the Figure 4.2, x_C is the contact length from the edge of the drop on the flat surface to the center of the fiber; ϕ_{flat} is the angle between the plane (A) and (B) as shown in Figure 4.3. The plane (A) is perpendicular to the flat surface and includes the fiber's axis in fiber length (y), while the plane (B) is perpendicular to the interface of liquid-vapor at the intersection of the liquid and the flat surface. Since the Young's contact angle between the liquid and the flat surface (θ_{flat}) with the fiber present is the same as if the fiber is not present, $\phi_{flat} = \theta_{flat}$ for $\theta_{flat} < 90^0$, and $\phi_{flat} = 180^0 - \theta_{flat}$ for $\theta_{flat} > 90^0$.

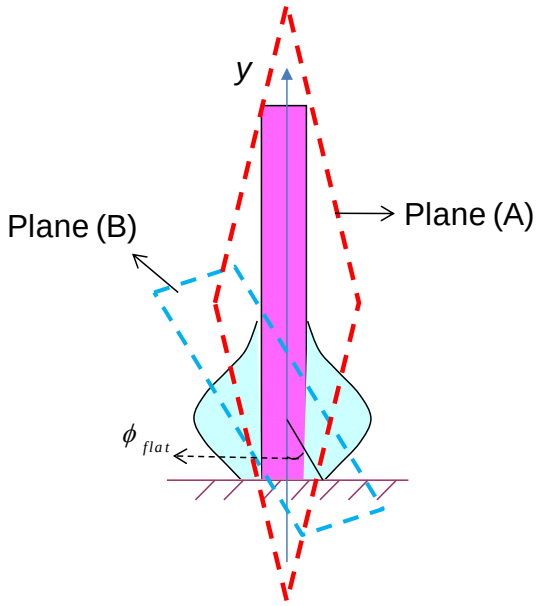

Figure 4.3. Schematic of angle ϕ_{flat}.

The Laplace pressure of a droplet on the flat surface and fiber combined system can be obtained by Equation (2.31). The free energy of the liquid droplet at this location can be expressed as following:

$$G_{flat \text{ and fiber}} = \gamma_{LV}\left(A_{LV-flat \text{ and fiber}} - A_{SL-on \text{ fiber}} \cos\theta_{fiber} - A_{SL-on \text{ flat}} \cos\theta_{flat}\right) + \gamma_{SV-flat} A_{total-flat} + \gamma_{SV-fiber} A_{total-fiber} \quad (4.6)$$

where γ, *LV*, *SL*, *SV*, A_{LV}, A_{SL}, A_{total} have the same meaning as the previous definitions, and subscripts *fiber*, *flat* and *flat and fiber* refer to "on fiber body," "on flat surface," and "on the flat surface and fiber combined system," respectively. $A_{LV\text{-}flat\ and\ fiber}$, $A_{SL\text{-}on\ fiber}$ and $A_{SL\text{-}on\ flat}$ are the interfacial surface areas of liquid-vapor on the flat surface and fiber combined system, solid-liquid on the fiber, and solid-liquid on the flat surface, respectively.

$$A_{SL-on \text{ flat}} = \pi\left(x_C^2 - r_f^2\right) \quad (4.7)$$

When a droplet resides simultaneously on both flat surface and a fiber as shown in Figure 4.2, the length of liquid from the edge of drop on the flat surface to the center of fiber (x_C) ranges from fiber radius (r_f) to the drop maximum thickness (h) and depends on the drop position. Based on Equation (2.28), x_C is a function of ϕ_{flat} and can be described as Equation (4.8)

$$\Delta P = \gamma_{LV}\left(\frac{1}{R_1} + \frac{1}{R_2}\right) = K \quad (2.28)$$

where K is constant, $R_1 = x\,\mathrm{cosec}\,\phi$ and $R_2 = \mathrm{d}\phi / ds$ are the principal radii of curvature, and s is the arc length of the drop, and $\phi = \phi_{flat}$ for the interfacial points at the intersection of liquid-vapor-flat.

$$x_C = \frac{1}{2}\left[(h + ar_f)\sin\phi_{flat} + \sqrt{(h + ar_f)^2 \sin^2\phi_{flat} - 4ahr_f}\right] \quad (4.8)$$

where $a = (n\cos\theta_{fiber} - 1) / (n - \cos\theta_{fiber})$ and $n = h / r_f$.

The length of a droplet on fiber ($L_{SL\text{-}on\ fiber}$) and the volume of liquid (V_0) are:

$$L_{SL-on\ \text{fiber}} = ar_f\left[F(\varphi_{fiber}, k) + bF(\varphi_{flat}, k)\right] + nr_f\left[E(\varphi_{fiber}, k) + bE(\varphi_{flat}, k)\right] \quad (4.9)$$

$$V_0 = \frac{\pi h}{3}\left\{(2a^2r_f^2 + 3ahr_f + 2h^2)\left[E(\varphi_{fiber}, k) + bE(\varphi_{flat}, k)\right] - a^2r_f^2\left[F(\varphi_{fiber}, k) + bF(\varphi_{flat}, k)\right]\right\}$$
$$+ \frac{\pi}{3}\left(r_f\sqrt{(h^2 - r_f^2)(r_f^2 - a^2r_f^2)} + bx_C\sqrt{(h^2 - x_C^2)(x_C^2 - a^2r_f^2)}\right) - \pi r_f^2 L_{SL-on\ \text{fiber}} \quad (4.10)$$

where $F(\varphi, k)$ and $E(\varphi, k)$ are the elliptical integrals of the first and second kind, respectively; subscript *fiber* and *flat* refer to "on fiber body" and "on flat surface," respectively; $b = 1$ for $\theta_{flat} > 90^0$, and $b = -1$ for $\theta_{flat} < 90^0$, respectively; $k^2 = 1 - a^2 / n^2$, and φ_{fiber}, φ_{flat} are the amplitudes of the elliptical integrals and can be obtained by the following equations:

$$\sin^2(\varphi_{fiber}) = (h^2 - r_f^2) \Big/ h^2k^2 \quad (4.11)$$

$$\sin^2(\varphi_{flat}) = (h^2 - x_C^2) \Big/ h^2k^2 \quad (4.12)$$

Since the drop maximum thickness (h) is constrained by the drop volume (V_0), and h increases with V_0 increasing, linear regression method can be used to obtain the maximum thickness at which the calculated drop volume (V_0) is almost equal to the real liquid volume

(V_{liquid}). Therefore, using fiber radius (r_f), liquid volume (V_{liquid}), liquid contact angles on fiber (θ_{fiber}) and on flat surface (θ_{flat}), the dimensions and interfacial surface areas of the drop (drop profile) can be obtained through the calculation. Table 4.1 lists the measured and predicted dimensions of different volume water droplets on a Teflon® flat surface and a glass fiber. The measured dimensions were obtained from photomicrographs (Figure 4.4) by measuring the fiber radius, the length of the drop, the width of the contact spot between the drop and the flat surface, and the widest width of the drop in number of pixels using Revolution™ v1.6.0b195 software. The dimensions measured in pixels were then converted to millimeters. The predicted dimensions were obtained by Matlab based on our Equations (4.6) and (4.12). Table 4.2 presents the measured (Figure 4.5) and predicted dimensions of different volume liquid droplets on a Teflon® flat surface and a glass fiber.

It can be seen that the predicted drop length ($L_{SL\text{-}on\ fiber}$), maximum thickness (h), and the contact length from the edge of the drop on the flat surface to the center of fiber (x_C) show good agreement with the corresponding measured values. The data in Tables 4.1 and 4.2 suggest that for different volume liquid droplets which have low contact angles with fibers the calculated dimensions agree well with measured ones.

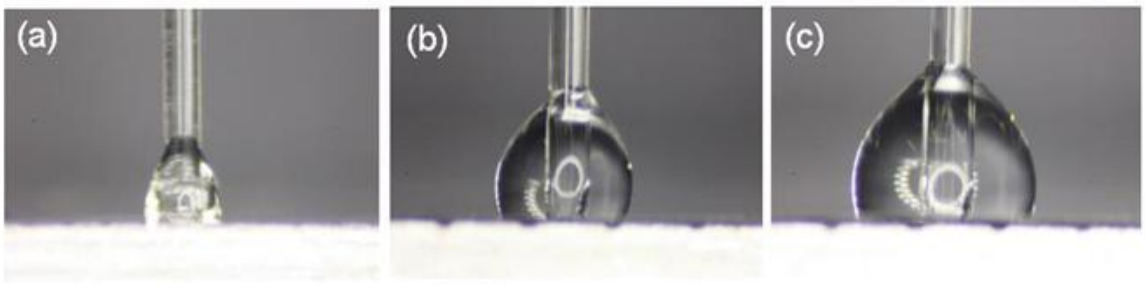

Figure 4.4. Water droplets sitting on a Teflon® flat surface and in contact with a glass fiber (r_f = 0.233mm): (a) 0.5μL, (b) 2.0μL, and (c) 4.0μL.

Table 4.1. Dimensions of water drop on a Teflon® flat surface and a glass fiber.

	$L_{SL\text{-}on\ fiber}$		x_C		h	
Volume V_0 (μL)	Measured	Predicted	Measured	Predicted	Measured	Predicted
0.5	1.04	1.08	0.49	0.51	0.50	0.56
2.0	1.60	1.66	0.75	0.79	0.83	0.86
4.0	1.85	2.05	1.02	0.99	1.08	1.09

Note: glass fiber r_f = 0.233mm, θ_{flat} = 115°, θ_{fiber} = 35°

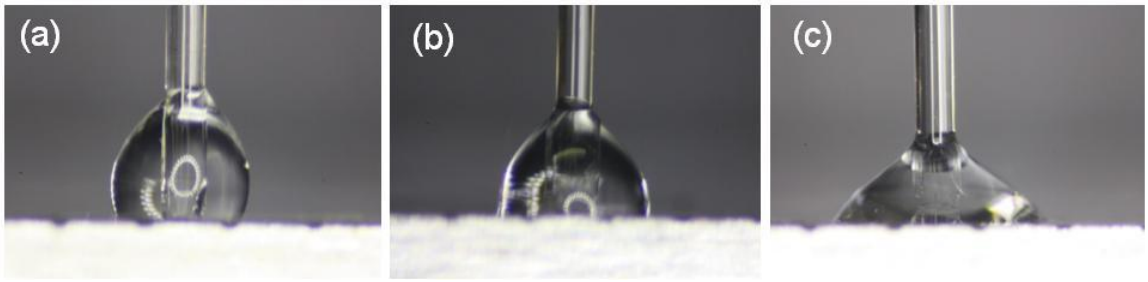

Figure 4.5. Different droplets (2.0 μL) sitting on a Teflon® flat surfaces and in contact with glass fibers (r_f = 0.233mm): (a) water, (b) EG, and (c) Kaydol.

Table 4.2. Dimensions of liquid drop on a Teflon® flat surface and a glass fiber.

Liquid	θ_{flat}	$L_{SL\text{-}on\ fiber}$		x_C		h	
		Measured	Predicted	Measured	Predicted	Measured	Predicted
water	115°	1.60	1.66	0.75	0.79	0.83	0.86
EG	85°	1.52	1.57	0.97	0.94	NM	0.95
Kaydol	56°	1.08	1.27	1.36	1.17	NM	1.40

Note: glass fiber r_f = 0.233mm, liquid volume V_0 = 2.0μL, NM means cannot measure.

The interfacial surface areas of liquid-vapor and solid-liquid are necessary to calculate the free energy of the drop on the flat surface and fiber combined system. To verify whether the calculation can be used to obtain the interfacial surface areas of a liquid droplet on the flat surface and fiber combined system, predicted drop profiles (white lines in Figure 4.6 – 4.9) are compared with corresponding experimental images.

The good match of drop profiles with the drop shape of different volumes (Figure 4.6), different liquids (Figure 4.7), different flat surfaces (Figure 4.8), and different fibers(Figure 4.9) suggests that the shape of liquid drop on the flat surface and fiber combined system can be assumed as an undulating bell which is cut off by the flat surface; the Young contact angle between the liquid and the flat surface is the same as if it resides only on the flat surface; the static contact angle on the fiber is not changed; the length of liquid from the edge of the drop on the flat surface to the center of fiber, x_C, can be obtained as a function of ϕ_{flat}., which equals to θ_{flat} for $\theta_{flat} < 90^0$, and is 180^0- θ_{flat} for $\theta_{flat} > 90^0$. The good match of drop profiles with the drop shapes also implies that our findings through mathematical formulas related to

the drop on the flat surface and fiber combined system can be used to obtain the interfacial surface areas (profile) of drops regardless of its volume, surface tension, the fiber surface energy, and fiber size.

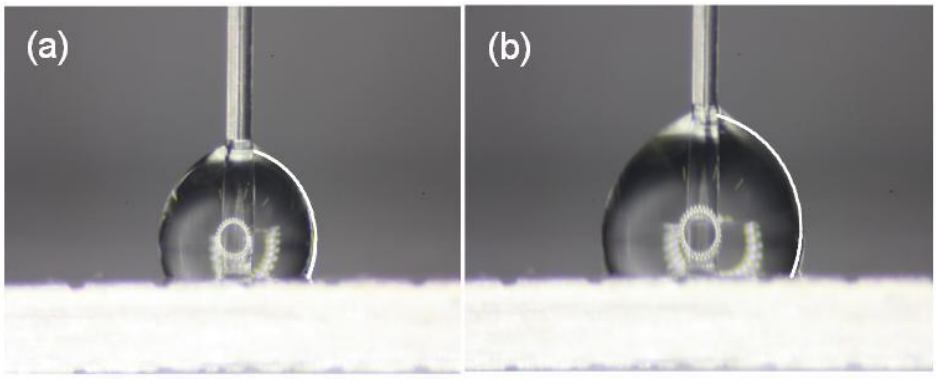

Figure 4.6. Water on a nylon fiber (r_f = 0.143mm) and a Teflon® flat surface with volumes (a) 2.0μL and (b) 4.0μL.

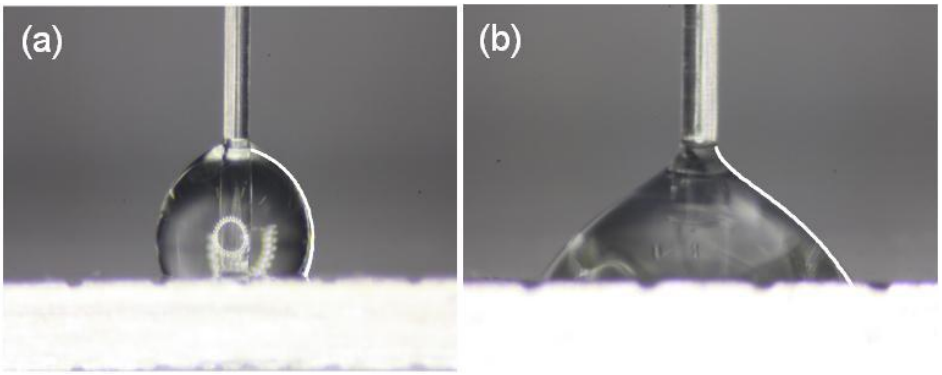

Figure 4.7. Different liquids of constant volume, V_0 = 2.0μL, on a nylon fiber (r_f = 0.143mm) and a Teflon® flat surface: (a) water, and (b) Kaydol.

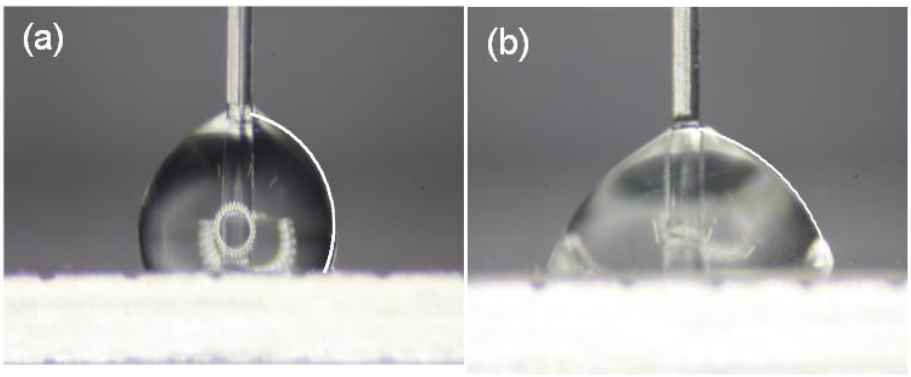

Figure 4.8. Water (V_0 = 4.0μL) on a nylon fiber (r_f = 0.143mm) and different flat surface: (a) Teflon® and (b) PET flat surfaces.

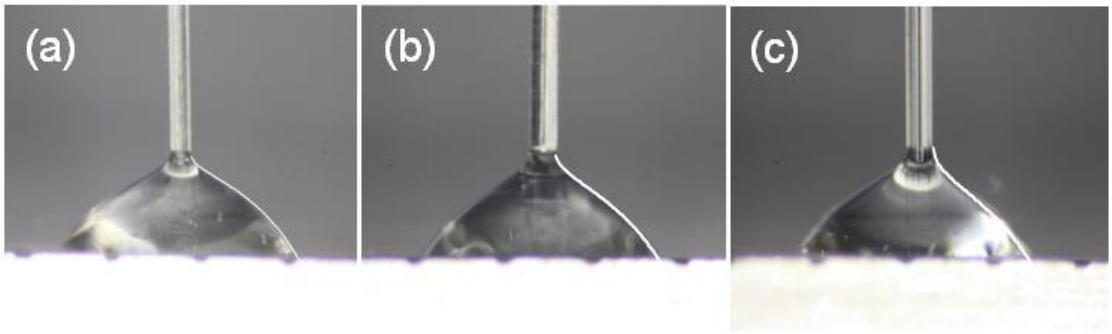

Figure 4.9. Kaydol (V_0 = 2.0μL) on a Teflon® flat surface and different fibers (a) PP (r_f = 0.1mm), (b) nylon (r_f = 0.143mm), and (c) glass (r_f = 0.145mm).

For a droplet transforming from a flat surface to the flat surface and fiber combined system, the change in the free energy $\Delta G_{Flat\&F\text{-}Flat}$ is:

$$\Delta G_{Flat\ \&\ F\text{-}Flat} = G_{flat\ \text{and}\ \text{fiber}} - (G_{flat} + \gamma_{SV-fiber} A_{total-fiber}) \quad (4.13)$$

which can be rewritten as:

$$\Delta G_{Flat\ \&\ \text{F-Flat}} = \gamma_{LV}\left[A_{LV-flat\ \text{and fiber}} - A_{LV-flat} + (A_{SL-flat} - A_{SL-on\ \text{flat}})\cos\theta_{flat} - A_{SL-on\ \text{fiber}}\cos\theta_{fiber}\right] \tag{4.14}$$

Likewise, the changes in the free energy for a droplet transferring from the flat surface and fiber combined system to the fiber body, $\Delta G_{F\text{-}Flat\&F}$, is:

$$\Delta G_{F-Flat\ \&\ \text{F}} = (G_{fibert} + \gamma_{SV-flat} A_{total-flat}) - G_{flat\ \text{and fiber}} \tag{4.15}$$

where subscript *total* refers to the total area of the solid surface as the previous definition. Equation (4.15) can be rewritten as:

$$\Delta G_{F-Flat\ \&\ \text{F}} = \gamma_{LV}\left[A_{\text{LV-fiber}} - A_{LV-flat\ \text{and fiber}} + A_{SL-on\ \text{flat}}\cos\theta_{flat} + (A_{SL-on\ \text{fiber}} - A_{SL-fiber}\cos\theta_{fiber}\right] \tag{4.16}$$

4.1.4. Laplace pressure and free energy of liquid on the fiber tip

For a droplet on fiber tip the shape of the drop is part of sphere as mentioned in Chapter 2. When the volume is small and the contact line is away from the edge, the drop rests on a flat surface and the contact angle is the static angle on fiber ($\theta = \theta_{fiber}$). As the liquid volume grows, the drop radius grows until the drop completely covers the tip of the fiber. As still more liquid is added, the apparent contact angle (θ) increases. As the drop continues to grow, eventually, the drop has expanded to the point where it now touches the side of the fiber; the drop collapses and encapsulates the tip. Before the drop collapse, the Laplace pressure and principle radius of curvature is just the sphere radius R_0 and can be provided by Equations

(2.29) and (2.30).

The free energy of a droplet only on the fiber tip is:

$$G_{tip} = \gamma_{LV} A_{LV-tip} - \gamma_{LV} \cos\theta_{fiber} A_{SL-tip} + \gamma_{SV-fiber} A_{total-fiber} \quad (4.17)$$

where θ_{fiber}, γ, *LV*, *SL*, *SV*, A_{LV}, A_{SL}, A_{total}, have the same meaning as the previous definitions, and subscript *fiber* refer to "on the fiber." The interfacial area of liquid-vapor $A_{LV\text{-}tip}$ and solid-liquid $A_{SL\text{-}tip}$ are:

$$A_{LV-tip} = 2\pi R_0^2 (1 - \cos\theta) \quad (4.18)$$

$$A_{SL-tip} = \pi r_f^2 \quad (4.19)$$

where $\theta = \theta_{fiber}$ for small volume drop, and $\theta = 90^0 + acos(r_f / R_0)$ for the liquid pinning at the edge of the fiber but prior to droplet collapse from the tip.

For a droplet transforming from a flat surface to the tip of fiber, the change in the free energy $\Delta G_{T\text{-}Flat}$ is:

$$\Delta G_{T\text{-}Flat} = (G_{tip} + \gamma_{SV-flat} A_{total-flat}) - (G_{flat} + \gamma_{SV-fiber} A_{total-fiber}) \quad (4.20)$$

which can be rewritten as:

$$\Delta G_{T\text{-}Flat} = \gamma_{LV} \left[A_{LV-tip} - A_{LV-flat} + A_{SL-flat} \cos\theta_{flat} - A_{SL-tip} \cos\theta_{fiber} \right] \quad (4.21)$$

After the drop collapses, the liquid stays on the tip and the body of the fiber. It is assumed that it takes the shape shown schematically in Figure 4.10, which consists of a portion that forms a part of sphere and a portion that forms part of a bell. The Laplace pressure in the

spherical portion is given by Equation (4.22) while the Laplace pressure in the bell portion is given by Equation (2.31)[6]:

$$\Delta P_{sphere} = \frac{2\gamma_{LV}}{R_{sphere}} \tag{4.22}$$

$$\Delta P_{bell} = \frac{2\gamma_{LV}}{r_f}\left(\frac{n - \cos\theta_{fiber}}{n^2 - 1}\right) \tag{2.31}$$

where R_{sphere} is the principle radius of the spherical tip, r_f is the fiber radius, θ_{fiber} is contact angle between the fiber and the liquid and $n = h / r_f$ (h is the maximum width of the bell shaped drop, as before).

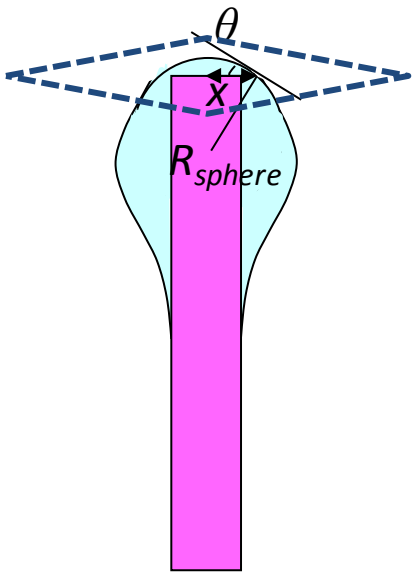

Figure 4.10. Schematic of liquid drop on the tip and the body of fiber.

For a static drop, the Laplace pressure should be same at each point of the liquid-vapor interface. Therefore, the Laplace pressure must be the same for both regions. Since Equation

(4.22) is equal to Equation (2.31), by combining these two equations, the following equation is obtained.

$$R_{sphere} = r_f \left(\frac{n^2 - 1}{n - \cos\theta_{fiber}}\right) \tag{4.23}$$

For the droplet on the tip and the body of the fiber, it is also expected that the conjunction area of the sphere and the bell portions includes the fiber tip as shown in Figure 4.10. Therefore, the length (x) of a drop from the drop edge to the center of the fiber at the combined plane of the sphere and the bell is:

$$x = R_{sphere} \sin\theta \tag{4.24}$$

where θ is the apparent angle at the combined plane of sphere and bell.

The volume of the drop, V_0, is just the sum of volume of the liquid in the spherical portion, V_{sphere}, and the volume in bell portion, V_{bell}, which can be obtained based on Equations (4.6) – (4.12).

$$V_{sphere} = \frac{\pi R_{sphere}^3 (2 - 3\cos\theta + \cos^3\theta)}{3} \tag{4.25}$$

The free energy of a droplet simultaneously on the tip and the body of fiber:

$$G_{tip\ \text{and}\ \text{fiber}} = \gamma_{LV} (A_{LV-in\ \text{sphere}} + A_{LV-in\ \text{bell}} - \cos\theta_{fiber} A_{SL-tip\ \text{and}\ \text{fiber}}) + \gamma_{SV-fiber} A_{total-fiber} \tag{4.26}$$

where θ_{fiber}, γ, LV, SL, SV, A_{LV}, A_{SL}, A_{total} have the same meaning as the previous definitions, and subscript *fiber*, *in sphere* and *in bell* refer to “on the fiber,” “in sphere portion” and “in

bell portion." The interfacial surface area of liquid-vapor in the spherical portion ($A_{LV\text{-}in\ sphere}$) and the interfacial surface area of solid-liquid ($A_{SL\text{-}tip\ and\ fiber}$) are:

$$A_{LV-in\ \text{sphere}} = 2\pi R_{sphere}^{2}\ (1-\cos\theta) \tag{4.27}$$

$$A_{SL-tip\ \text{and fiber}} = \pi r_f^{2} + 2\pi r_f L_{SL-fiber} \tag{4.28}$$

where $L_{SL\text{-}fiber}$ is the length of drop on the fiber body. Since the bell-shaped portion is a bell cut off by the flat plane, which is the same as the case of drops on both the flat surface and the fiber body, $A_{LV\text{-}in\ bell}$ and $L_{SL\text{-}fiber}$ can be obtained based on Equation (4.6) – (4.12).

As shown in Equations (4.23) – (4.28), R_{sphere}, x, volume V_{sphere}, V_{bell} are the functions of apparent angle θ and n. For each θ and V_0 there should be one corresponding n and one system free energy $G_{tip\ and\ fiber}$. Since n increases with increasing drop volume, the linear regression method was also used to get n and system free energy $G_{tip\ and\ fiber}$ for each θ, which ranges 0 to 180^0. The real θ is the one at which system has minimum free energy. After θ, R_{sphere}, x, n are obtained, the interfacial surface areas of solid-liquid and liquid-vapor of drop simultaneously on the tip and the body of fiber can be provided. Matlab has been run based on the assumptions and equations to carry out the free energy of the drop. Figure 4.11 shows the images of water, EG and Kaydol and the corresponding drop profiles (white line). Since the drop is small, the water drop, 0.5 μL, will stay on the nylon fiber tip after depositing water on it. The profile of the water drop fits well with the experimental images (Figure 4.11.a). For 0.5 μL EG and 1.0 μL Kaydol, the predicted drop profiles of the droplet on the fiber tip and the fiber body are in good agreement with the liquid shapes as shown in Figure

4.11.b and Figure 4.11.c.

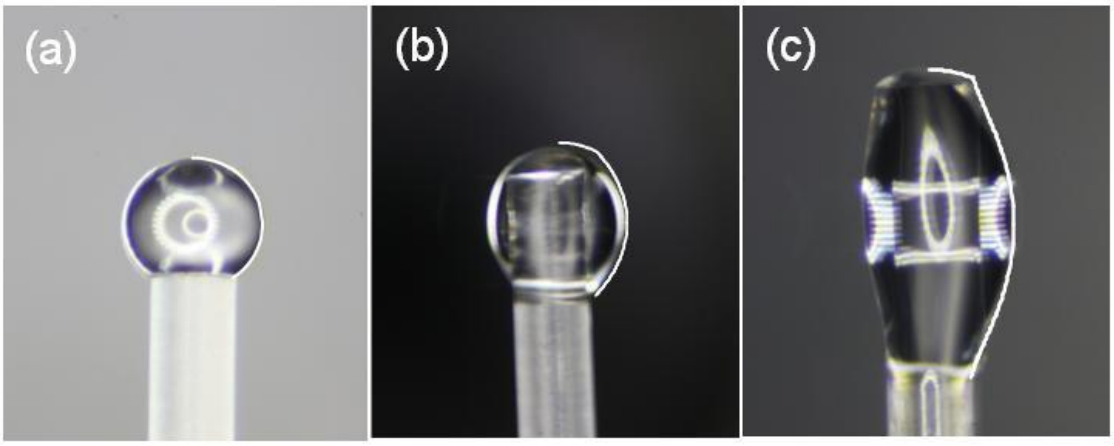

Figure 4.11. Different liquid on a nylon fiber (r_f = 0.288mm) after dropping the drop on the tip of the fiber: (a) water (0.5μL), (b) EG (0.5μL), and (c) Kaydol (1.0μL).

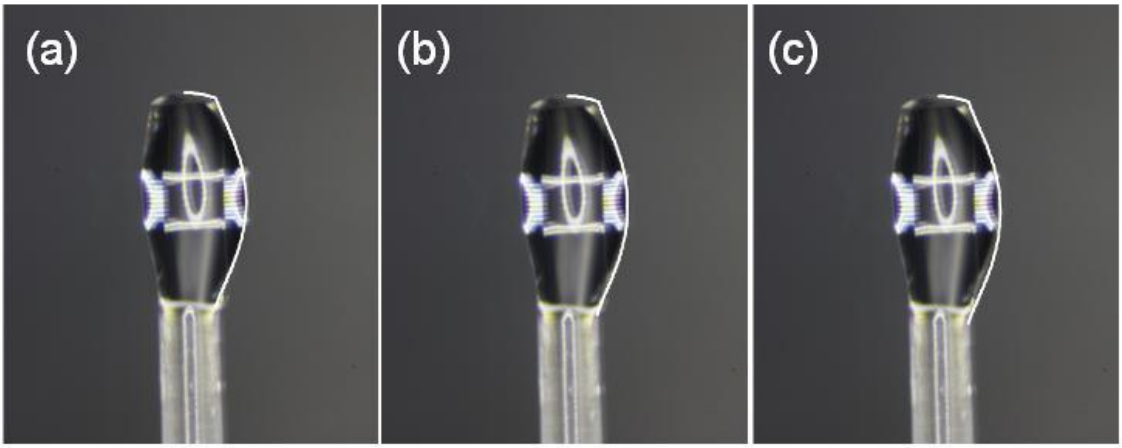

Figure 4.12. Fittings of the Kaydol drop on a nylon fiber after dropping the drop on the tip of the fiber (r_f = 0.288mm and V_{liquid} = 1.0μL) with different calculation volume V_0: (a) 0.9μL, (b) 1.0μL, and (c) 1.1μL.

Since the liquid volume V_0 ($V_0 = V_{sphere}+V_{bell}$) affects the calculation related to the droplet profiles, different liquid volumes were applied to determine the fitting error caused by V_0 and θ_{fiber}. Figure 4.12 shows the fittings of the Kaydol drop image (V_{liquid} = 1.0 μL) with the profiles calculated with different Kaydol volume V_0: 0.9 μL, 1.10 μL and1.1 μL. It shows that the predicted drop length and the maximum thickness increase as the volume of liquid increases. In Figure 4.12, (b) shows the best agreement between the true shape and the predicted profile.

There were two assumptions (1) the liquid drop shape consists of a part of sphere and a part of a bell, and (2) the conjunction area of the sphere and bell portion includes the fiber tip. These assumptions are essential to carry out the droplet profiles. The developed mathematical formulae can be used to obtain the interfacial surface area of liquid-vapor and the interfacial area of solid-liquid at the tip and the body of fiber.

For a droplet transferring from the tip and the body of fiber to the fiber tip, the change in the free energy $\Delta G_{T\text{-}T\&F}$ is:

$$\Delta G_{T-T\&F} = G_{tip} - G_{tip \text{ and fiber}} \tag{4.29}$$

which can be reformulated as:

$$\Delta G_{T-T\&F} = \gamma_{LV}\left[A_{LV-tip} - A_{LV-in \text{ sphere}} - A_{LV-in \text{ bell}} + (A_{SL-tip \text{ and fiber}} - A_{SL-tip})\cos\theta_{fiber}\right] \tag{4.30}$$

Likewise, the changes in the free energy for a droplet transferring from the fiber body to the tip and the body of fiber, $\Delta G_{T\&F\text{-}F}$, and transferring from the flat surface and the fiber body combined system to the tip and the body of fiber, $\Delta G_{T\&F\text{-}Flat\&F}$, are:

$$\Delta G_{T\&F-F} = \gamma_{LV}\left[A_{LV-in\ \text{sphere}} + A_{LV-in\ \text{bell}} - A_{LV-fiber} + (A_{SL-fiber} - A_{SL-tip\ \text{and fiber}})\cos\theta_{fiber}\right] \quad (4.31)$$

$$\Delta G_{T\&F\text{-Flat }\&F} = (G_{T\&F} + \gamma_{SV-flat}\,A_{total-flat}) - (G_{Flat\ \&F} + \gamma_{SV-fiber}\,A_{total-fiber}) \quad (4.32)$$

which can be rewritten as:

$$\begin{aligned}\Delta G_{T\&F\text{-Flat }\&F} = {} & \gamma_{LV}\left[A_{LV-in\ \text{sphere}} + A_{LV-in\ \text{bell}} - A_{LV-flat\ \text{and fiber}} + A_{SL-on\ \text{flat}}\cos\theta_{flat}\right] \\ & - \gamma_{LV}\,(A_{SL-tip\ \text{and fiber}} + A_{SL-on\ fiber})\cos\theta_{fiber}\end{aligned} \quad (4.33)$$

In our assumptions regarding a drop on the flat surface and fiber combined system, the shape of liquid drop was an undulating bell which was cut off by the flat surface, and the contact angles on the combined system were the same as the drop which was deposited on a flat surface and on a fiber. In the assumption related to drop on the tip and the body of fiber, the drop contains of a part bell and a part sphere and the conjunction area of the bell and the sphere portions including the fiber tip. The profiles of drops obtained by the math formula developed in this study based on the assumptions had good agreement with the experimental results. The free energies were carried out by varying the volume, liquid surface tension, surface energy of the flat surface and a fiber. By comparing the free energies of the drops, the motion and final location of liquid drops can be predicted. Understanding the wetting behavior of drops on fiber standing on a flat surface provides the capability of an engineering design for the desired applications.

4.2. Liquid transferring from one location to another

It is known that the driving force caused by pressure difference may move a drop from one location to another as long as the driving force can overcome the resistive force. According to the thermodynamic theory, system prefers the state in which it has lowest free energy. When a fiber is brought vertically into contact with a droplet sited on a flat surface and then the fiber is lifted, the drop can transfer to the tip of fiber (Figure 4.13.a), move to both the tip and the body of fiber (b), climb onto the fiber body (Figure 4.13.c) or remain on flat surface (Figure 4.13.d).

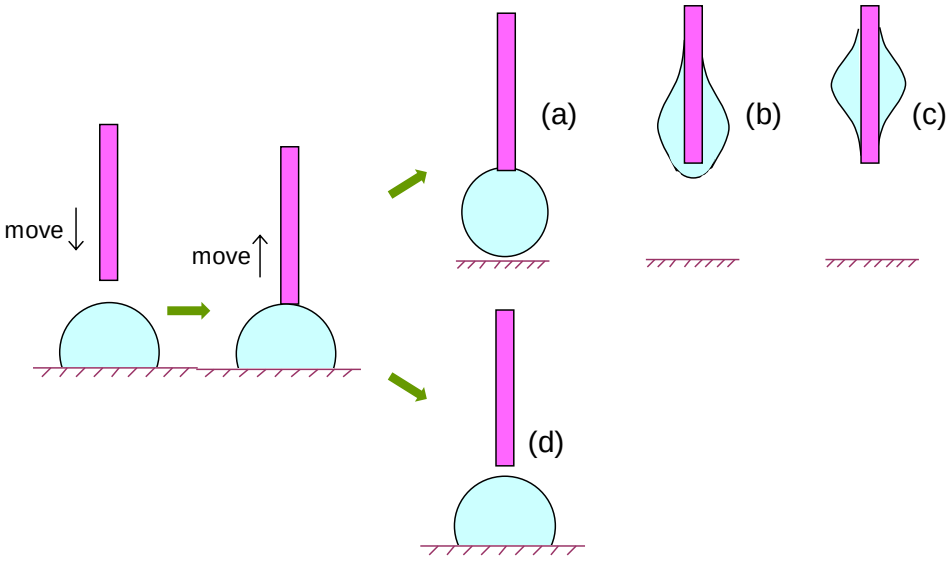

Figure 4.13. Schematics of a liquid droplet after vertically moving a fiber into contact with it and then lifting the fiber, the drop moves to: (a) the fiber tip, (b) the tip and the body of fiber, (c) the fiber body, or it (d) remains on the flat surface.

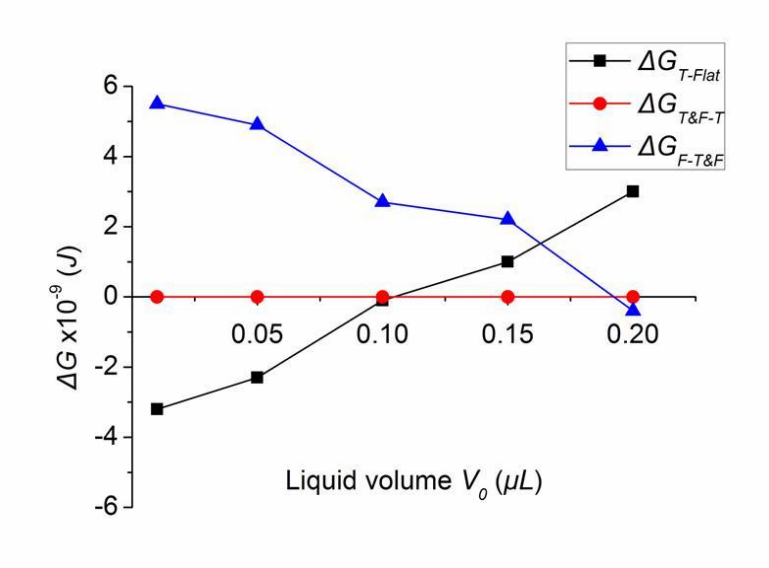

(a)

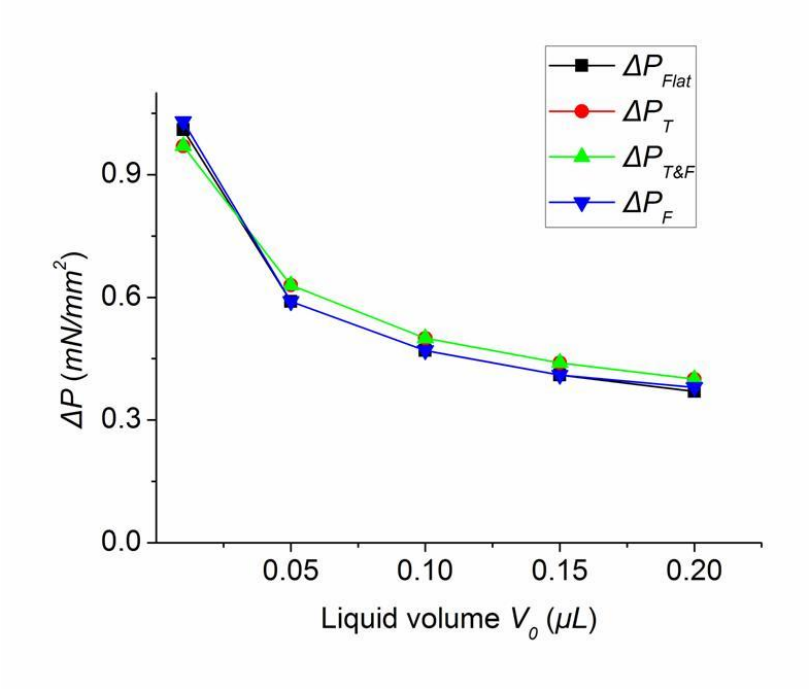

(b)

Figure 4.14. Water on a Teflon® flat surface and a nylon fiber tip or body (r_f = 0.143mm, θ_{fiber} = 72°, θ_{flat} = 115°): (a) changes in free energy ΔG, and (b) Laplace pressure ΔP.

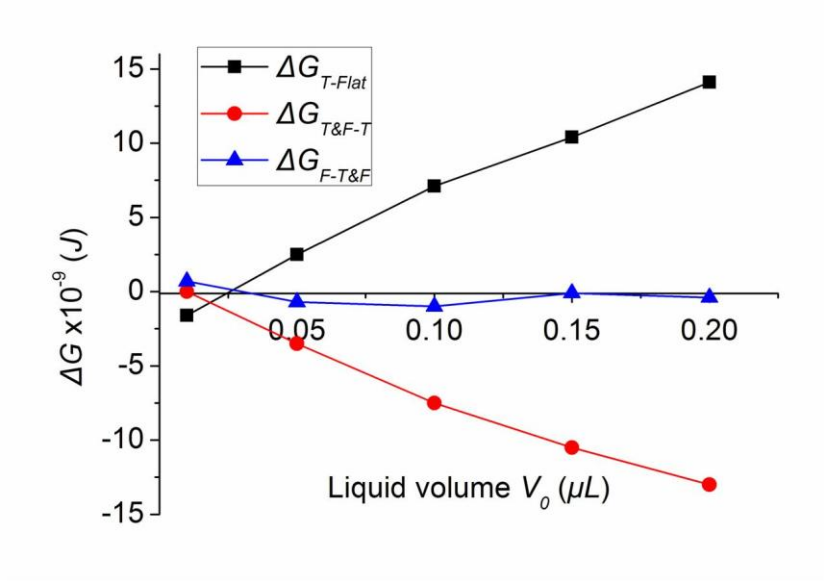

(a)

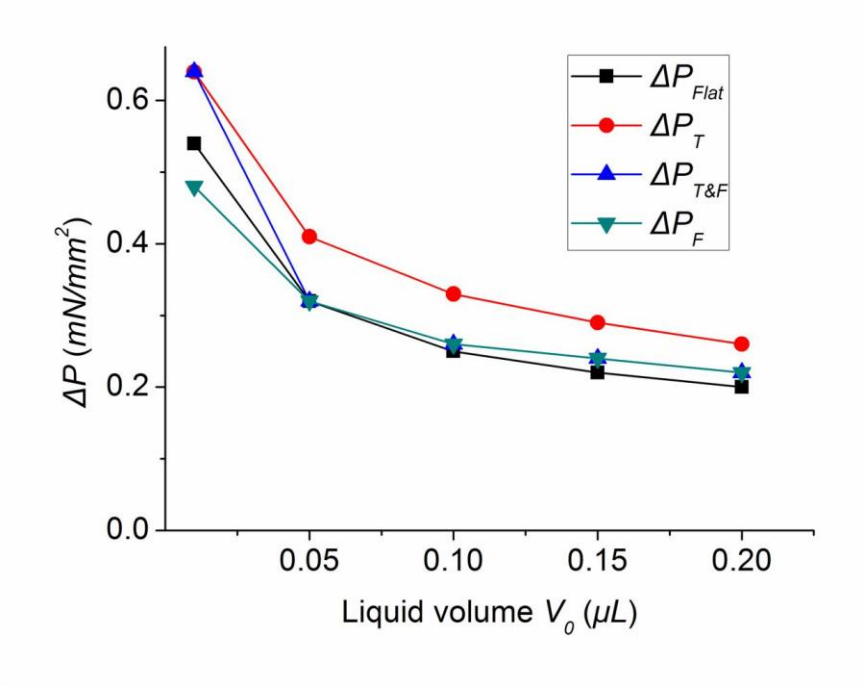

(b)

Figure 4.15. EG on a Teflon® flat surface and a nylon fiber tip or body (r_f = 0.143mm, θ_{fiber} = 42°, θ_{flat} = 85°): (a) changes in free energy ΔG, and (b) Laplace pressure ΔP.

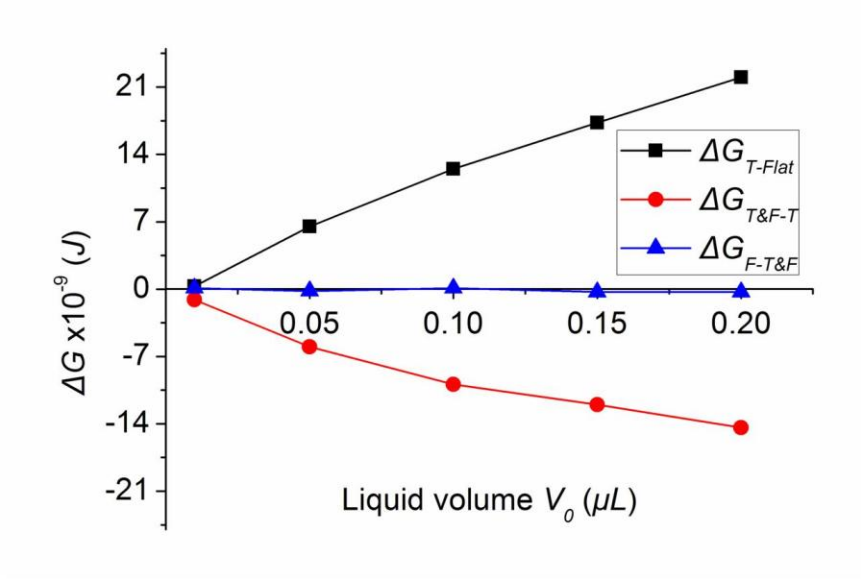

(a)

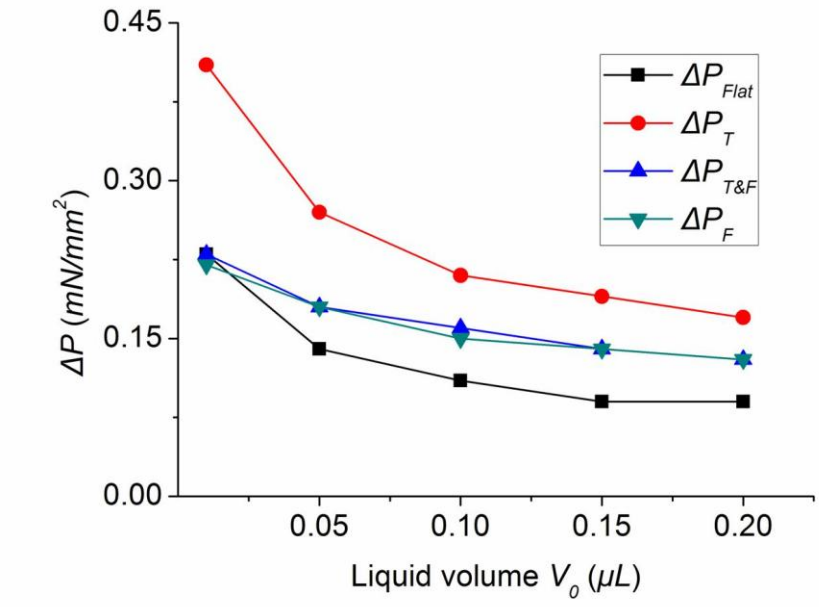

(b)

Figure 4.16. Kaydol on a Teflon® flat surface and a nylon fiber tip or body (r_f = 0.143mm, θ_{fiber} = 17°, θ_{flat} = 56°): (a) changes in free energy ΔG, and (b) Laplace pressure ΔP.

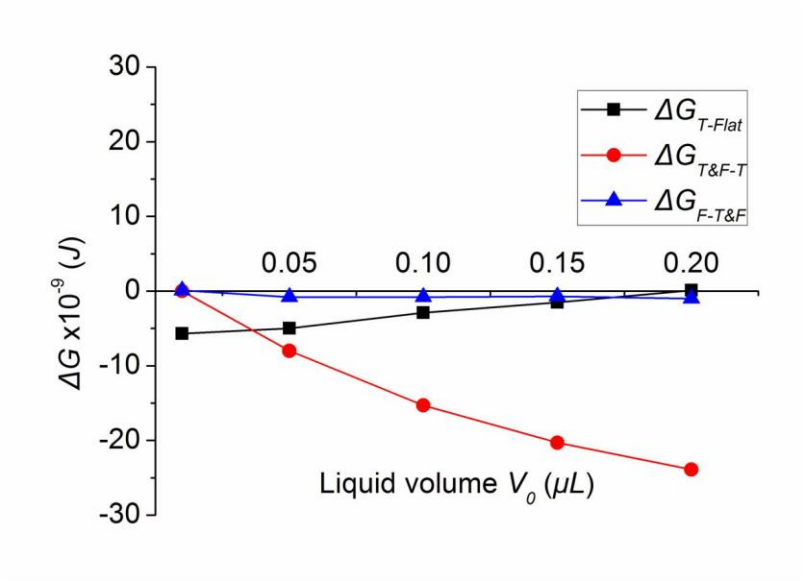

(a)

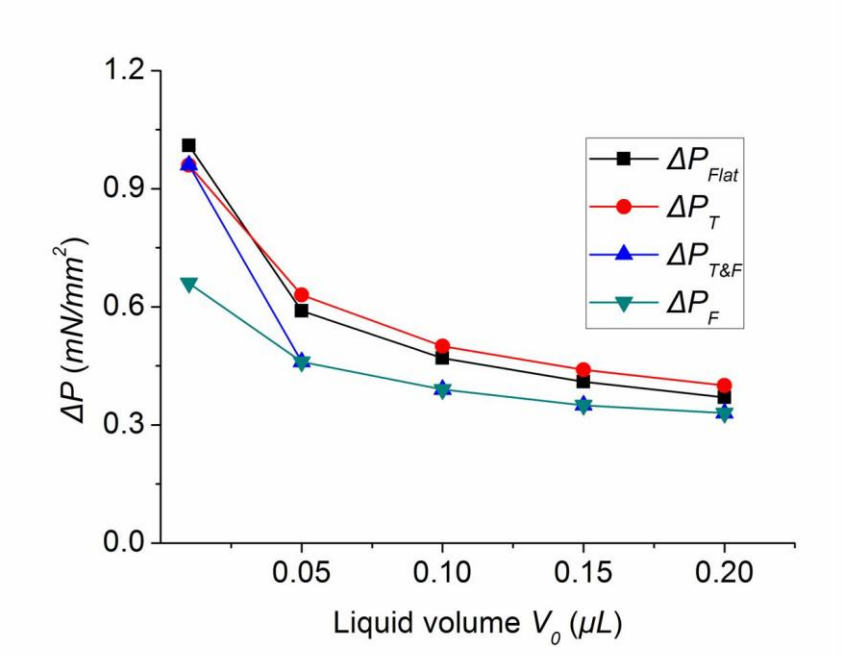

(b)

Figure 4.17. Water on a Teflon® flat surface and a glass fiber tip or body (r_f = 0.145mm, θ_{fiber} = 35°, θ_{flat} = 115°): (a) changes in free energy ΔG, and (b) Laplace pressure ΔP.

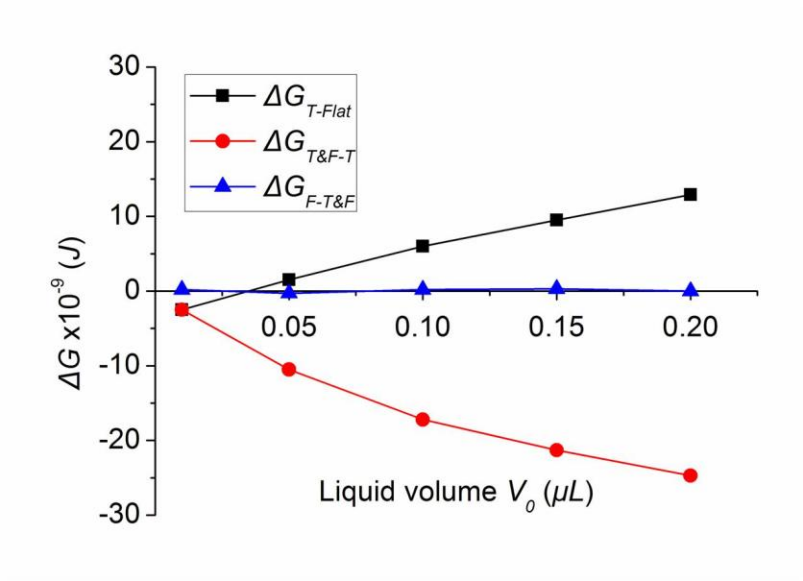

(a)

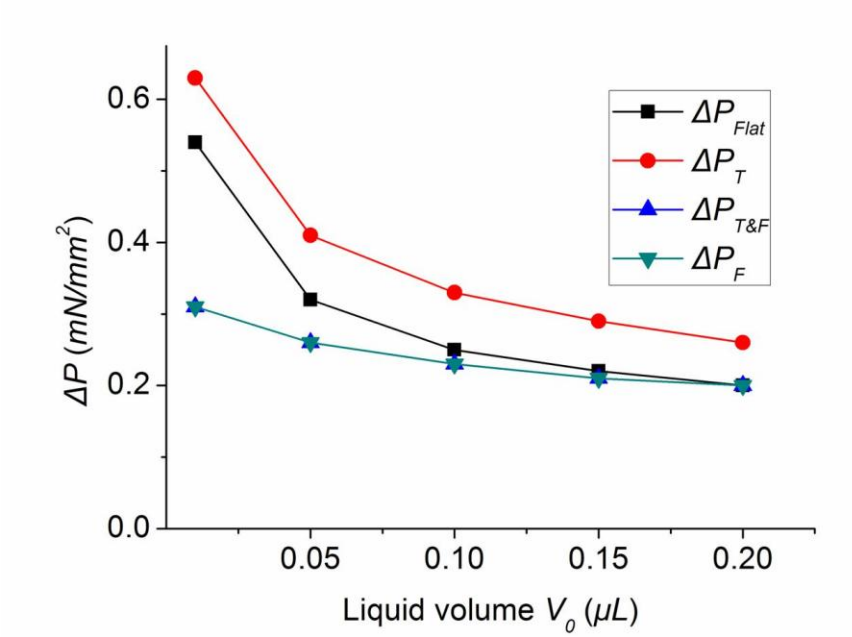

(b)

Figure 4.18. EG on a Teflon® flat surface and a glass fiber tip or body (r_f = 0.145mm, θ_{fiber} = 0°, θ_{flat} = 85°): (a) changes in free energy ΔG, and (b) Laplace pressure ΔP.

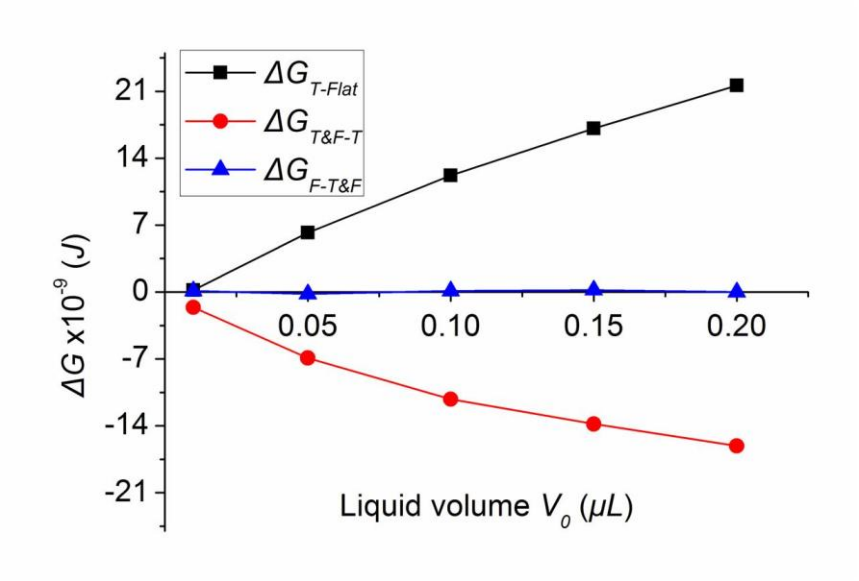

(a)

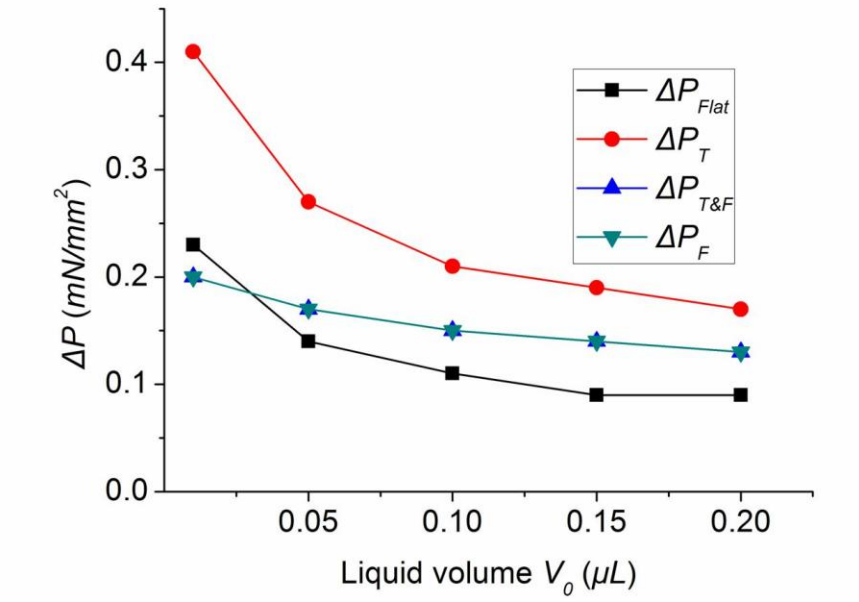

(b)

Figure 4.19. Kaydol on a Teflon® flat surface and a glass fiber tip or body (r_f = 0.145mm, θ_{fiber} = 0°, θ_{flat} =56°): (a) changes in free energy ΔG, and (b) Laplace pressure ΔP.

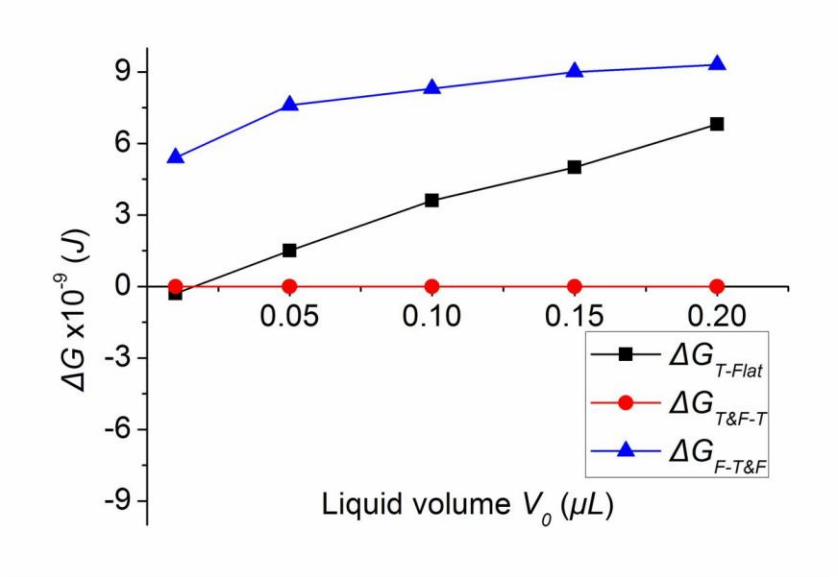

(a)

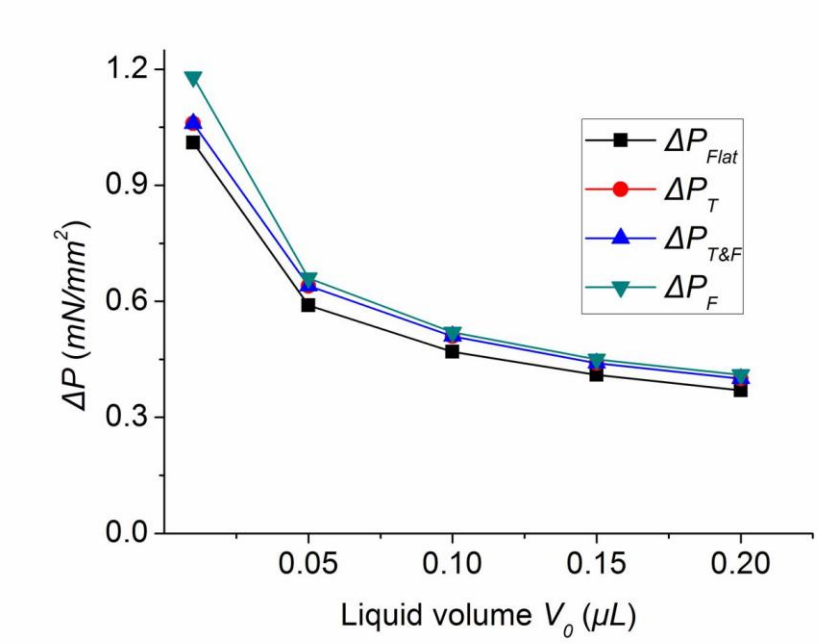

(b)

Figure 4.20. Water on a Teflon® flat surface and a PP fiber tip or body (r_f = 0.1mm, θ_{fiber} = 97°, θ_{flat} = 115°): (a) changes in free energy ΔG, and (b) Laplace pressure ΔP.

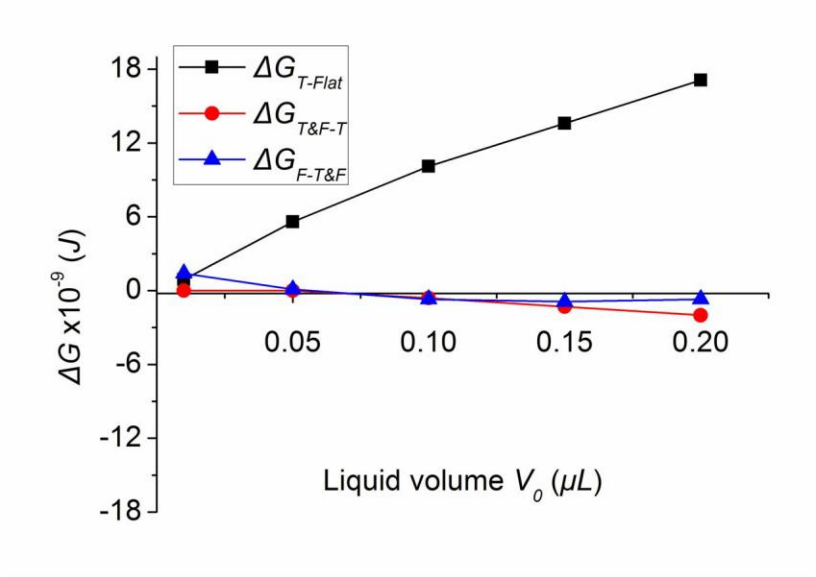

(a)

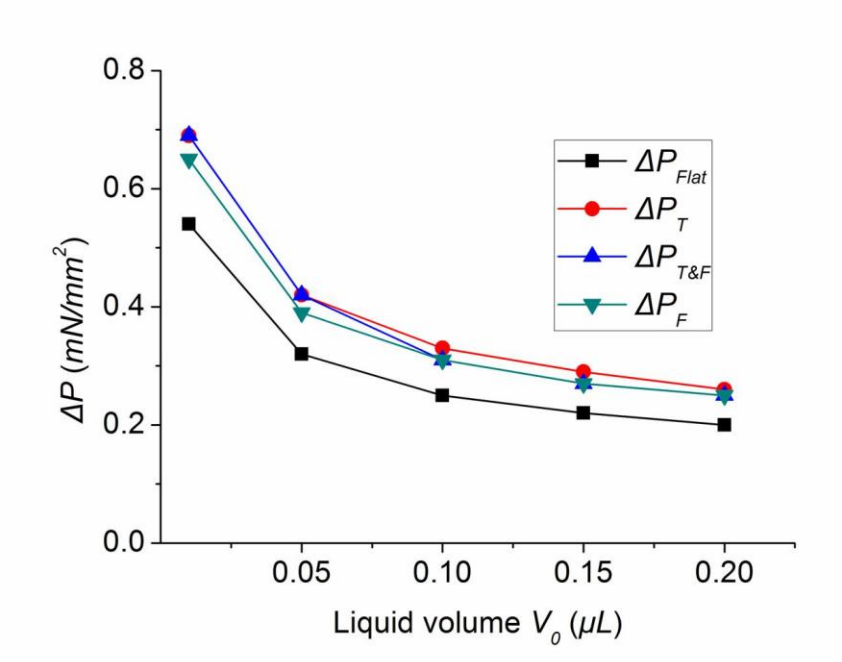

(b)

Figure 4.21. EG on a Teflon® flat surface and a PP fiber tip or body (r_f = 0.1mm, θ_{fiber} = 69°, θ_{flat} = 85°): (a) changes in free energy ΔG, and (b) Laplace pressure ΔP.

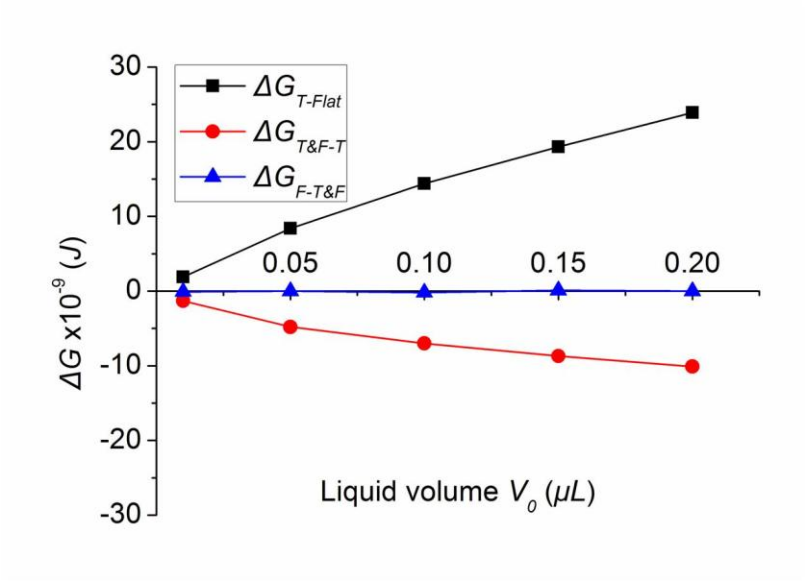

(a)

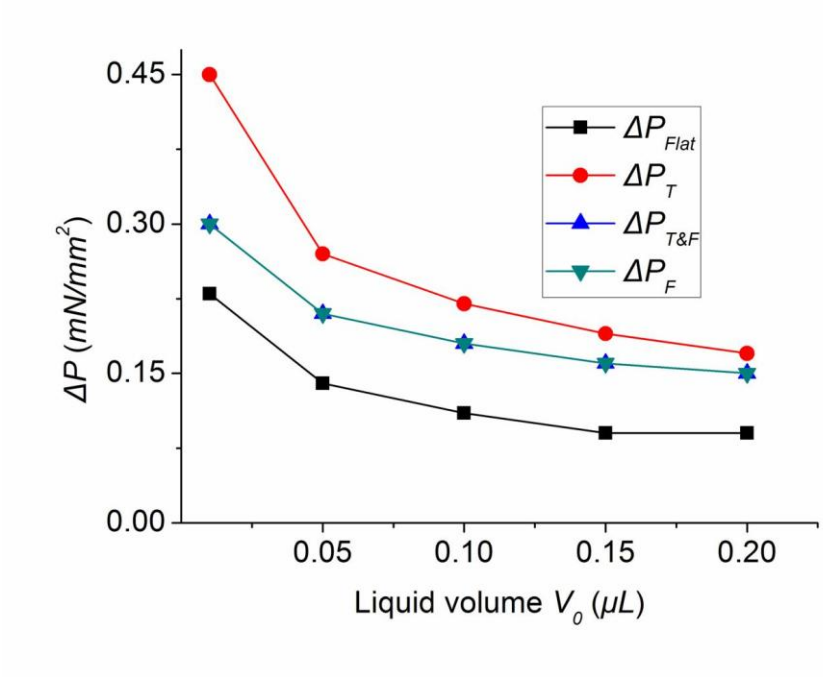

(b)

Figure 4.22. Kaydol on a Teflon® flat surface and a PP fiber tip or body (r_f = 0.1mm, θ_{fiber} = 69°, θ_{flat} = 85°): (a) changes in free energy ΔG, and (b) Laplace pressure ΔP.

Based on Equations (4.1) – (4.33), Figures 4.14 – 4.22 show the calculated change of free energy ΔG and Laplace pressure ΔP of liquid after vertically moving a fiber into contact with the liquid and then lifting the fiber (data is presented in Appendices 1 – 9). The liquids used in these tables are water, ethylene glycol (EG) and Kaydol; the fibers are nylon, glass and polypropylene (PP) monofilaments with different radii; and the flat surface is Teflon® film.

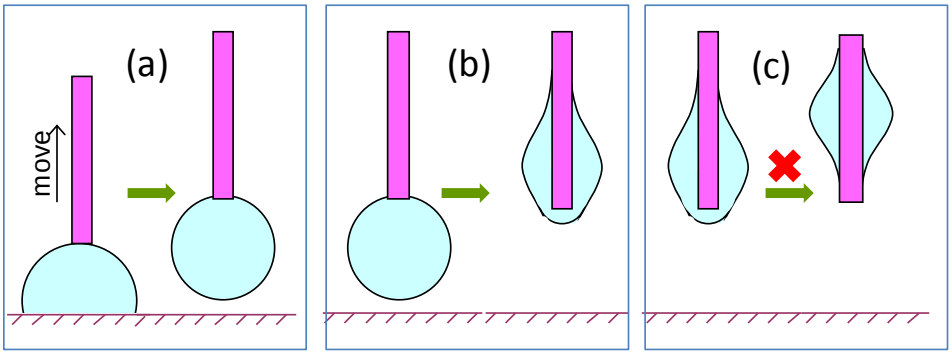

Figure 4.23. Schematics of the motion of a liquid droplet on a fiber after vertically lifting the fiber contacted with the droplet which rests on a flat surface. The droplet moves to: (a) the fiber tip, (b) the tip and the body of fiber, and (c) the fiber body,

It is known that the pressure difference will cause the drop to change the shape or even move it. In the Figures (4.14 – 4.22) most Laplace pressures on flat surfaces are close or smaller than on the fiber tip ($\Delta P_{Flat} \leq \Delta P_T$), which means there is no driving force to transfer the liquid from a Teflon® flat surface to the fiber tip. However, the change of free energy from a Teflon® flat surface to a fiber tip $\Delta G_{T\text{-}Flat}$ is negative for small volume liquids (Figures 4.14, 4.15, 4.17, 4.18, 4.20), which suggests that the liquid transferring between these two locations can happen (as shown in Figure 4.23.a). This prediction agrees with our laboratory

observation that small volume liquid transfers to the tip of the fiber after the fiber is lifted from the surface as shown in Figure 4.24. For large volume liquid drop $\Delta G_{T\text{-}Flat}$ is positive which means the drop cannot move to fiber tip after lifting the fiber and Figure 4.25 verified this prediction.

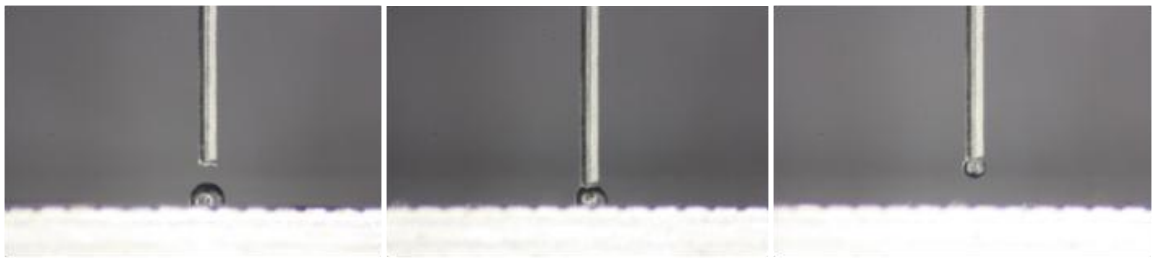

Figure 4.24. Transferring of a small volume of water (0.1 µL) resting on a Teflon® flat surface to a nylon fiber (r_f = 0.143mm) after vertically moving the fiber into contact with the droplet and then lifting the fiber: (a) on flat surface, (b) on both flat surface and fiber, and (c) on fiber tip.

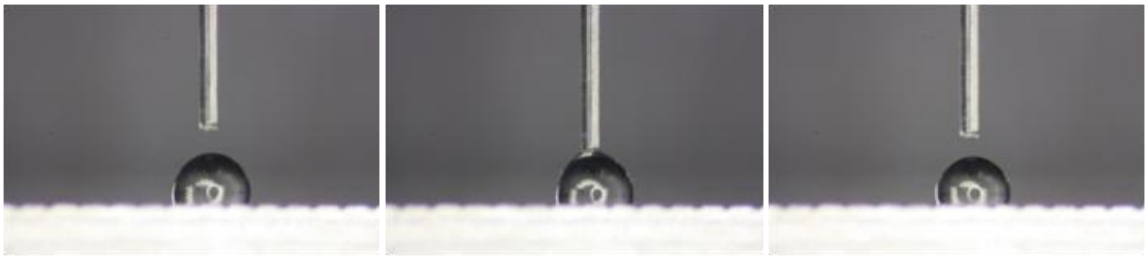

Figure 4.25. Transferring of a large volume of water (2.0 µL) resting on a Teflon® flat surface to a nylon fiber (r_f = 0.143mm) after vertically moving the fiber into contact with the droplet and then lifting the fiber: (a) on flat surface, (b) on both flat surface and fiber, and (c) remaining on the flat surface.

According to the changes in free energy of liquid transfer from a flat surface to a fiber, it can be predicted that the maximum liquid volume, which transfers to the fiber tip, increases with increasing liquid surface tension (Figure 4.14, 4.15, 4.16) and fiber surface energy (Figure 4.14, 4.17, 4.20). The predictions agree with our experimental observations. A liquid having high surface tension such as water (γ_{LV} = 72.8mN/m) better transfers to the fiber tip than a liquid having low surface tension such as Kaydol (γ_{LV} = 31mN/m). A liquid rather moves to a fiber tip (glass) with high surface energy instead of moving to a fiber with low surface energy (PP).

A drop with small volume or on a high surface energy fiber ($\theta_{fiber} > 90^0$) will only move to the fiber tip as mentioned in Chapter 2. It is assumed that $G_{tip\ and\ fiber}$ equals to G_{tip} for these liquids, since it is required to have the free energy of the drop at a fiber tip and body in order to understand the influence of energy of different liquids at different locations.

When $\theta_{fiber} << 90^0$ or a liquid volume is large enough, $\Delta G_{T\&F\text{-}T} < 0$. This indicates that the majority of liquid drop will move from the fiber tip to the fiber body shown in Figure 4.23.b. The $\Delta G_{F\text{-}T\&F}$ is very small for a low surface tension liquid. In consideration of calculation errors, it can be assumed that there is no energy difference between low surface tension liquid on the tip and the body of the fiber and that on the fiber body. Therefore, the drop will stay on the tip and the body instead of moving to the fiber body as shown in Figure 4.23. c.

The motion prediction of a liquid droplet from the fiber tip to the tip and the body of fiber

and to the fiber body was obtained with the prerequisite that the liquid drop was already on the fiber tip. If the drop cannot transfer to the fiber from the flat surface after the fiber lifting as shown in Figure 4.23.a, the following motion of drop on fiber would not be observed. From Figures (4.14 – 4.22), it is found that to transfer liquid from flat surface to fiber tip, low surface tension liquid or large volume liquid needs large fiber radius; it is easy for liquid to transfer to the tip of fiber which has low surface energy.

The predictions from our calculations and our laboratory observations suggest that the force caused by the difference of droplet Laplace pressure makes it possible for a droplet to transfer from one location to another; however, the final motion of the droplet is decided by the change of free energy.

When a fiber is horizontally moved into a droplet resting on a flat surface as shown in Figure 4.26, the drop can remain in contact with both the flat surface and the fiber, climb onto the fiber body, touch both the tip and the body of fiber, or move to the tip of fiber depending on which location has the lowest free energy.

Based on Equations (4.1) – (4.33), Figures 4.27 – 4.34 and the tables provided in Appendices 10 – 17 list the changes in the free energies of liquids with different volumes for drops transferring from a Teflon® flat surface to the Teflon® flat surface and fiber combined systems $\Delta G_{Flat\&F\text{-}Flat}$, from the Teflon® flat surface and fiber combined system to the fiber bodies $\Delta G_{F\text{-}Flat\&F}$, from the fiber bodies to the tip and the body of fiber $\Delta G_{T\&F\text{-}F}$, from the tip

and the body of fiber to the fiber tips $\Delta G_{T\text{-}T\&F}$, and from the Teflon® flat surface and fiber combined system to the tip and the body of fiber $\Delta G_{T\&F\text{-}Flat\&F}$. The liquids used in these tables are water, ethylene glycol (EG), and Kaydol; the fibers are glass, nylon and polypropylene monofilaments with different radii; and the flat surfaces is Teflon® film.

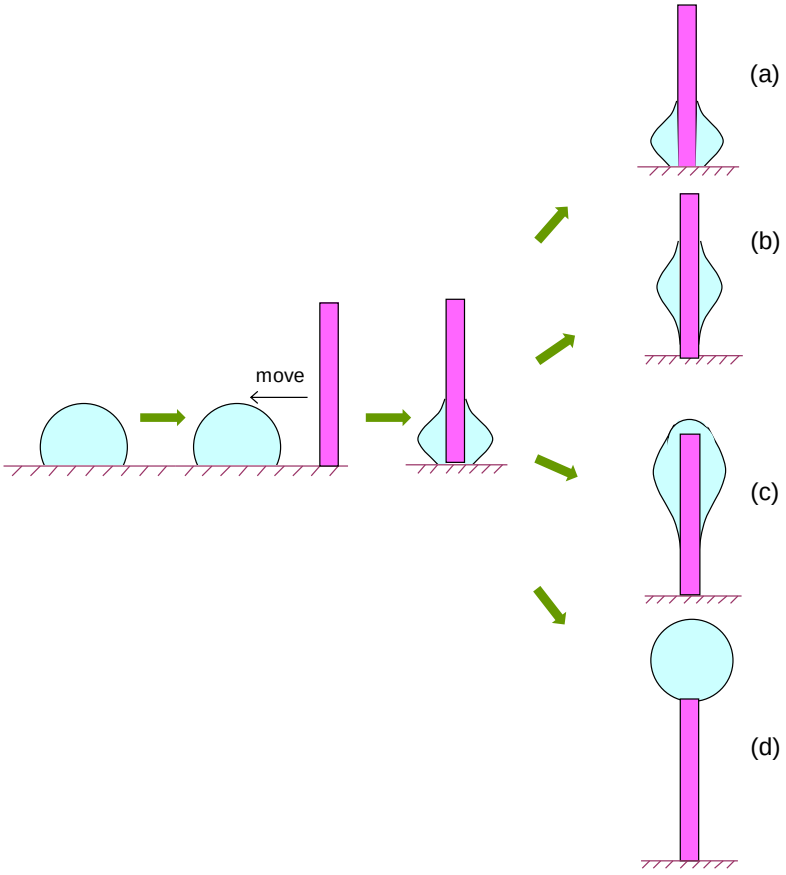

Figure 4.26. Schematics of a liquid droplet on a fiber after horizontally moving the fiber into the center of the droplet which rests on a flat surface. The droplet can: (a) reside on both the flat surface and the fiber, (b) it can move onto the fiber body, (c) on the tip and the body of fiber, or (d) only on the fiber tip.

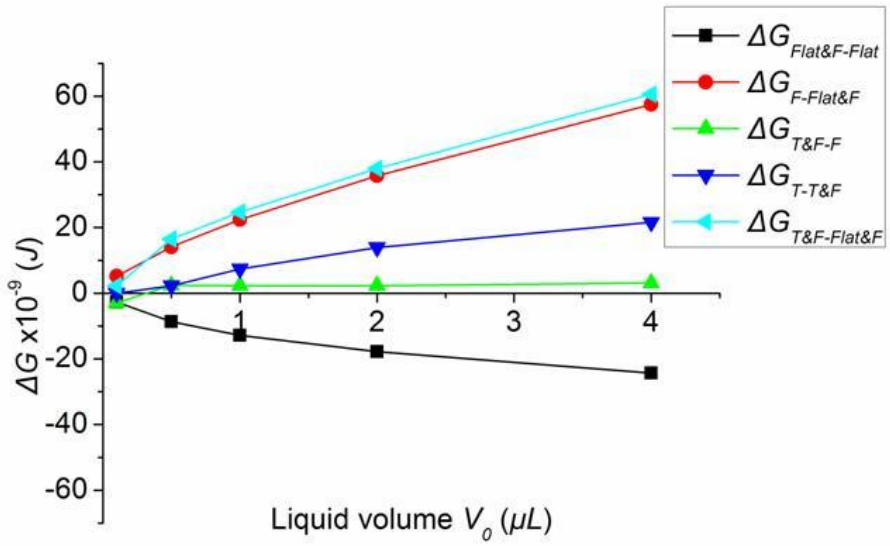

(a)

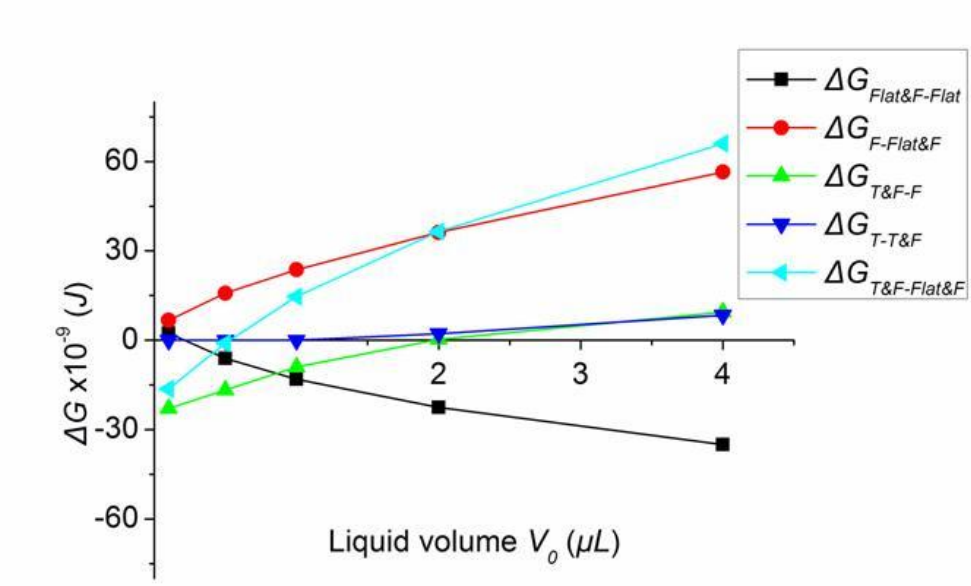

(b)

Figure 4.27. ΔG of water on a Teflon® flat surface and a nylon fiber (θ_{fiber} = 72°, θ_{flat} = 115°): (a) r_f = 0.143mm, and (b) r_f = 0.288mm.

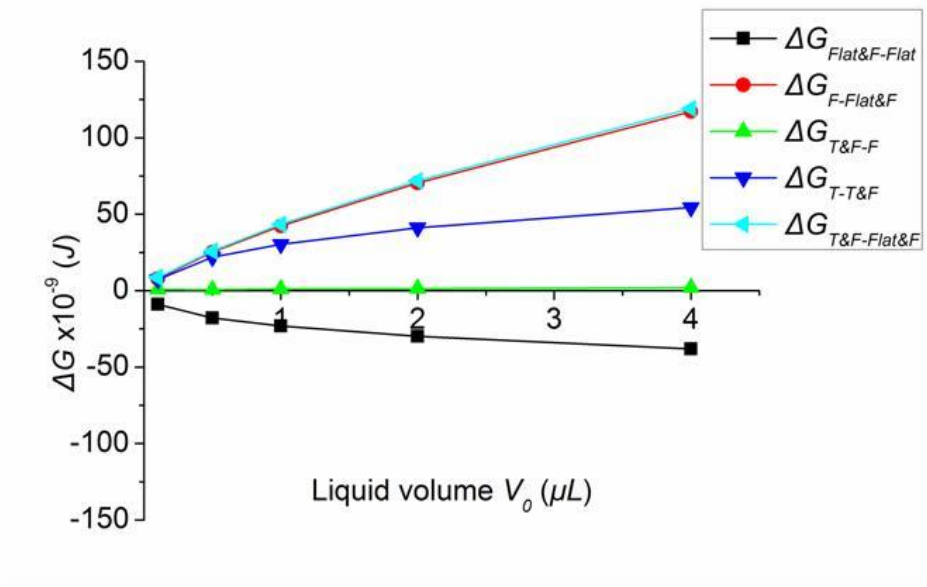

(a)

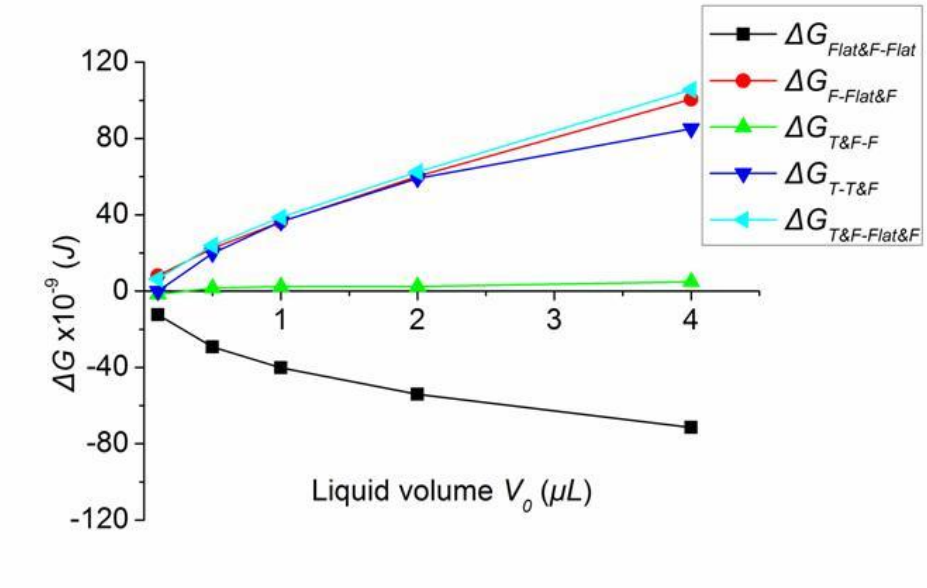

(b)

Figure 4.28. ΔG of EG on a Teflon® flat surface and a nylon fiber (θ_{fiber} = 42°, θ_{flat} = 85°): (a) r_f = 0.143mm, and (b) r_f = 0.288mm.

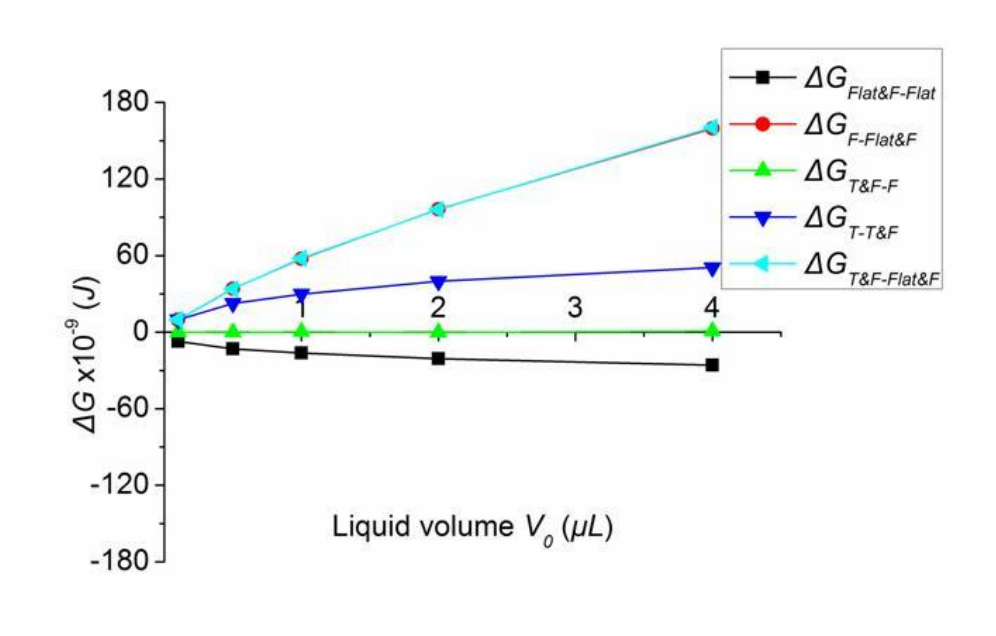

(a)

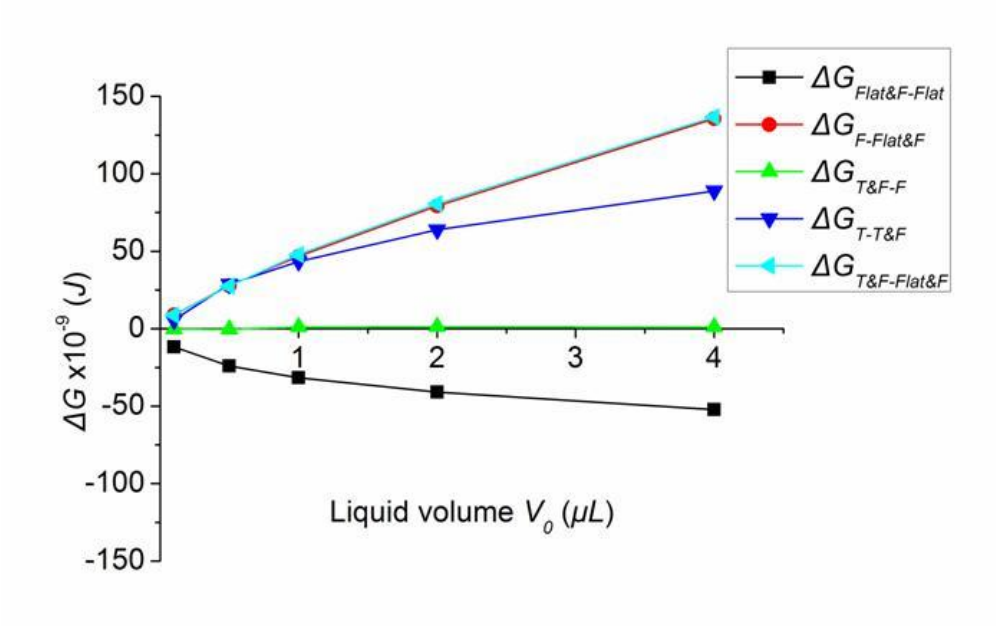

(b)

Figure 4.29. ΔG of Kaydol on a Teflon® flat surface and a nylon fiber (θ_{fiber} = 17°, θ_{flat} = 56°): (a) r_f = 0.143mm, and (b) r_f = 0.288mm.

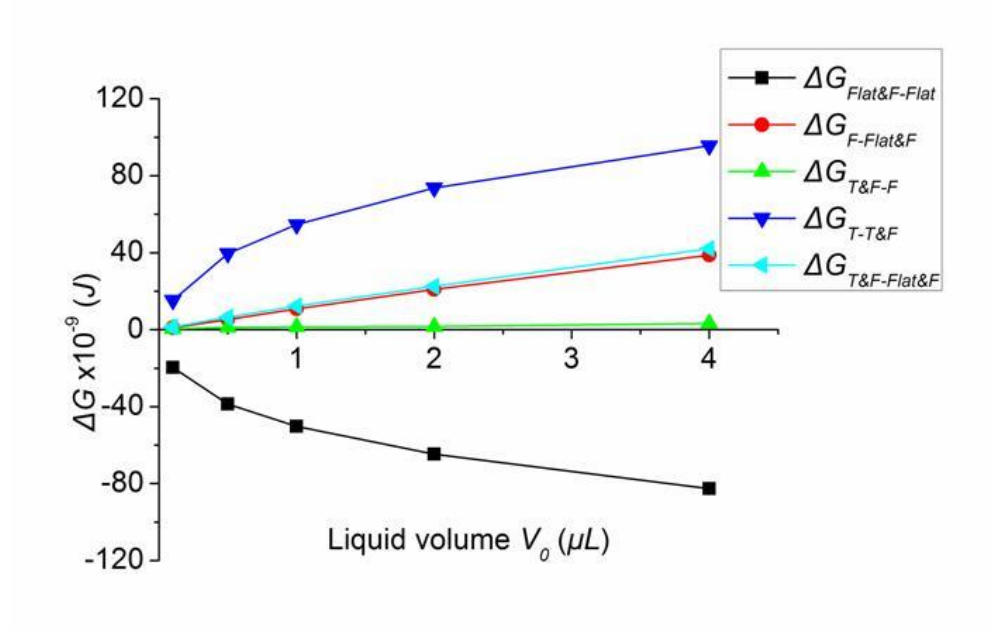

(a)

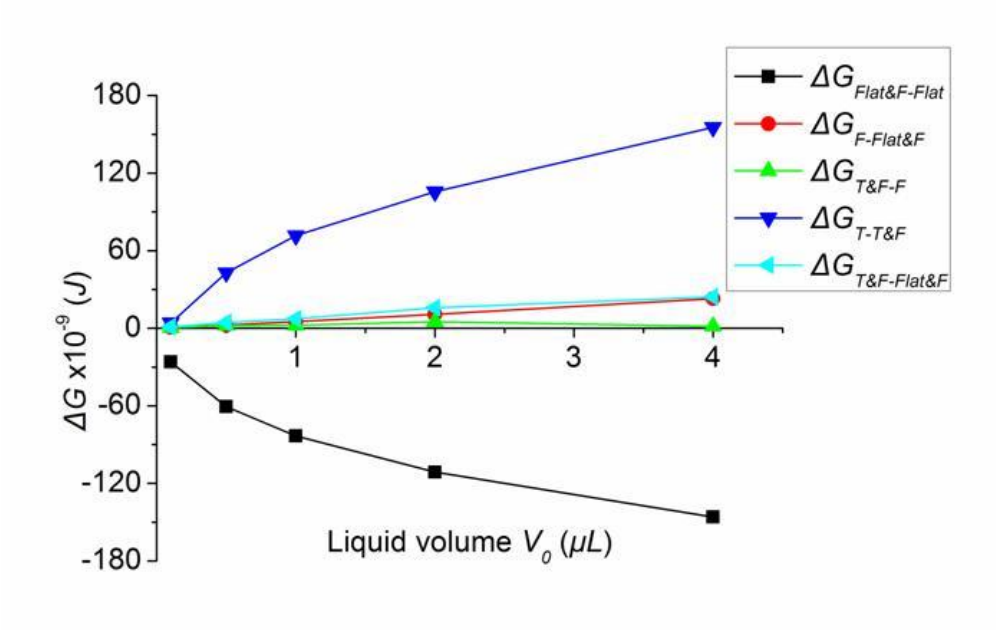

(b)

Figure 4.30. ΔG of water on a Teflon® flat surface and a glass fiber (θ_{fiber} = 35°, θ_{flat} = 115°): (a) r_f = 0.145mm, and (b) r_f = 0.271mm.

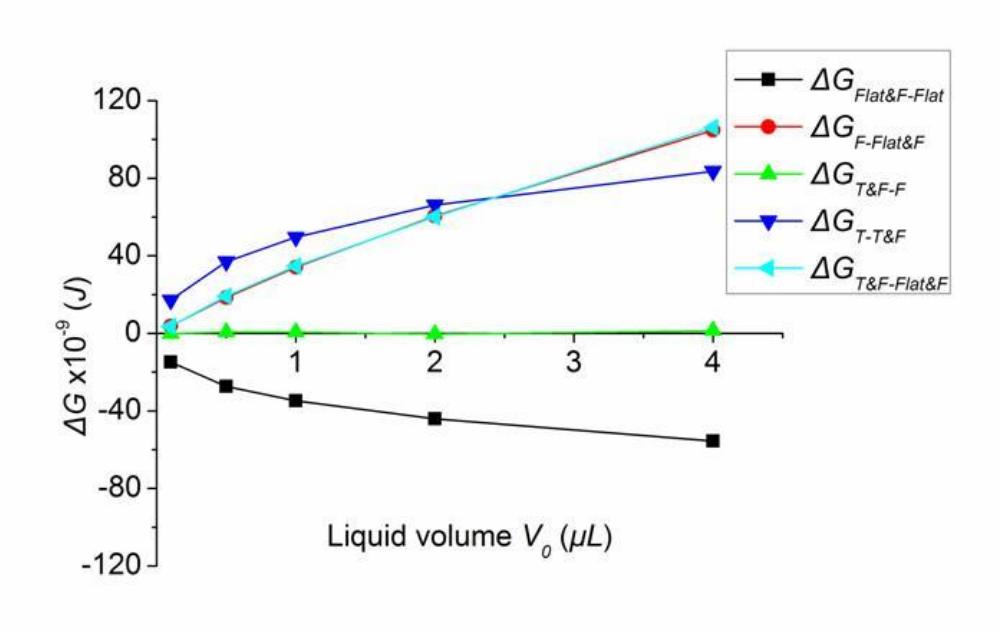

(a)

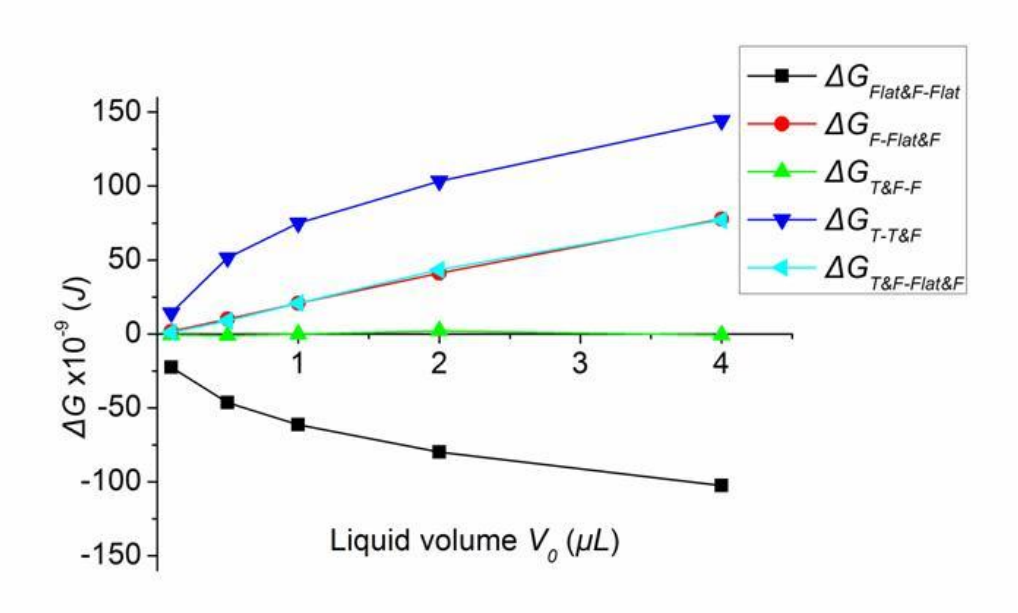

(b)

Figure 4.31. ΔG of EG on a Teflon® flat surface and a glass fiber (θ_{fiber} = 0°, θ_{flat} = 85°): (a) r_f = 0.145mm, and (b) r_f = 0.271mm.

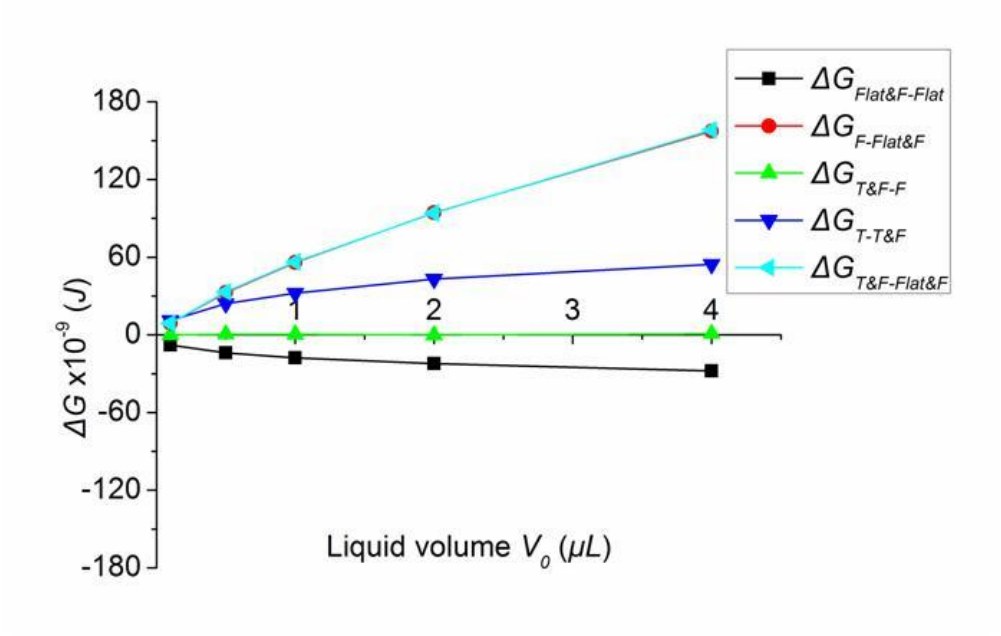

(a)

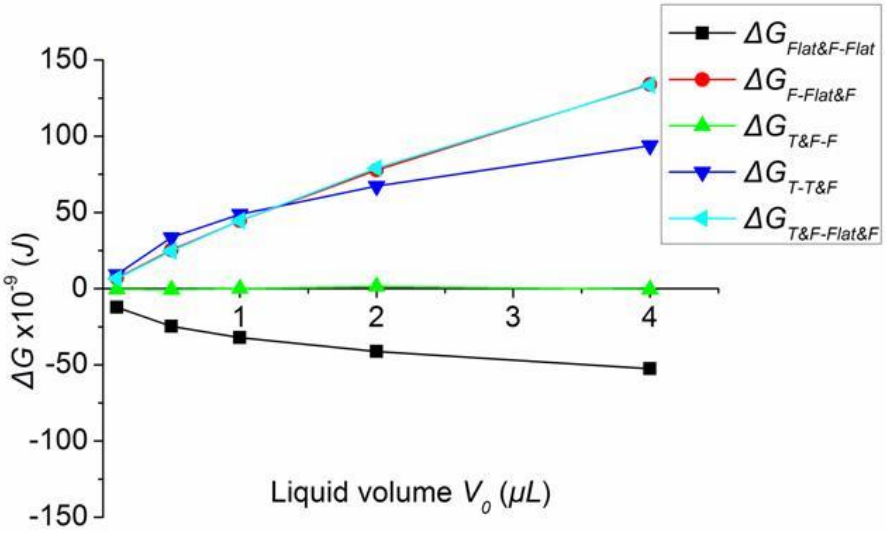

(b)

Figure 4.32. ΔG of Kaydol on a Teflon® flat surface and a glass fiber (θ_{fiber} = 0°, θ_{flat} = 56°): (a) r_f = 0.145mm, and (b) r_f = 0.271mm.

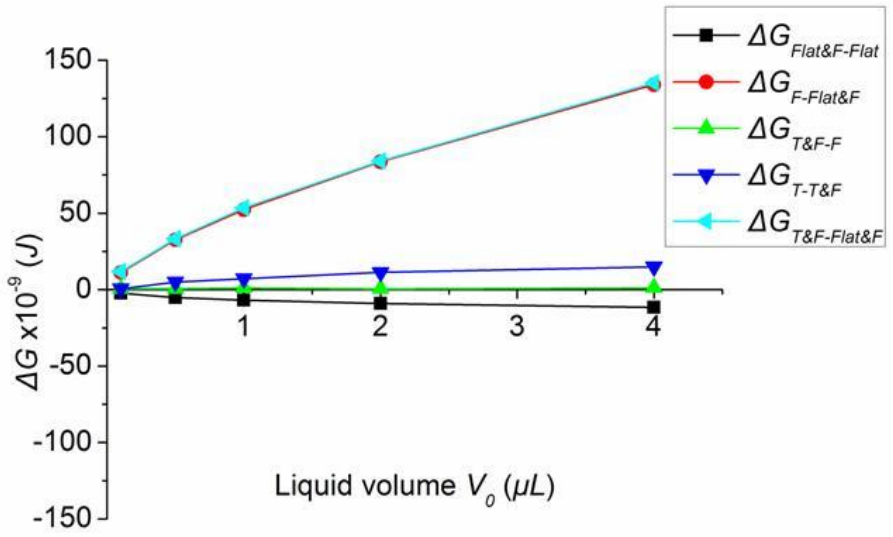

(a)

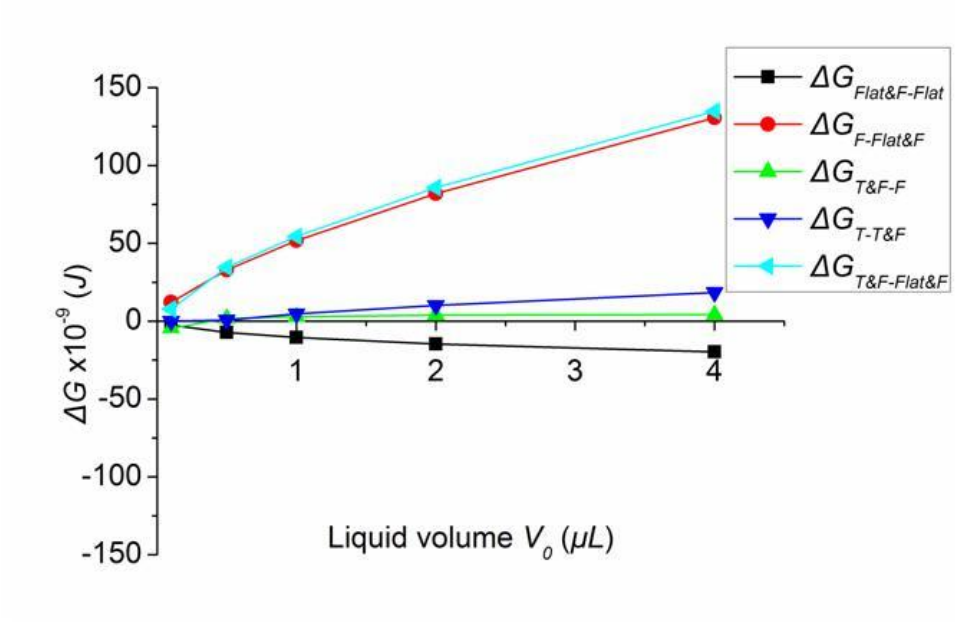

(b)

Figure 4.33. ΔG of EG on a Teflon® flat surface and a PP fiber (θ_{fiber} = 69°, θ_{flat} = 85°): (a) r_f = 0.1mm, and (b) r_f = 0.19mm.

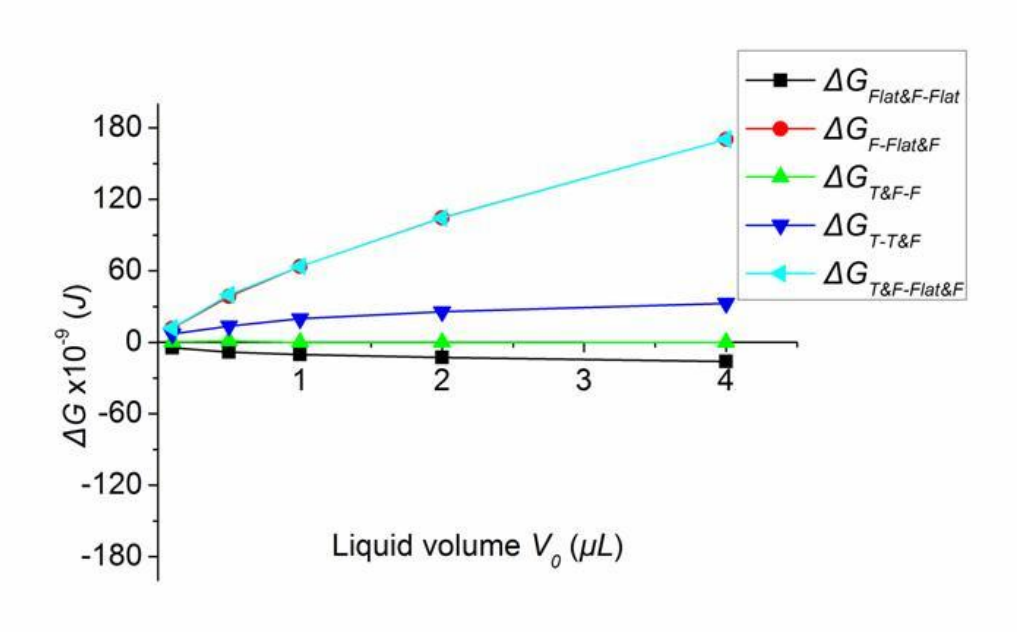

(a)

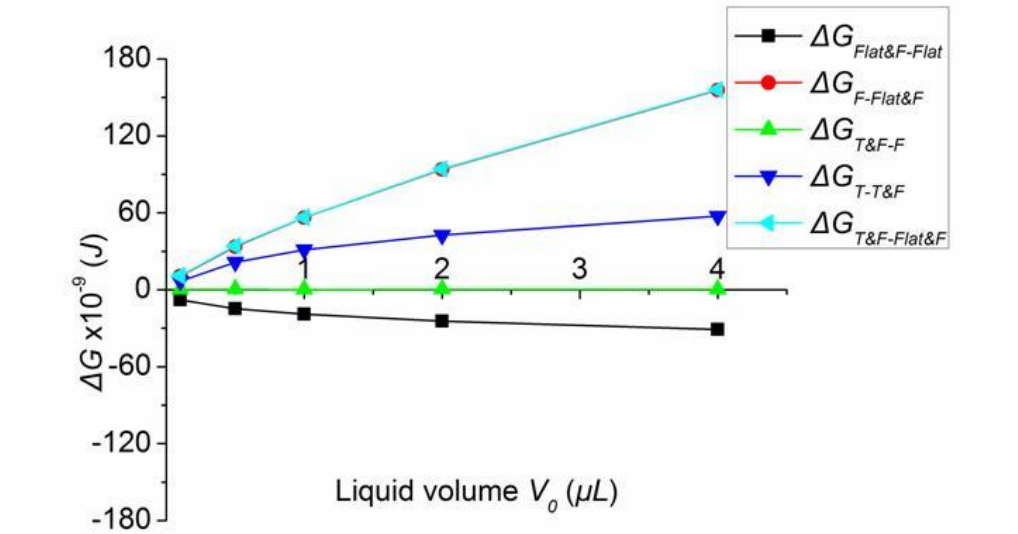

(b)

Figure 4.34. ΔG of Kaydol on a Teflon® flat surface and a PP fiber (θ_{fiber} = 29°, θ_{flat} = 56°): (a) r_f = 0.1mm, and (b) r_f = 0.19mm.

In figures (4.27 – 4.34) all the $\Delta G_{Flat\&F\text{-}Flat}$ are negative which suggests that liquid drop can move from the flat surface to the flat surface and fiber combined systems as long as the liquid touches the fibers. Liquid neither can transfer from the flat surface and fiber combined systems to fiber bodies ($\Delta G_{F\text{-}Flat\&F} > 0$), nor from the tip and the body of fiber to the fiber tip ($\Delta G_{T\text{-}T\&F} > 0$), nor from the flat surface and fiber combined systems to the tip and the body of fiber ($\Delta G_{T\&F\text{-}Flat\&F} > 0$). Except water on nylon fiber in Figure 4.27, a liquid would not move from the fiber body to the tip and body since $\Delta G_{T\&F\text{-}F}$ is very small and there is no free energy difference between these two statuses. The exception may be caused by the high water contact angle on nylon fiber (72^0), because the interfacial surface areas of solid-liquid and liquid-vapor were obtained based on Carroll's equation[6] which requires small contact angles ($\theta_{fiber} < 60^0$) or large volume.

Since it has lowest free energy when the drop is deposited on the flat surface and fiber combined system, it can be predicted that a liquid droplet will stay on the bottom of the fiber standing on a flat surface (flat surface and fiber combined systems) as long as the droplet connects with the fiber. To verify this prediction, different fibers (nylon, glass and PP) were horizontally moved into 2.0 µL and 4.0 µL water, EG and Kaydol drops resting on the Teflon® flat film. The images of these experiments are shown in Figures (4.35 – 4.40). The images prove that for fibers having different surface energy and liquid having different surface tension and volume, the prediction had good agreement with the experimental results.

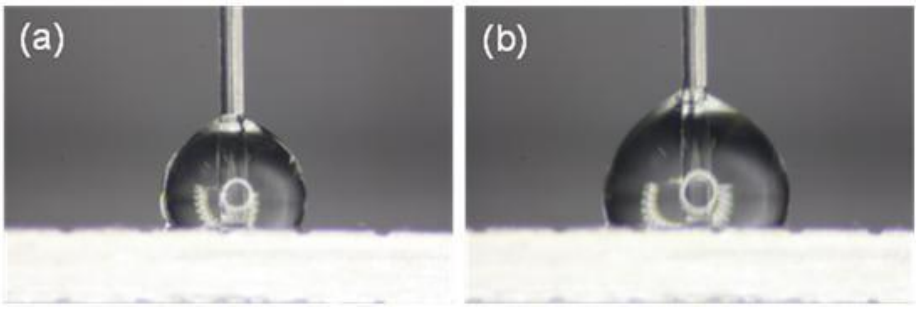

Figure 4.35. 2.0 µL and 4.0 µL water on a Teflon® flat surface and a nylon fiber (r_f = 0.143mm) after horizontally moving the nylon fiber into the droplet.

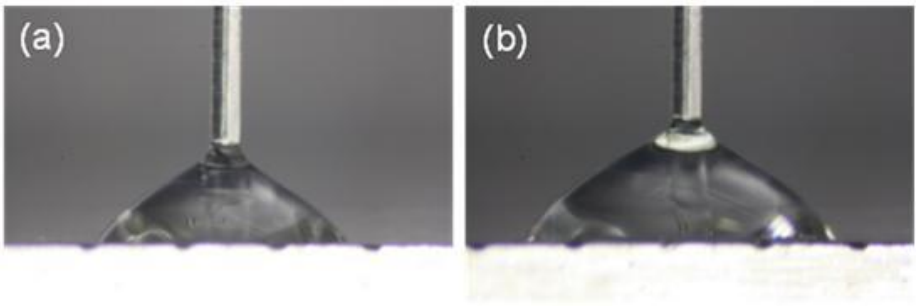

Figure 4.36. 2.0 µL and 4.0 µL Kaydol on a Teflon® flat surface and a nylon fiber (r_f = 0.143mm) after horizontally moving the nylon fiber into the droplet.

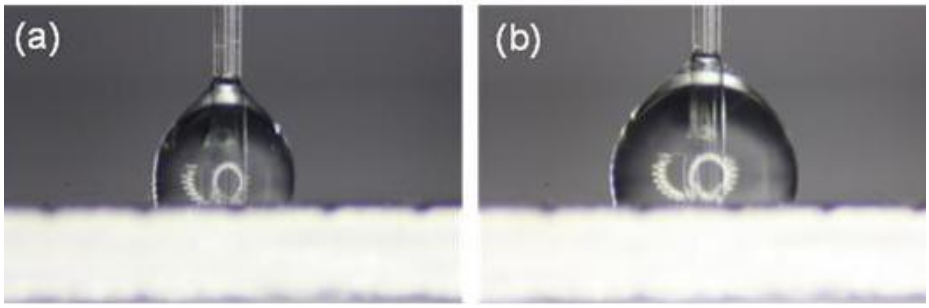

Figure 4.37. 2.0 µL and 4.0 µL water on a Teflon® flat surface and a glass fiber (r_f = 0.145mm) after horizontally moving the nylon fiber into the droplet.

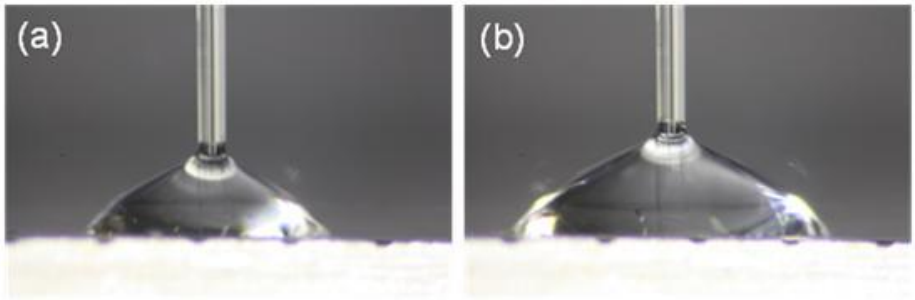

Figure 4.38. 2.0 µL and 4.0 µL Kaydol on a Teflon® flat surface and a glass fiber (r_f = 0.145mm) after horizontally moving the nylon fiber into the droplet.

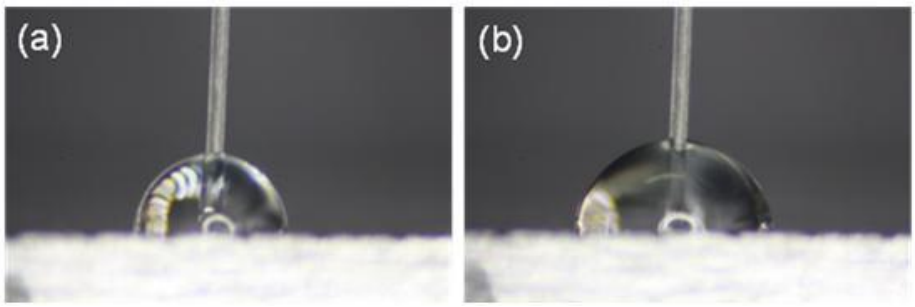

Figure 4.39. 2.0 µL and 4.0 µL EG on a Teflon® flat surface and a PP fiber (r_f = 0.1mm) after horizontally moving the nylon fiber into the droplet.

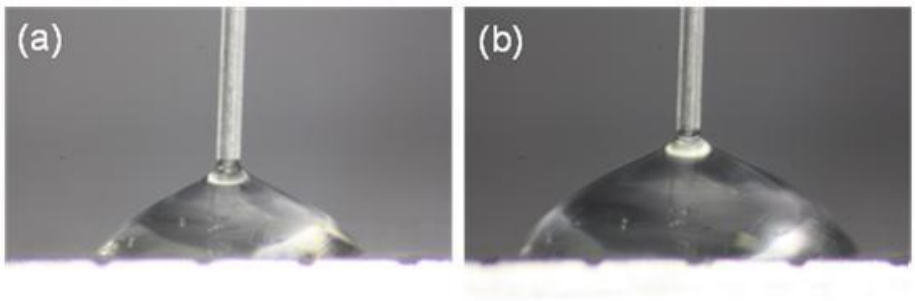

Figure 4.40. 2.0 µL and 4.0 µL Kaydol on a Teflon® flat surface and a PP fiber (r_f = 0.1mm) after horizontally moving the nylon fiber into the droplet.

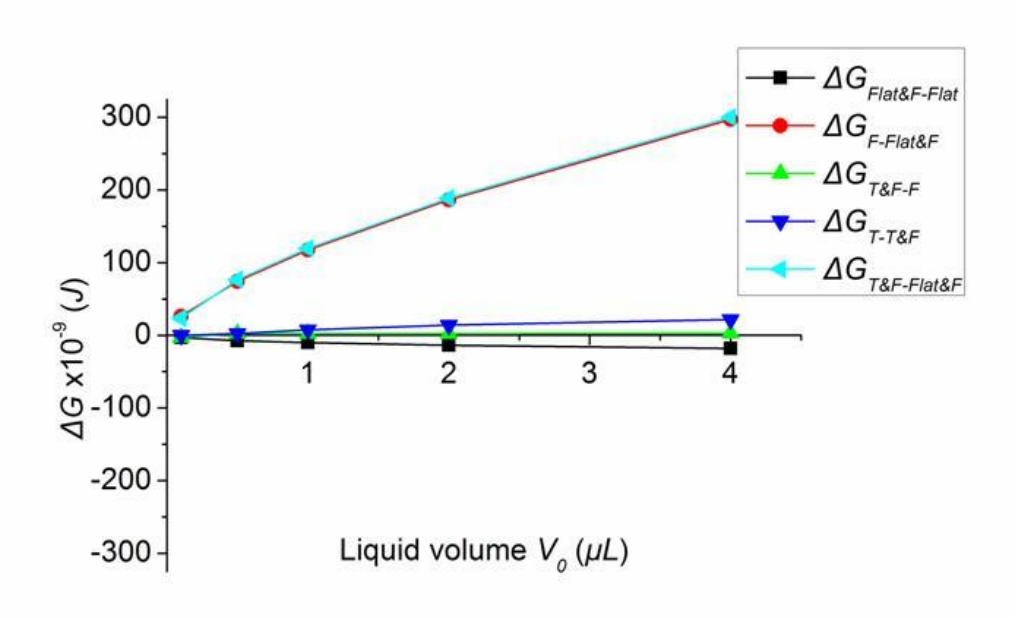

(a)

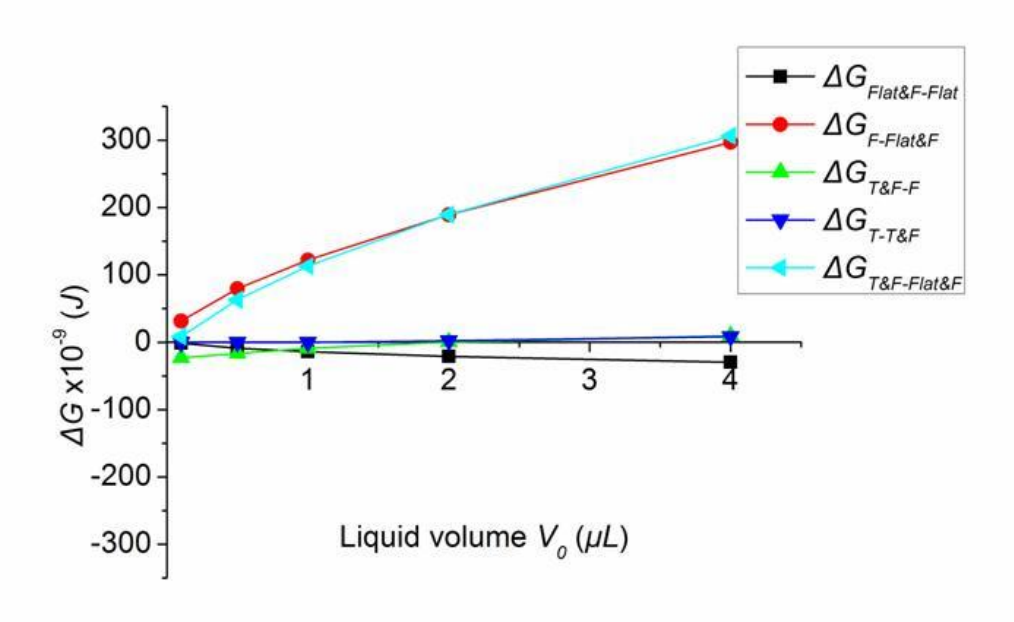

(b)

Figure 4.41. ΔG of water on a PET flat surface and a nylon fiber (θ_{fiber} = 72°, θ_{flat} = 72°): (a) r_f = 0.143mm, and (b) r_f = 0.288mm.

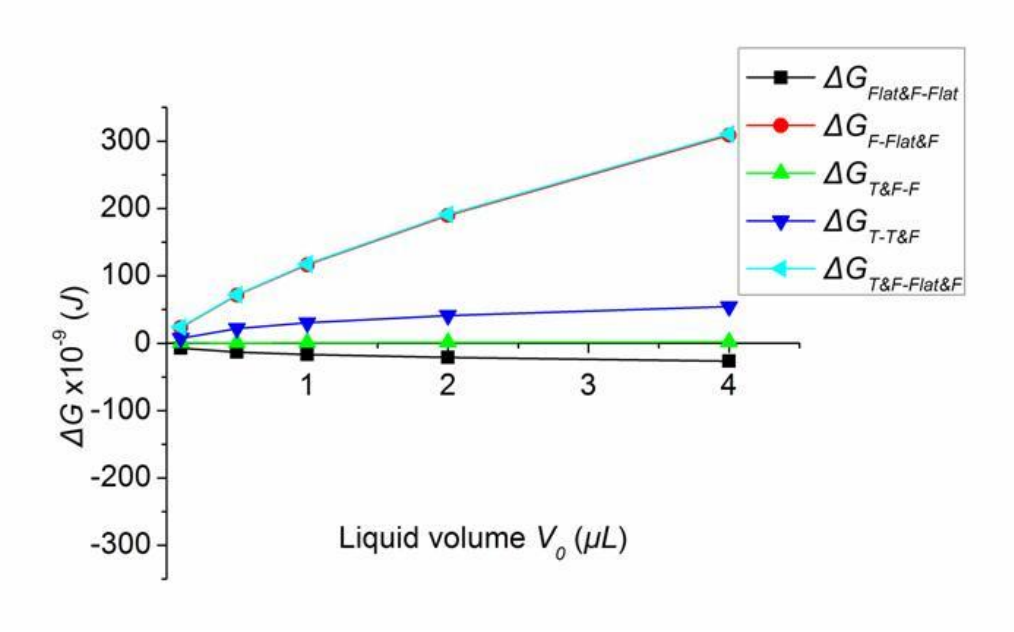

(a)

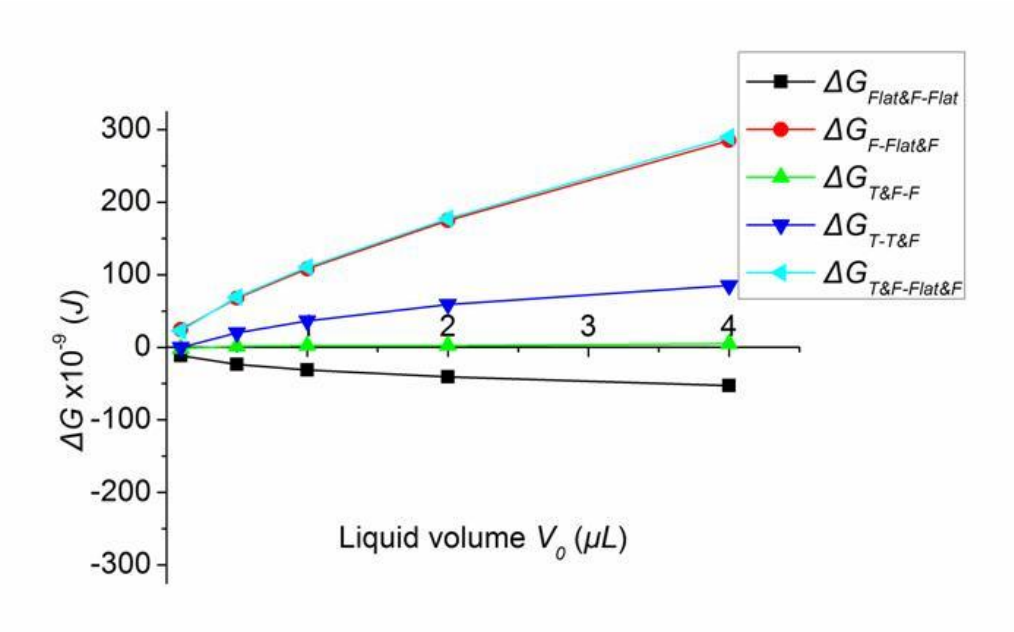

(b)

Figure 4.42. ΔG of EG on a PET flat surface and a nylon fiber (θ_{fiber} = 42°, θ_{flat} = 47°): (a) r_f = 0.143mm, and (b) r_f = 0.288mm.

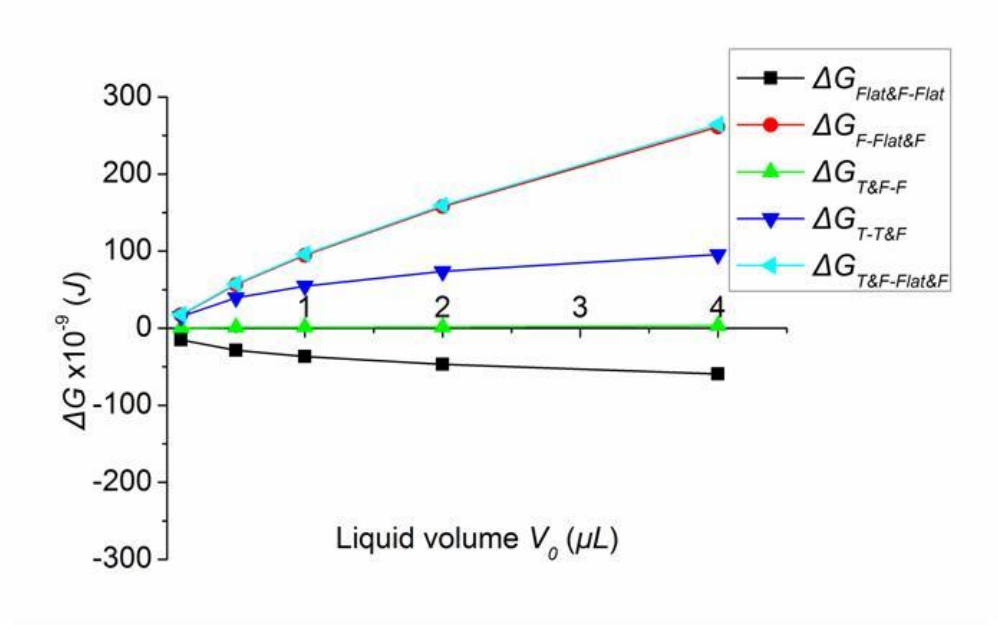

(a)

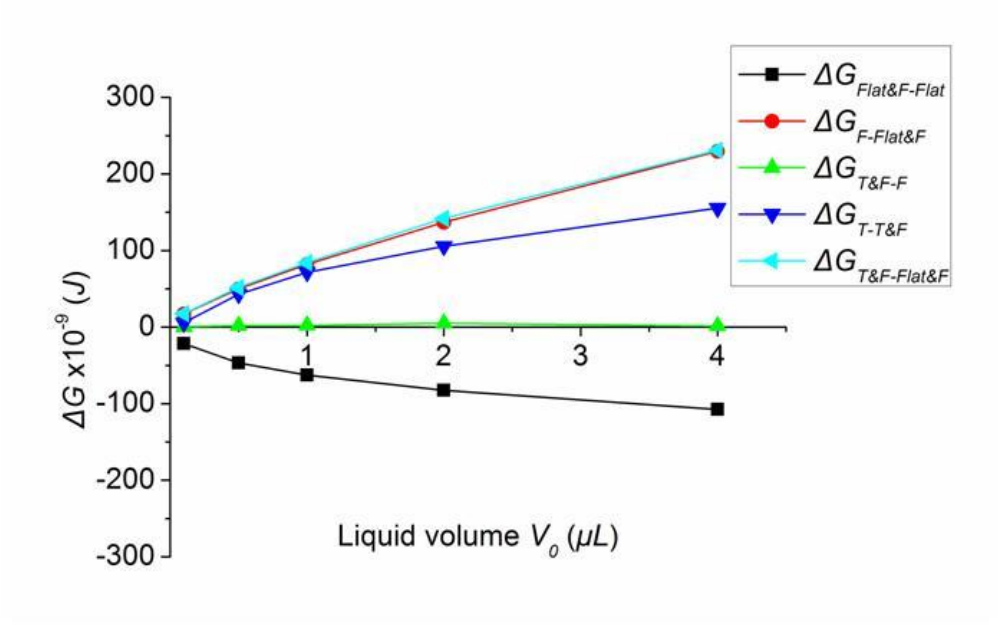

(b)

Figure 4.43. ΔG of water on a PET flat surface and a glass fiber (θ_{fiber} = 35°, θ_{flat} = 72°): (a) r_f = 0.145mm, and (b) r_f = 0.271mm.

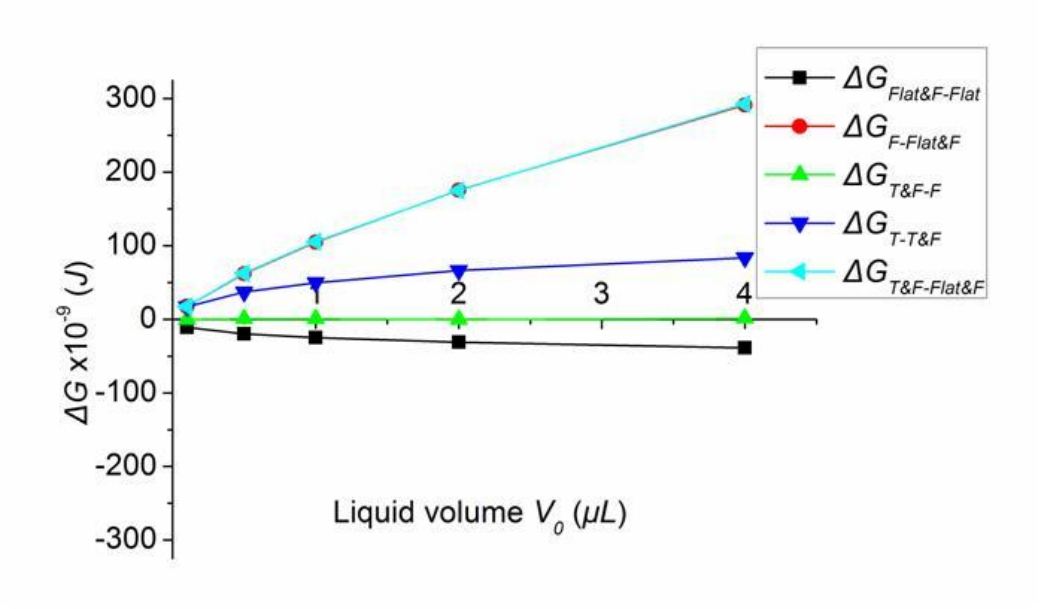

(a)

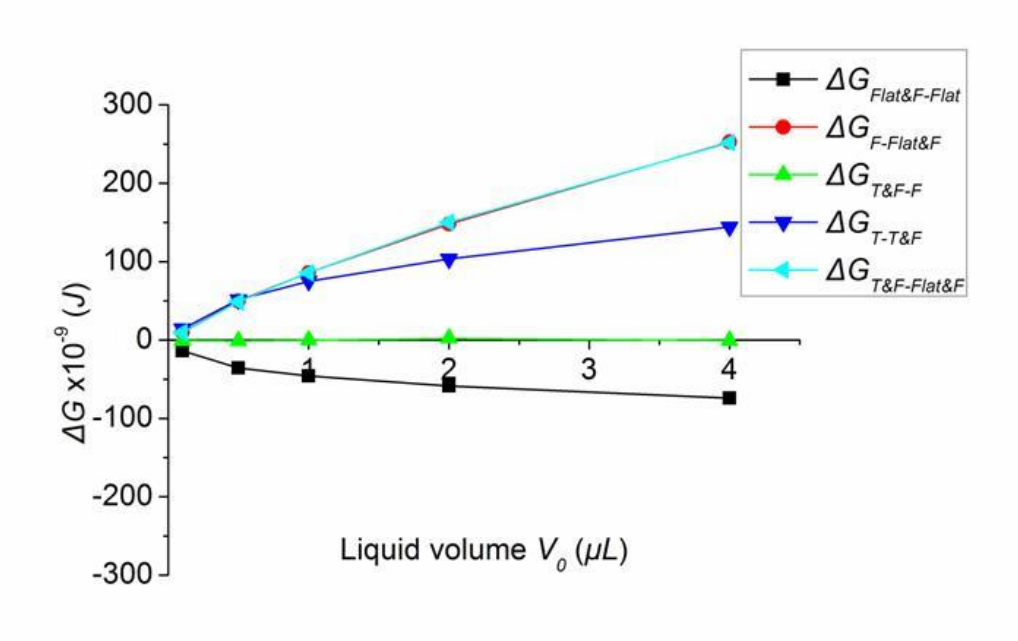

(b)

Figure 4.44. ΔG of EG on a PET flat s surface and a glass fiber (θ_{fiber} = 0°, θ_{flat} = 47°): (a) r_f = 0.145mm, and (b) r_f = 0.271mm.

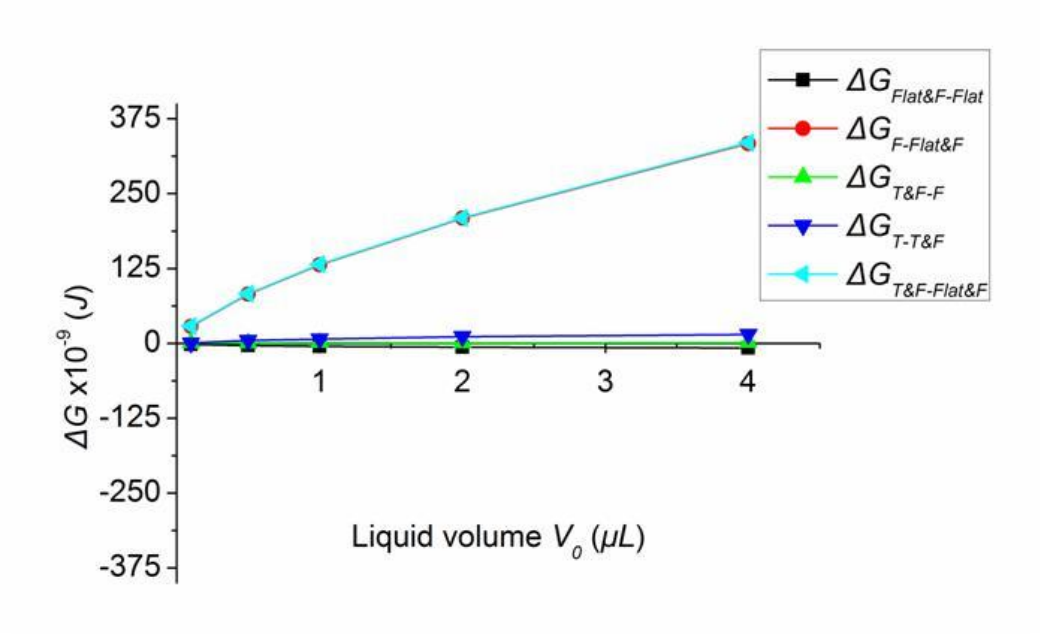

(a)

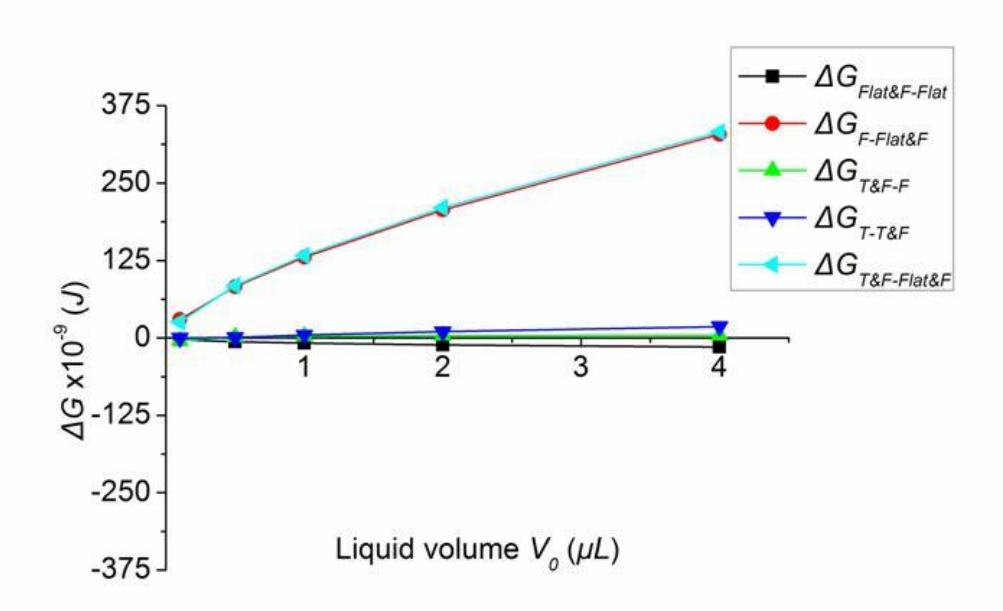

(b)

Figure 4.45. ΔG of EG on a PET flat surface and a PP fiber (θ_{fiber} = 69°, θ_{flat} = 47°): (a) r_f = 0.1mm, and (b) r_f = 0.19mm.

To study the influence of flat surfaces on the ability of the liquid to transfer, high surface energy flat polyester (PET) film were used. Figures (4.41 – 4.45) and the tables provided in Appendices 18 – 22 present the changes of free energy of water and EG on nylon, glass and PP fibers and PET film.

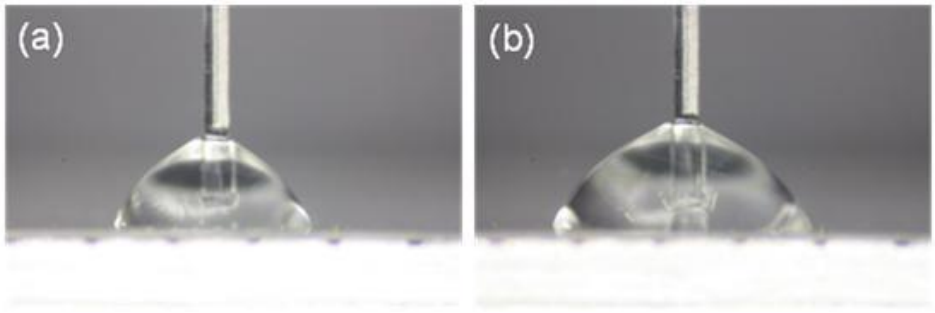

Figure 4.46. Water on both PET flat surface and nylon fiber (r_f = 0.143mm) after horizontally moving the nylon fiber into the droplet: (a) 2.0 µL, and (b) 4.0 µL.

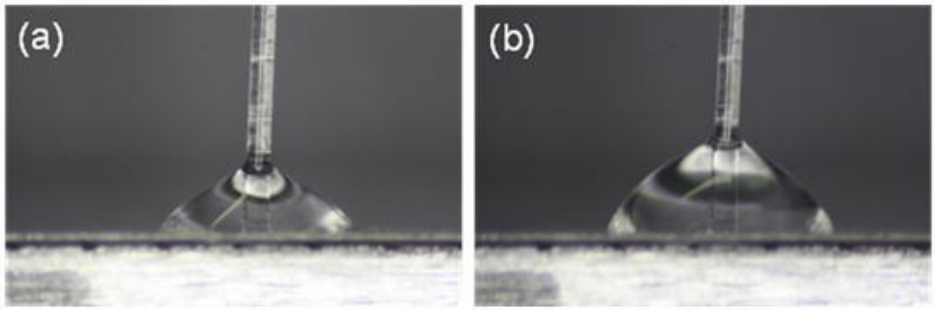

Figure 4.47. EG on both PET flat surface and nylon fiber (r_f = 0.143mm) after horizontally moving the nylon fiber into the droplet: (a) 2.0 µL, and (b) 4.0 µL.

The figures of water and EG on glass, nylon and PP fibers on PET flat surface show the same

result as the liquid on Teflon® flat surface: $\Delta G_{Flat\&F\text{-}Flat} < 0$, $\Delta G_{F\text{-}Flat\&F} > 0$, $\Delta G_{T\&F\text{-}Flat\&F} > 0$, $\Delta G_{T\text{-}T\&F} \geq 0$, and $\Delta G_{T\&F\text{-}F} \approx 0$. It can be predicted that liquid will stay on the flat surface and fiber combined systems if the liquid can touch the fibers resting on PET flat surface. The prediction works well with our experimental observations shown in the images (Figure 4.46 – Figure 4.50).

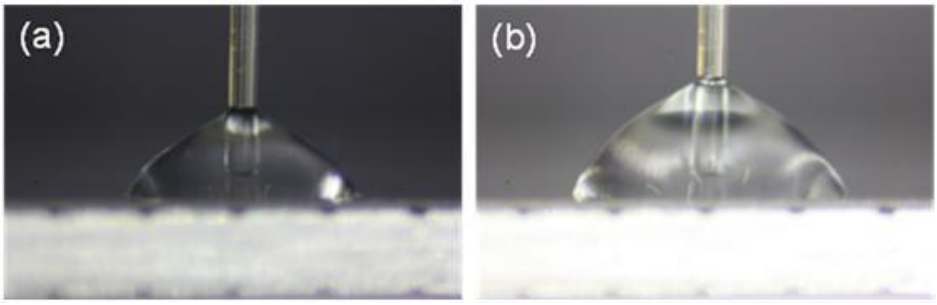

Figure 4.48. Water on both PET flat surface and glass fiber (r_f = 0.145mm) after horizontally moving the nylon fiber into the droplet: (a) 2.0 µL, and (b) 4.0 µL.

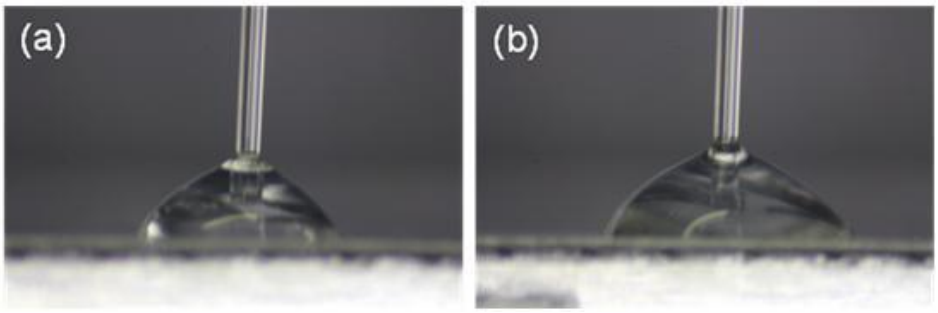

Figure 4.49. EG on both PET flat surface and glass fiber (r_f = 0.145mm) after horizontally moving the nylon fiber into the droplet: (a) 2.0 µL, and (b) 4.0 µL.

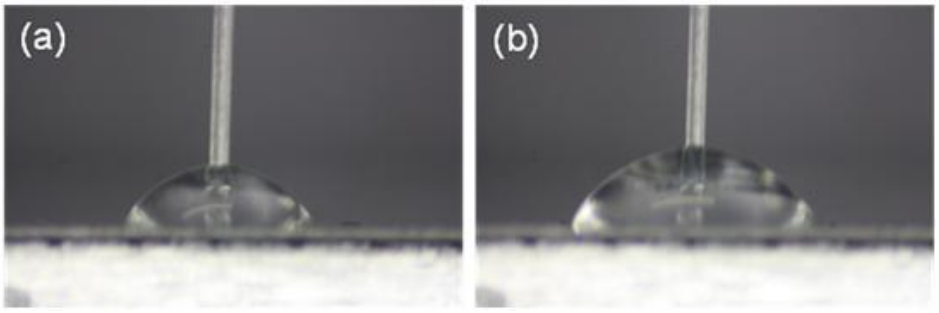

Figure 4.50. EG on both PET flat surface and PP fiber (r_f = 0.15mm) after horizontally moving the PP fiber into the droplet: (a) 2.0 µL, and (b) 4.0 µL.

It is possible for a droplet to move to a new location if the driving force caused by Laplace pressure difference can overcome the resistive force; however, whether the motion occurs spontaneously or not depends on the change in free energy. The calculated change of free energies of a liquid drop on a fiber resting on a flat surface indicated that the drop has the lowest free energy on the flat surface and fiber combined system.

Different liquids have different abilities to transfer from one surface to another. Based on the changes in free energy and liquid Laplace pressures, and observation in our experimental, it was found that the calculations agree well with experimental observations for liquids with low surface tensions, i.e. for which the liquid has a contact angle with fiber that is less than 60º. At higher contact angles, the agreement is not as good and may be due to inaccuracies in Carroll's equations[6], which require small contact angles or large volume to obtain accurate results. Since the average water contact angle on nylon is 72º, in Figure 4.27, positive $\Delta G_{Flat\&F\text{-}Flat}$ was obtained for water having very small volume on a Teflon® flat surface and a

nylon fiber. However, based on other data in the figures, Carroll's equations still are approximately correct in this range.

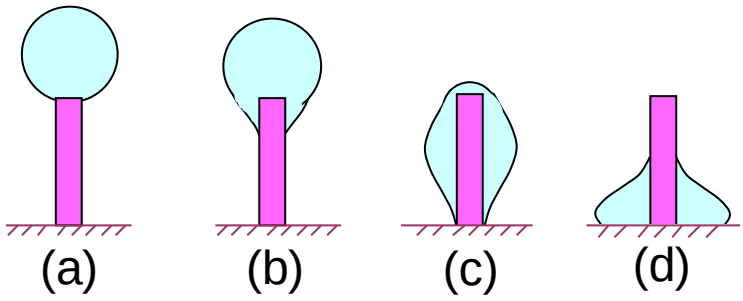

Figure 4.51. Schematics of a drop on a fiber with increasing the drop volume: (a) on the tip, (b) on the tip and the body of fiber, (c) on both tip and fiber and touching flat surface, and (d) on the flat surface and fiber combined system.

The changes in free energy of drop at different locations suggest that it has lowest free energy when liquid is on the flat surface and fiber combined system. It can be predicted that liquid will stay at this location if the liquid drop touches the fibers, which was observed in our experiments. Even though the changes in free energy were calculated to predict the motion and final location of drops from a flat surface to a fiber standing on the flat surface, the changes in free energy also can be used to predict what will happen if the drop is dropped on the fiber tip or on the body of fiber. The data in Figures (4.27 – 4.34) and Figures (4.41 – 4.45) suggest that liquid of small volume will stay on the tip of fiber shown in Figure 4.51.a; liquid of large volume will be on the tip and the body of fiber shown in Figure 4.51.b; if the drop, on fiber body or on the tip and the body of fiber (Figure 4.51.c), touches the flat surface

it will go to the bottom of the fiber (the flat surface and fiber combined system) shown in Figure 4.51.d.

It should be mentioned that the motion of liquid drop on a fiber standing on a flat surface only can happen when the drop can access the new location. For example, a drop cannot move along a fiber body when it is on the middle of the fiber as shown in Figure 4.52.a due to the constant Laplace pressure and constant system free energy; if the drop connected with the flat surface it can move to the flat surface and fiber combined system as shown in Figure 4.52.b and Figure 4.52.c because of the existence of the free energy difference between the two locations.

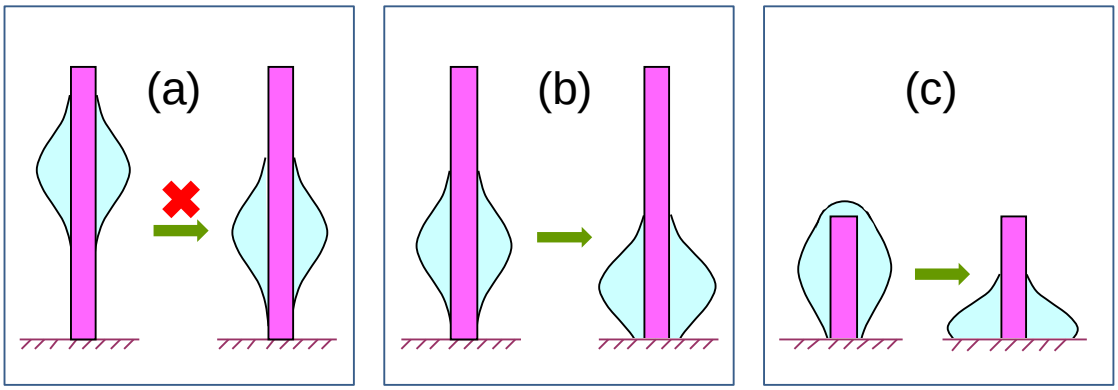

Figure 4.52. Schematics of a drop motion: (a) on the middle of the fiber, (b) and (c) on the fiber and connected with the flat surface.

To predict the final location of a drop on a solid surface it is assumed that the drop is at ideal status at which it keeps ideal shape and it has access to the closed location. Through the

calculation not only the changes in free energy but also the length of drop (L) can be provided.

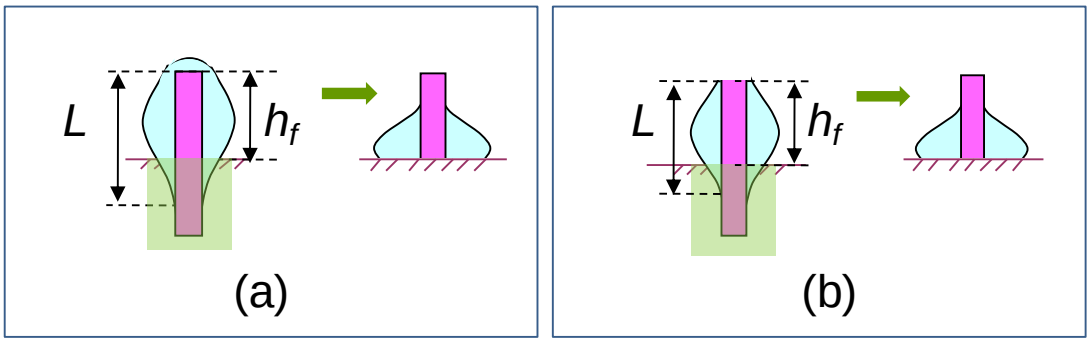

Figure 4.53. Schematics of a drop when the ideal length of a drop (L) is longer than the fiber height (h_f): (a) a drop is on the tip and the body of fiber, and (b) a drop is on the fiber.

If the length (L) of drop on the tip and the body of fiber is longer than the fiber height (h_f), the drop will move to the flat surface and fiber combined system as shown in Figure 4.53.a. When the length of drop on the fiber body is longer than the fiber height ($L > h_f$), the drop also goes to the flat surface and fiber combined system as shown in Figure 4.53.b. To keep a drop away from the flat surface after it is applied on the tip or body of a fiber, the fiber height (h_f) should longer than the critical fiber height (h_C) which is equal to the drop length (L). Table 4.3 and 4.4 listed the critical fiber height for EG and Kaydol drops on nylon and PP fiber when the drops are simultaneously on the tip and the body of fiber ($h_{C\text{-}T\&F}$), on fiber body ($h_{C\text{-}F}$), and on the flat surface and fiber combined system ($h_{C\text{-}Flat\&F}$).

Table 4.3. h_C for EG and Kaydol drops on a Teflon® flat surface and a nylon fiber.

Fiber radius r_f	Liquid volume V_0	EG			Kaydol		
(mm)	(μL)	$h_{C\text{-}T\&F}$	$h_{C\text{-}Flat\&F}$	$h_{C\text{-}F}$	$h_{C\text{-}T\&F}$	$h_{C\text{-}Flat\&F}$	$h_{C\text{-}F}$
0.143	0.1	0.71	0.44	0.72	0.96	0.43	0.98
0.143	0.5	1.26	0.76	1.26	1.51	0.69	1.54
0.143	1.0	1.57	0.94	1.58	1.84	0.83	1.86
0.143	2.0	1.96	1.16	1.96	2.22	1.01	2.24
0.143	4.0	2.42	1.44	2.43	2.69	1.22	2.70
0.19	0.1	0.61	0.43	0.68	0.98	0.43	0.99
0.19	0.5	1.25	0.76	1.26	1.61	0.71	1.62
0.19	1.0	1.58	0.96	1.59	1.95	0.87	1.96
0.19	2.0	1.99	1.19	2.00	2.33	1.06	2.36
0.19	4.0	2.47	1.47	2.48	2.84	1.28	2.85
0.229	0.1	0.57	0.41	0.65	0.95	0.43	0.98
0.229	0.5	1.22	0.76	1.24	1.63	0.73	1.67
0.229	1.0	1.58	0.96	1.59	1.99	0.89	2.03
0.229	2.0	2.00	1.20	2.01	2.42	1.09	2.45
0.229	4.0	2.50	1.49	2.51	2.94	1.32	2.95
0.288	0.1	0.00	0.39	0.60	0.90	0.42	0.94
0.288	0.5	1.18	0.75	1.19	1.66	0.74	1.70
0.288	1.0	1.54	0.96	1.56	2.06	0.92	2.10
0.288	2.0	1.98	1.21	2.00	2.51	1.13	2.55
0.288	4.0	2.53	1.52	2.53	3.04	1.37	3.09

Note: $\theta_{fiber\text{-}EG} = 42°$, $\theta_{fiber\text{-}Kaydol} = 17°$, $\theta_{flat\text{-}EG} = 85°$, $\theta_{flat\text{-}EG} = 56°$

Table 4.4. h_C for EG and Kaydol drops on a Teflon® flat surface and a PP fiber.

Fiber radius r_f	Liquid volume V_0	EG			Kaydol		
(mm)	(μL)	$h_{C\text{-}T\&F}$	$h_{C\text{-}Flat\&F}$	$h_{C\text{-}F}$	$h_{C\text{-}T\&F}$	$h_{C\text{-}Flat\&F}$	$h_{C\text{-}F}$
0.1	0.1	0.56	0.36	0.59	0.83	0.38	0.83
0.1	0.5	1.02	0.64	1.05	1.34	0.61	1.35
0.1	1.0	1.33	0.80	1.33	1.63	0.74	1.65
0.1	2.0	1.67	1.01	1.68	2.01	0.91	2.01
0.1	4.0	2.10	1.27	2.11	2.44	1.11	2.46
0.15	0.1	0.00	0.34	0.54	0.83	0.39	0.83
0.15	0.5	0.93	0.63	1.02	1.41	0.64	1.41
0.15	1.0	1.30	0.80	1.31	1.72	0.79	1.73
0.15	2.0	1.67	1.01	1.67	2.10	0.96	2.12
0.15	4.0	2.11	1.27	2.11	2.57	1.17	2.59
0.19	0.1	0.00	0.33	0.51	0.80	0.38	0.81
0.19	0.5	0.04	0.62	0.98	1.41	0.65	1.43
0.19	1.0	1.18	0.79	1.28	1.75	0.81	1.78
0.19	2.0	1.64	1.01	1.65	2.17	0.99	2.19
0.19	4.0	2.10	1.27	2.10	2.64	1.21	2.67

Note: $\theta_{fiber\text{-}EG} = 69°$, $\theta_{fiber\text{-}Kaydol} = 29°$, $\theta_{flat\text{-}EG} = 85°$, $\theta_{flat\text{-}EG} = 56°$

It is found that for fiber having same size and made from the same material, it needs longer fiber to keep low surface tension drop away from the flat surface; the longer fiber is also necessary to prevent a large drop wetting the flat surface; and low surface energy fiber works better on blocking a drop moves from the tip or body to the flat surface as shown in Figures (4.54 – 4.56).

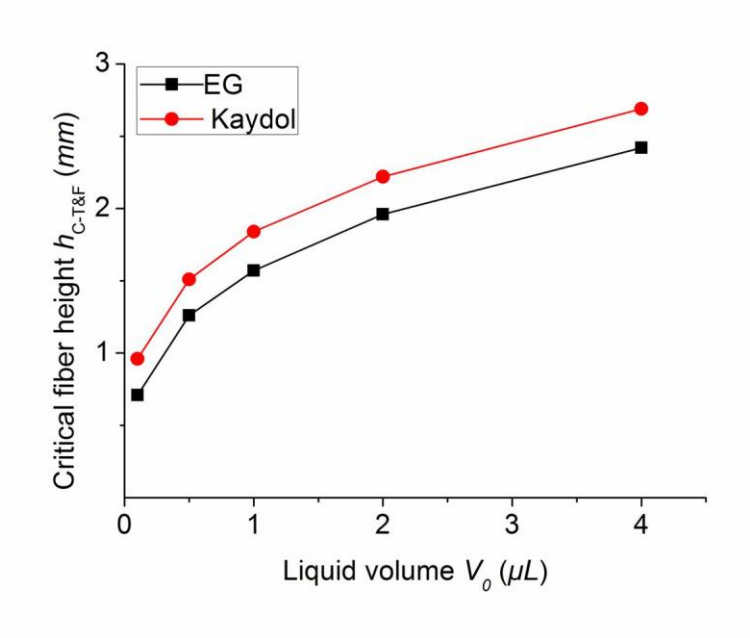

(a)

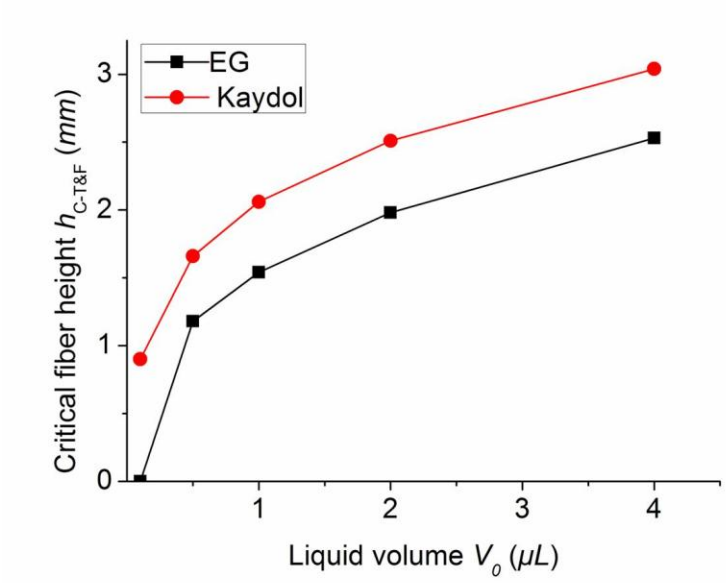

(b)

Figure 4.54. The critical fiber height ($h_{C\text{-}T\&F}$) of different liquid on nylon fiber: (a) r_f = 0.143mm, and (b) r_f = 0.288mm.

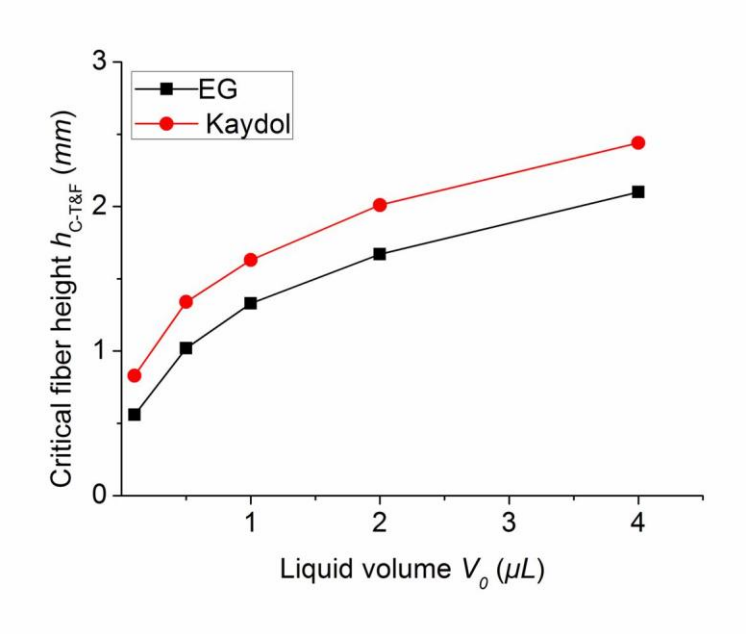

(a)

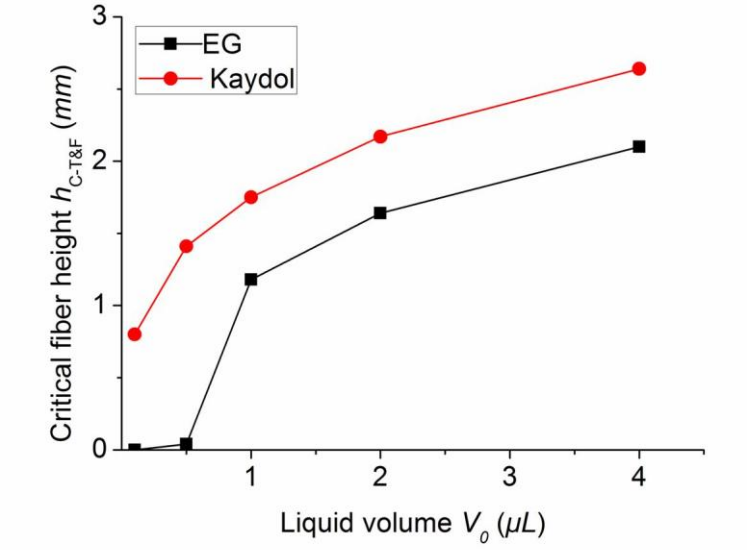

(b)

Figure 4.55. The critical fiber height ($h_{C\text{-}T\&F}$) of different liquid on PP fiber: (a) r_f = 0.1mm, and (b) r_f = 0.19mm.

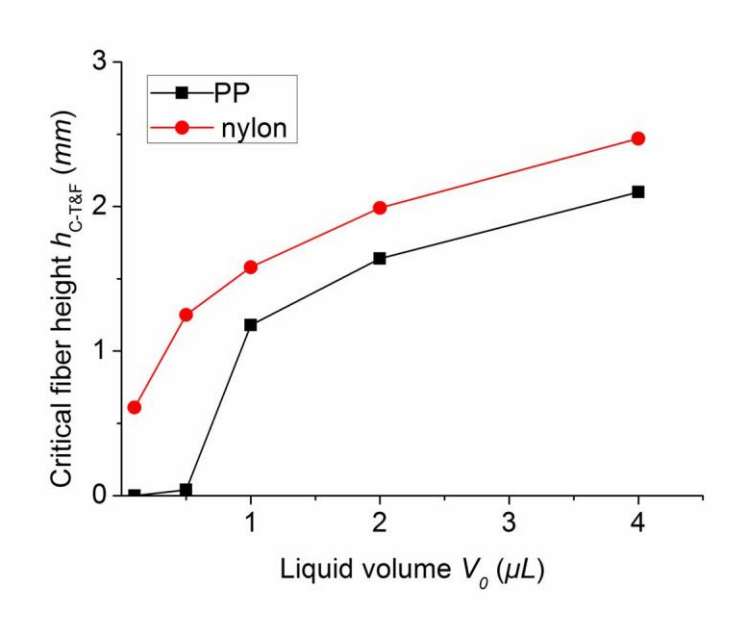

(a)

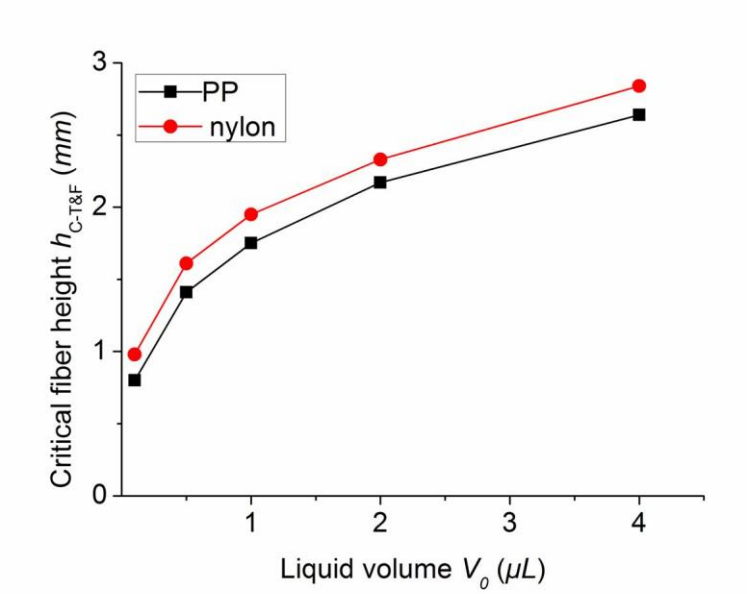

(b)

Figure 4.56. The critical fiber height ($h_{C\text{-}T\&F}$) of liquid on different fiber (r_f = 0.19mm): (a) EG and (b) Kaydol.

The assumption and equations developed in this chapter can be used to calculate the length of a drop and its free energy at different locations. A drop has lowest free energy on a flat surface and fiber combined system. However, a drop cannot move to the combined system from the fiber tip if the fiber height is longer than the drop length on the fiber. Based on this information it is possible to prevent big size oil wetting flat surface with proper design of fiber shape and spacing as shown in Figure 4.57.

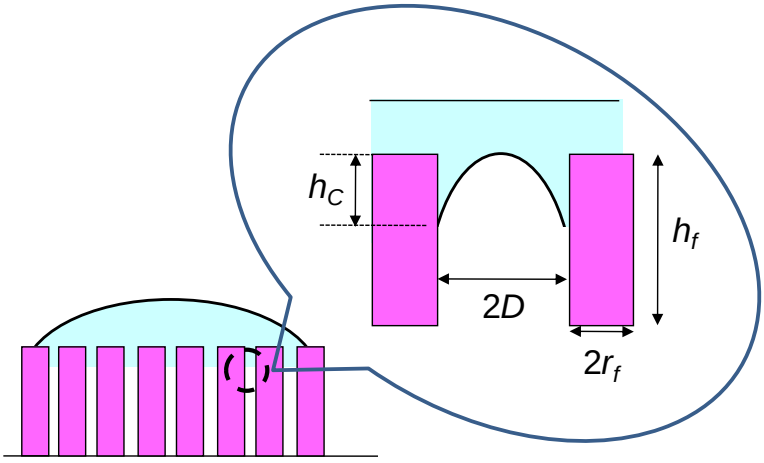

Figure 4.57. Schematics of a large drop on the top of fibers standing on a flat surface.

Most oil repellent materials reported recently can only prevent large size oil droplets from wetting them. These materials can do nothing with small size oil droplets. It is necessary for superoleophobic or oil self-cleaning materials to keep oil on top of the materials from which they can easily roll off. However, it would be even better if the material can lift small oil droplets from its base to the top.

In our work we found that if low surface tension liquid on flat surface comes into contact with a fiber on the flat surface, the liquid should move to locate on both flat surface and fiber. However, the liquid should not climb onto the fiber body or its tip. It was found that for water on glass fibers, no matter what the size of the droplet, the droplet would locate on both the Teflon® flat surface and the glass fiber instead of climbing onto the glass fiber (Figure 4.4). For liquid with different surface tensions such as water, EG and Kaydol, all the droplets with the same volume did not climb onto a glass fiber from a Teflon® flat surface (Figure 4.5). Therefore, it appears that cylindrical fibers are unable to lift small droplets from the bottom of a fiber resting on a flat surface onto the fiber body or tip. As a consequence, other fiber geometries should be considered.

Chapter 5 Liquid Moving on Conical Fibers

We found that liquid does not spontaneously move along a cylindrical fiber due to the lack of a driving force when the fiber radius is constant; the Laplace pressure is same at every point of the droplet. As mentioned in Chapter 2, a drop can travel along fiber which has a variation in radius. According to Equation (2.31), the Laplace pressure increases if the radius of cylinder decreases. Therefore, a Laplace pressure difference should exist for a liquid on a conical fiber where the radius increases from the tip to base as shown in Figure 2.13. The Laplace pressure of a drop on the small radius section of the cone is larger than on the large radius section, which suggests that the drop may move along the cone axis in the direction of increasing radius, if gravity can be ignored.

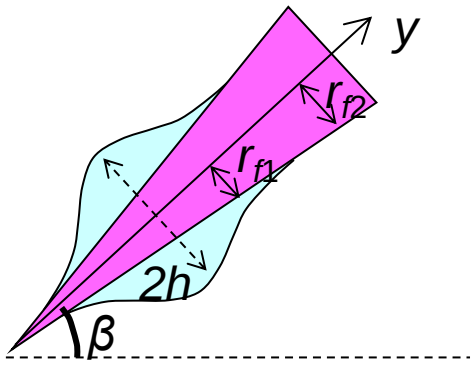

Figure 2.13. Schematic of a liquid drop on a titled conical fiber. Radius of the cone increases from the tip to base of the cone (marked as *y* direction), and the cone is tilted at an angle β with horizon direction.

5.1. Factors influencing the Laplace pressure change

For an undulating drop on a conical fiber the change in the Laplace pressure along the conical fiber $d\Delta P/dy$ can be reformulated as Equation (2.37).

$$\left.\frac{d\Delta P}{dy}\right|_{V_0} = -\frac{2\gamma_{LV}}{\left(r_f + R_0\right)^2}\left.\frac{dr_f}{dy}\right|_{V_0} = -\left.\frac{2\gamma_{LV}\tan\alpha}{\left(r_f + R_0\right)^2}\right|_{V_0} \tag{2.37}$$

For a very thin, flat, uniform film on the fiber, the change in the Laplace pressure along the conical fiber length $d\Delta P / dy$ can be rewritten as Equation (2.38).

$$\left.\frac{d\Delta P}{dy}\right|_{V_0} = -\left.\frac{\gamma_{LV}\tan\alpha}{r_f^2}\right|_{V_0} \tag{2.38}$$

5.2. Motion of droplet on conical fiber

It is easy to see that the values of the conical fiber gradient $\tan\alpha$, the local cone radius r_f, and the liquid surface tension γ_{LV} will influence the change of Laplace pressure along the conical fiber length. $d\Delta P / dy$ will increase with increasing $\tan\alpha$ and γ_{LV}, and it will also increase with decreasing fiber radius r_f for constant liquid volume as seen in Equations (2.37) and (2.38).

When a drop moves on a fiber, there are three forces acting on it: the driving force, F_{driv}, caused by the difference in Laplace pressure, the gravitational force, F_G, and the viscous force, F_η, where F_η, F_{driv}, and F_G were defined in Equations (2.41), (2.46) and (2.47). If $F_{driv} \geq F_G + F_\eta$, the driving force overcomes the resistance of gravitational force and viscous

force and the droplet will move along the fiber.

Based on Equation, (2.41), (2.46) and (2.47), the relationships in Equations (2.48) and (2.49) should be satisfied in order for a droplet to move.

$$\tan\ \alpha\ \geq\ (\rho g V_0 \sin\ \beta + \frac{3\pi\eta\ k r_f v}{\theta})\frac{(r_f + R_0)^2}{2\gamma_{LV} V_0} \tag{2.48}$$

$$v \leq \left[\frac{2\gamma_{LV}\ \tan\ \alpha}{(r_f + R_0)^2} - \rho g \sin\ \beta\right]\frac{\theta V_0}{3\pi\eta\ k r_f} \tag{2.49}$$

According to Equation (2.49) we predicted that the velocity of a drop is related to the liquid surface tension, the liquid volume, and the radius and gradient of the cone. With an increase in the gradient of the cone or the liquid volume, the velocity of the drop should increase. Likewise it should decrease if the radius of cone increases. We found that liquid did not move on cylindrical fibers (Figure 5.1) but it would move on conical ones in the direction of increasing radius as shown in Figure 5.2; the liquid moved faster on a large gradient cone than on a small one as shown in Figures 5.3 and 5.4; large volume liquid drops move more quickly and further than small volume ones as shown in Figures 5.5 and 5.6. What we observed agrees well with the predictions based on equation (2.49). However, more detail on the relationship between liquid motion and its influence factors should be obtained to provide critical information on liquid movement.

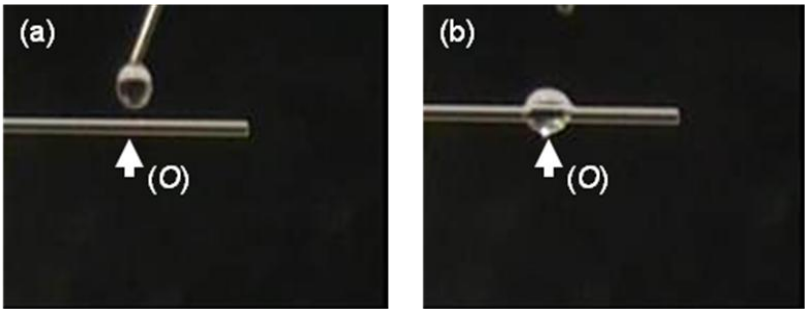

Figure 5.1. Motion of water on glass cylinder: (a) water loading on a glass cylinder at the location *O*, and (b) water on the cylinder at the location *O* after the loading.

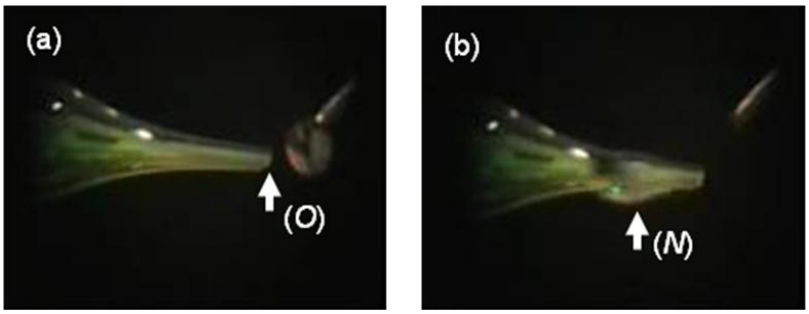

Figure 5.2. Motion of water on glass cone: (a) water loading on a glass cone at the location *O*, and (b) water on cone at the new location *N* after the loading.

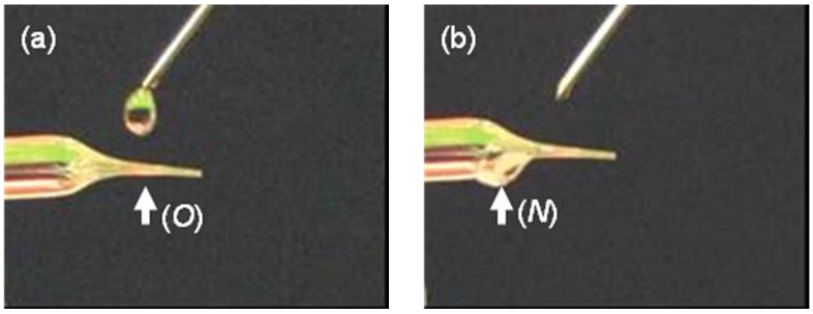

Figure 5.3. Motion of water on large gradient glass cone: (b) water loading on a glass cone at the location *O*, and (b) water on the cone at the new location *N* after the loading.

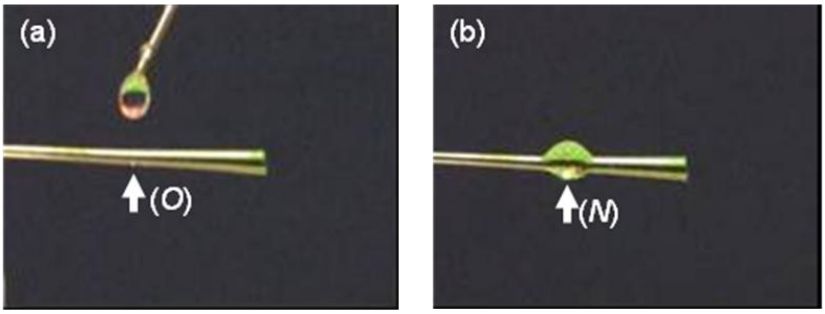

Figure 5.4. Motion of water on small gradient glass cone: (a) water loading on a glass cone at the location *O*, and (b) water on the cone at the new location *N* after the loading.

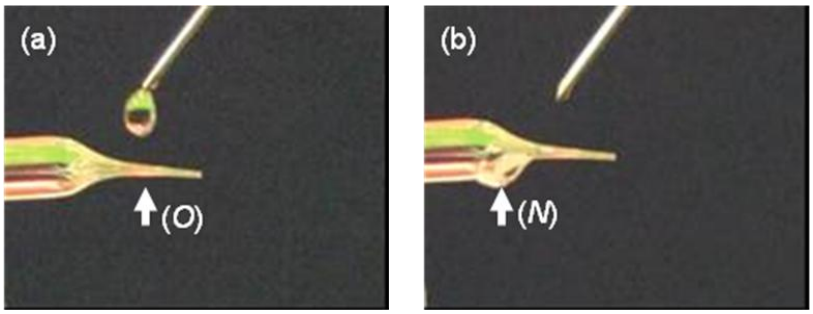

Figure 5.5. Motion of large volume water (2.0 μL) on glass cone: (a) water loading on a glass cone at the location *O*, and (b) water on the cone at the new location *N* after the loading.

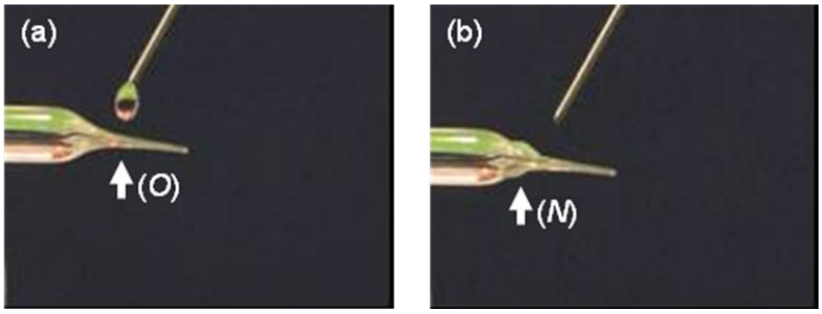

Figure 5.6. Motion of small volume water (1.0 μL) on glass cone: (a) water loading on a glass cone at the location *O*, and (b) water on the cone at the new location *N* after loading.

Chapter 6 Conclusions

Understanding the ability of a liquid to transfer from a flat surface to fibers can provide basic information enabling the design and preparation of superoleophobic or oil self-cleaning materials. Based on the literature review, we found that a Laplace pressure of a liquid determines the shape of a droplet on a solid surface. The Laplace pressure must be same throughout a static droplet; otherwise, the Laplace pressure difference will change the shape of droplet and even move it when the force caused by this pressure difference overcomes the resistive forces such as gravitational and viscosity forces. Laplace pressure differences make it possible for a droplet to transfer from one location to another. The final shape and location of droplets on different materials or different geometrical structures are determined by the system free energy. Thermodynamics requires that the system free energy of the new location be smaller than the former one, $\Delta G < 0$. Based on experimental observations and the prediction of the ability of a liquid to transfer, it was found that the theory can be used to predict and explain low surface tension liquid (oil) transfer and the final location of the liquid.

Some oil repellent materials created by academic or industrial laboratories can prevent large oil droplets from absorbing into them. In the study, it was found that the height of fiber standing on flat surface should be longer than the length of the drop on the tip and the body of fiber or that on fiber body to prevent the drop wetting the flat surface; longer fiber is needed to avoid low surface tension liquid or large volume drop falling to the flat surface;

low surface energy fiber works better than the higher one on keeping liquid on the fiber. For superoleophobic or oil self-cleaning materials, an oil droplet must stay on top of the materials and easily roll off from it. However, it would be preferred if the material can lift small oil droplets from its base to top. We found that if a low surface tension liquid on a flat surface touches a cylindrical fiber resting on the flat surface and normal to it, the drop should move such that it lies on both the flat surface and the fiber. However, the liquid does not climb the cylindrical fiber or transfer to its tip. If subsequently the fiber is raised, then the droplet may remain with the flat surface, transfer to the fiber tip, or transfer to the tip and the body of fiber. This motion can be reversed when one applies a droplet on the fiber tip and then touches it to the flat surface.

According to Carroll's derivation of the Laplace pressure of droplet on cylindrical fiber, there should be a gradient in the Laplace pressure for a droplet on a conical fiber due to gradient in the radius. Therefore, it should be possible for a droplet to move along a conical fiber in the direction of increasing radius when the force caused by the Laplace pressure overcomes the resistive force such as gravitational force and viscosity force. The theoretical equations derived from Carroll's equation and our laboratory observations proved that droplets do move along a conical fiber. However, the critical relationships between liquid motion and droplet size, surface tension, conical fiber geometry should be obtained to provide information on liquid transferring ability.

Chapter 7 Future Work

The calculation of changes in free energy predicted that the height of fiber standing on a flat surface should be longer than the drop length after dropping the drop on the tip or the body of fiber. Study about fiber shape and spacing on flat surface should be done to provide information on preventing big size oil wetting flat surface.

Our laboratory observations proved that droplets do move along a conical fiber. However, the critical relationships between liquid motion and droplet size, surface tension (liquid and fiber), conical fiber geometry (gradient of cone) still need to be determined. To provide these critical relationships we plan to determine:

(1) The relationship between liquid motion and droplet size with different liquid volumes.

(2) The relationship between liquid motion and liquid surface tension by applying different surface tension liquid: water, glycerol, EG, Kaydol and dodecane.

(3) The relationship between liquid motion and fiber surface tension by using different surface tension fibers: glass, nylon, copper, and PP.

(4) The relationship between liquid motion and the gradient of the cone by using different cones.

References

1. Tadanaga, K.; Morinaga, J.; Matsuda, A.; Minami, T., Superhydrophobic superhydrophilic micropatterning on flowerlike alumina coating film by the sol-gel method *Chem. Mater.* **2000,** 12, (3), 590-592.

2. Liu, H.; Feng, L.; Zhai, J.; Jiang, L.; Zhu, D., Reversible Wettability of a Chemical Vapor Deposition Prepared ZnO Film between Superhydrophobicity and Superhydrophilicity. *Langmuir* **2004,** 20, (14), 5659-5661.

3. Hoefnagels, H. F.; Wu, D.; de With, G.; Ming, W., Biomimetic superhydrophobic and highly oleophobic cotton textiles. *Langmuir* **2007,** 23, (26), 13158-13163.

4. Neinhuis, C.; Barthlott, W., Characterization and distribution of water-repellent, self-cleaning plant surfaces. *Annals Botany* **1997,** 79, (6), 667-677.

5. Cassie, A. B. D.; Baxter, S., Large Contact Angles of Plant and Animal Surfaces. *Nature* **1945,** 155, (3923), 21-22.

6. Carroll, B. J., Accurate Measurement of Contact-Angle, Phase Contact Areas, Drop Volume, and Laplace Excess Pressure in Drop-on-Fiber Systems. *J. Colloid Interface Sci.* **1976,** 57, (3), 488-495.

7. Lorenceau, E.; Quere, D., Drops on a conical wire. *J. Fluid Mech.* **2004,** 510, 29-45.

8. Nakajima, A.; Hashimoto, K.; Watanabe, T.; Takai, K.; Yamauchi, G.; Fujishima, A., Transparent Superhydrophobic Thin Films with Self-Cleaning Properties. *Langmuir* **2000,** 16, (17), 7044-7047.

9. Michielsen, S.; Lee, H. J., Design of a Superhydrophobic Surface Using Woven Structures. *Langmuir* **2007,** 23, (11), 6004-6010.

10. Lee, H. J.; Michielsen, S., Preparation of a superhydrophobic rough surface. *J. Polym. Sci. Part B: Polym. Phys.* **2006,** 45, 253-261.

11. Zhu, M.; Zuo, W.; Yu, H.; Yang, W.; Chen, Y., Superhydrophobic surface directly created by electrospinning based on hydrophilic material. *J. Mater. Sci.* **2006,** 41, (12), 3793-3797.

12. Zhai, L.; Cebeci, F. C.; Cohen, R. E.; Rubner, M. F., Stable superhydrophobic coatings from polyelectrolyte multilayers. *Nano Lett.* **2004,** 4, (7), 1349-1353.

13. Ulrike, M.; Ralf, F.; Wolfgang, M.; Jurgen, R., Towards ultrahydrophobic surfaces: a biomimetic approach. *J. Phys.: Condens. Matter* **2005,** 17, (9), S639-S648.

14. Otten, A.; Herminghaus, S., How plants keey dry: a Physicist's point of view. *Langmuir* **2004,** 20, 2405-2408.

15. Tuteja, A.; Choi, W.; Ma, M. L.; Mabry, J. M.; Mazzella, S. A.; Rutledge, G. C.; McKinley, G. H.; Cohen, R. E., Designing superoleophobic surfaces. *Science* **2007,** 318, (5856), 1618-1622.

16. Zimmermann, J.; Rabe, M.; Artus, G. R. J.; Seeger, S., Patterned superfunctional surfaces based on a silicone nanofilament coating. *Soft Matter* **2008,** 4, 450-452.

17. Cao, L.; Hu, H.-H.; Gao, D., Design and Fabrication of Micro-textures for Inducing a Superhydrophobic Behavior on Hydrophilic Materials. *Langmuir* **2007,** 23, (8), 4310-4314.

18. Tuteja, A.; Choi, W.; Mabry, J. M.; McKinley, G. H.; Cohen, R. E., Robust omniphobic surfaces. *Proc. N. A. S.* **2008,** 105, (47), 18200-18205.

19. Brewer, S. A.; Willis, C. R., Structure and oil repellency - Textiles with liquid repellency to hexane. *Appl. Surf. Sci.* **2008,** 254, (20), 6450-6454.

20. Cao, L.; Price, T. P.; Weiss, M.; Gao, D., Super Water- and Oil-Repellent Surfaces on

Intrinsically Hydrophilic and Oleophilic Porous Silicon Films. *Langmuir* **2008,** 24, (5), 1640-1643.

21. Steele, A.; Bayer, I.; Loth, E., Inherently Superoleophobic Nanocomposite Coatings by Spray Atomization. *Nano Lett.* **2009,** 9, (1), 501-505.

22. Yan, H.; Kurogi, K.; Tsujii, K., High oil-repellent poly(alkylpyrrole) films coated with fluorinated alkylsilane by a facile way. *Colloids Surfaces A: Physicochem. Eng. Aspects* **2007,** 292, (1), 27-31.

23. Hsieh, C.-T.; Chen, J.-M.; Kuo, R.-R.; Lin, T.-S.; Wu, C.-F., Influence of surface roughness on water- and oil-repellent surfaces coated with nanoparticles. *Appl. Surf. Sci.* **2005,** 240, (1-4), 318-326.

24. Reihs, K.; Duff, D.-G.; Wiessmeier, G.; Koehler, B.; Voetz, M.; Gonzalez-Blanco, J.; Wenz, E., Method for producing an ultraphobic surface on an aluminum base. *U.S. Patent* **2003**, 6,652,669.

25. Reihs, K., Long-time stable water-repellent and oil-repellent surface *U.S. Patent* **2009**, 7,563,505.

26. Lamon, S.; McDonogh, R., Oleophobic coated membranes *U.S Patent* **2003**, 6,521,012.

27. Yamaguchi, F.; Yamamoto, I.; Kusumi, K., Water- and oil-repellent treatment of textile *U.S Patent* **2006**, 7,147,669.

28. Pal, S.; Weiss, H.; Keller, H.; Muller-Plathe, F., Effect of Nanostructure on the Properties of Water at the Water-hydrophobic Interface: A Molecular Dynamics Simulation. *Langmuir* **2005,** 21, (8), 3699-3709.

29. Balkenende, A. R.; van de Boogaard, H. J. A. P.; Scholten, M.; Willard, N. P., Evaluation

of Different Approaches To Assess the Surface Tension of Low-Energy Solids by Means of Contact Angle Measurements. *Langmuir* **1998,** 14, (20), 5907-5912.

30. Fowkes, F. M., Additivity of intermolecular forces at interfaces: I. Determination of contribution to surface and interfacial tensions of dispersion forces in various liquids. *J. Phys. Chem.* **1963,** 67, 2538-2541.

31. Lee, H. J.; Michielsen, S., Lotus effect: Superhydrophobicity. *J. Text. Inst.* **2006,** 97, (5), 455-464.

32. Rosario, R.; Gust, D.; Garcia, A. A.; Hayes, M.; Taraci, J. L.; Clement, T.; Dailey, J. W.; Picraux, S. T., Lotus Effect Amplifies Light-Induced Contact Angle Switching. *J. Phys. Chem. B* **2004,** 108, (34), 12640-12642.

33. Sun, M.; Luo, C.; Xu, L.; Ji, H.; Ouyang, Q.; Yu, D.; Chen, Y., Artificial Lotus Leaf by Nanocasting. *Langmuir* **2005,** 21, (19), 8978-8981.

34. Zheng, Q. S.; Yu, Y.; Zhao, Z. H., Effects of Hydraulic Pressure on the Stability and Transition of Wetting Modes of Superhydrophobic Surfaces. *Langmuir* **2005,** 21, (26), 12207-12212.

35. Wenzel, R. N., Resistance of solid surfaces to wetting by water. *Ind. Eng. Chem.* **1936,** 28, 988-994.

36. Cassie, A. B. D.; Baxter, S., Wettability of porous surfaces. *Trans. Faraday Soc.* **1944,** 40, 0546-0550.

37. He, B.; Patankar, N. A.; Lee, J., Multiple Equilibrium Droplet Shapes and Design Criterion for Rough Hydrophobic Surfaces. *Langmuir* **2003,** 19, (12), 4999-5003.

38. Bico, J.; Tordeux, C.; Quere, D., Rough wetting. *Europhys. Lett.* **2001,** 55, (2), 214-220.

39. Brochard, F., Spreading of Liquid-Drops on Thin Cylinders - the Manchon-Droplet Transition. *J. Chem. Phys.* **1986,** 84, (8), 4664-4672.

40. de Gennes, P. G., Wetting: statics and dynamics. *Rev. Mod. Phys.* **1985,** 57, (3), 827.

41. Neimark, A. V., Thermodynamic equilibrium and stability of liquid films and droplets on fibers. *J. Adhesion Sci. Technol.* **1999,** 13, (10), 1137-1154.

42. Lorenceau, E.; Senden, T.; Quéré, D., WETTING OF FIBERS. In *Molecular Gels. Materials with Self-Assembled Fibrillar Networks*, Weiss, R. G.; Terech, P., Eds. 2006; pp 223-237.

43. Extrand, C. W., Model for contact angles and hysteresis on rough and ultraphobic surfaces. *Langmuir* **2002,** 18, (21), 7991-7999.

44. Extrand, C. W., Modeling of Ultralyophobicity: Suspension of Liquid Drops by a Single Asperity. *Langmuir* **2005,** 21, (23), 10370-10374.

45. Oliver, J. F.; Huh, C.; Mason, S. G., RESISTANCE TO SPREADING OF LIQUIDS BY SHARP EDGES. *Journal of Colloid and Interface Science* **1977,** 59, (3), 568-581.

46. Chang, F.-M.; Hong, S.-J.; Sheng, Y.-J.; Tsao, H.-K., Wetting Invasion and Retreat across a Corner Boundary. *The Journal of Physical Chemistry C* 114, (3), 1615-1621.

47. Yamaki, J. I.; Katayama, Y., New Method of Determining Contact Angle between Monofilament and Liquid. *J. Appl. Poly. Sci.* **1975,** 19, (10), 2897-2909.

48. Song, B.; Bismarck, A., Surface and Interfacial Tension Measurement, Theory and Applications. In *Surface and Interacial Tension Measurement, Theory, and Application*, Hartland, S., Ed. Marcel Dekker, Inc.: New York, 2004.

49. Wagner, H. D., Spreading of liquid droplets on cylindrical surfaces: Accurate

determination of contact angle. *J. Appl. Phys.* **1990,** 67, (3), 1352-1355.

50. Liu, J.; Xia, R.; Li, B.; Feng, X., Directional Motion of Droplets in a Conical Tube or on a Conical Fibre. *Chin. Phys. Lett.* **2007,** 24, (11), 3210-3213.

51. de Gennes, P. G., Deposition of Langmuir-Blodgett layers. *Colloid Polym. Sci.* **1986,** 264, (5), 463-465.

52. Aussillous, P.; Quere, D., Quick deposition of a fluid on the wall of a tube. *Phys. Fluids* **2000,** 12, (10), 2367-2371.

53. Hoffman, R. L., Study of Advancing Interface .1. Interface Shape in Liquid-Gas Systems. *J. Colloid Interface Sci.* **1975,** 50, (2), 228-241.

54. Tanner, L. H., The spreading of silicone oil drops on horizontal surfaces. *J. Phys. D: Appl. Phys.* **1979,** 12, (9), 1473-1484.

Appendix

Appendix 1. ΔG and ΔP of water on a Teflon® flat surface and nylon fiber tip or body.

Fiber radius r_f (mm)	Liquid volume V_0 (μL)	Free energy, $J\times10^{-9}$			Laplace pressure, mN/mm^2			
		$\Delta G_{T\text{-}Flat}$	$\Delta G_{T\&F\text{-}T}$	$\Delta G_{F\text{-}T\&F}$	ΔP_{Flat}	ΔP_T	$\Delta P_{T\&F}$	ΔP_F
0.143	0.01	-3.2	0.0	5.5	1.01	0.97	0.97	1.03
0.143	0.05	-2.3	0.0	4.9	0.59	0.63	0.63	0.59
0.143	0.10	-0.1	0.0	2.7	0.47	0.50	0.50	0.47
0.143	0.15	1.0	0.0	2.2	0.41	0.44	0.44	0.41
0.143	0.20	3.0	0.0	-0.4	0.37	0.40	0.40	0.38
0.19	0.01	-4.7	0.0	7.9	1.01	0.74	0.74	1.08
0.19	0.05	-5.8	0.0	10.3	0.59	0.61	0.61	0.59
0.19	0.10	-4.2	0.0	7.9	0.47	0.50	0.50	0.47
0.19	0.15	-2.6	0.0	7.1	0.41	0.44	0.44	0.41
0.19	0.20	-1.6	0.0	6.4	0.37	0.40	0.40	0.37

Note: $\theta_{fiber} = 72°$, $\theta_{flat} = 115°$

Appendix 2. ΔG and ΔP of EG on a Teflon® flat surface and nylon fiber tip or body.

Fiber radius r_f (mm)	Liquid volume V_0 (μL)	Free energy, $J\times10^{-9}$			Laplace pressure, mN/mm^2			
		$\Delta G_{T\text{-}Flat}$	$\Delta G_{T\&F\text{-}T}$	$\Delta G_{F\text{-}T\&F}$	ΔP_{Flat}	ΔP_T	$\Delta P_{T\&F}$	ΔP_F
0.143	0.01	-1.6	0.0	0.7	0.54	0.64	0.64	0.48
0.143	0.05	2.5	-3.5	-0.7	0.32	0.41	0.32	0.32
0.143	0.10	7.1	-7.5	-1.0	0.25	0.33	0.26	0.26
0.143	0.15	10.4	-10.5	-0.1	0.22	0.29	0.24	0.24
0.143	0.20	14.1	-13.0	-0.4	0.20	0.26	0.22	0.22
0.19	0.01	-3.6	0.0	3.0	0.54	0.48	0.48	0.45
0.19	0.05	-0.8	-1.2	-0.5	0.32	0.40	0.37	0.30
0.19	0.10	3.3	-5.3	-1.3	0.25	0.33	0.25	0.25
0.19	0.15	7.0	-9.2	-1.2	0.22	0.29	0.23	0.22
0.19	0.20	10.0	-12.0	-1.1	0.20	0.26	0.21	0.21

Note: $\theta_{fiber} = 42°$, $\theta_{flat} = 85°$

Appendix 3. ΔG and ΔP of Kaydol on a Teflon® flat surface and nylon fiber tip or body.

Fiber radius r_f (mm)	Liquid volume V_0 (μL)	Free energy, $J\times10^{-9}$			Laplace pressure, mN/mm^2			
		$\Delta G_{T\text{-}Flat}$	$\Delta G_{T\&F\text{-}T}$	$\Delta G_{F\text{-}T\&F}$	ΔP_{Flat}	ΔP_T	$\Delta P_{T\&F}$	ΔP_F
0.143	0.01	0.3	-1.1	0.1	0.23	0.41	0.23	0.22
0.143	0.05	6.5	-6.0	-0.2	0.14	0.27	0.18	0.18
0.143	0.10	12.5	-9.9	0.1	0.11	0.21	0.16	0.15
0.143	0.15	17.3	-12.0	-0.3	0.09	0.19	0.14	0.14
0.143	0.20	22.0	-14.4	-0.3	0.09	0.17	0.13	0.13
0.19	0.01	-1.3	0.0	0.3	0.23	0.31	0.31	0.19
0.19	0.05	4.0	-4.9	-0.3	0.14	0.26	0.15	0.15
0.19	0.10	9.8	-9.9	0.4	0.11	0.21	0.14	0.14
0.19	0.15	14.8	-13.1	0.0	0.09	0.19	0.13	0.13
0.19	0.20	19.0	-15.5	-0.1	0.09	0.17	0.12	0.12

Note: $\theta_{fiber} = 17°$, $\theta_{flat} = 56°$

Appendix 4. ΔG and ΔP of water on a Teflon® flat surface and glass fiber tip or body.

Fiber radius r_f (mm)	Liquid volume V_0 (μL)	Free energy, $J\times10^{-9}$			Laplace pressure, mN/mm^2			
		$\Delta G_{T\text{-}Flat}$	$\Delta G_{T\&F\text{-}T}$	$\Delta G_{F\text{-}T\&F}$	ΔP_{Flat}	ΔP_T	$\Delta P_{T\&F}$	ΔP_F
0.145	0.01	-5.7	0.0	0.1	1.01	0.96	0.96	0.66
0.145	0.05	-5.0	-8.0	-0.8	0.59	0.63	0.46	0.46
0.145	0.10	-2.9	-15.3	-0.8	0.47	0.50	0.39	0.39
0.145	0.15	-1.5	-20.3	-0.7	0.41	0.44	0.35	0.35
0.145	0.20	0.1	-23.9	-1.0	0.37	0.40	0.33	0.33
0.191	0.01	-3.0	0.0	-2.6	1.01	0.76	0.76	0.62
0.191	0.05	-10.3	-4.5	-0.4	0.59	0.61	0.43	0.42
0.191	0.10	-8.6	-12.2	-1.8	0.47	0.50	0.36	0.36
0.191	0.15	-6.8	-19.2	-1.0	0.41	0.44	0.33	0.33
0.191	0.20	-5.6	-23.3	-1.4	0.37	0.40	0.30	0.30

Note: $\theta_{fiber} = 35°$, $\theta_{flat} = 115°$

Appendix 5. ΔG and ΔP of EG on a Teflon® flat surface and glass fiber tip or body.

Fiber radius r_f (mm)	Liquid volume V_0 (μL)	Free energy, $J\times10^{-9}$			Laplace pressure, mN/mm^2			
		$\Delta G_{T\text{-}Flat}$	$\Delta G_{T\&F\text{-}T}$	$\Delta G_{F\text{-}T\&F}$	ΔP_{Flat}	ΔP_T	$\Delta P_{T\&F}$	ΔP_F
0.145	0.01	-2.5	-2.5	0.2	0.54	0.63	0.31	0.31
0.145	0.05	1.5	-10.5	-0.3	0.32	0.41	0.26	0.26
0.145	0.10	6.0	-17.2	0.2	0.25	0.33	0.23	0.23
0.145	0.15	9.5	-21.3	0.3	0.22	0.29	0.21	0.21
0.145	0.20	12.9	-24.7	0.0	0.20	0.26	0.20	0.20
0.191	0.01	-1.1	0.0	-4.6	0.54	0.50	0.50	0.24
0.191	0.05	-2.4	-9.8	0.3	0.32	0.40	0.22	0.22
0.191	0.10	1.8	-17.8	0.4	0.25	0.33	0.20	0.20
0.191	0.15	5.6	-22.9	-0.4	0.22	0.29	0.19	0.19
0.191	0.20	8.7	-26.9	-0.7	0.20	0.26	0.18	0.18

Note: $\theta_{fiber} = 0°$, $\theta_{flat} = 85°$

Appendix 6. ΔG and ΔP of Kaydol on a Teflon® flat surface and glass fiber tip or body.

Fiber radius r_f (mm)	Liquid volume V_0 (μL)	Free energy, $J\times10^{-9}$			Laplace pressure, mN/mm^2			
		$\Delta G_{T\text{-}Flat}$	$\Delta G_{T\&F\text{-}T}$	$\Delta G_{F\text{-}T\&F}$	ΔP_{Flat}	ΔP_T	$\Delta P_{T\&F}$	ΔP_F
0.145	0.01	0.2	-1.6	0.1	0.23	0.41	0.20	0.20
0.145	0.05	6.2	-6.9	-0.2	0.14	0.27	0.17	0.17
0.145	0.10	12.2	-11.2	0.1	0.11	0.21	0.15	0.15
0.145	0.15	17.1	-13.8	0.2	0.09	0.19	0.14	0.14
0.145	0.20	21.6	-16.1	0.0	0.09	0.17	0.13	0.13
0.191	0.01	1.1	0.0	-3.0	0.23	0.32	0.32	0.16
0.191	0.05	3.7	-6.4	0.2	0.14	0.26	0.14	0.14
0.191	0.10	9.5	-11.6	0.3	0.11	0.21	0.13	0.13
0.191	0.15	14.6	-14.9	-0.2	0.09	0.19	0.12	0.12
0.191	0.20	18.9	-17.5	-0.5	0.09	0.17	0.12	0.12

Note: $\theta_{fiber} = 0°$, $\theta_{flat} = 56°$

Appendix 7. ΔG and ΔP of water on a Teflon® flat surface and PP fiber tip or body.

Fiber radius r_f (mm)	Liquid volume V_0 (μL)	Free energy, $J\times10^{-9}$			Laplace pressure, mN/mm^2			
		$\Delta G_{T\text{-}Flat}$	$\Delta G_{T\&F\text{-}T}$	$\Delta G_{F\text{-}T\&F}$	ΔP_{Flat}	ΔP_T	$\Delta P_{T\&F}$	ΔP_F
0.1	0.01	-0.3	0.0	5.4	1.01	1.06	1.06	1.18
0.1	0.05	1.5	0.0	7.6	0.59	0.64	0.64	0.66
0.1	0.10	3.6	0.0	8.3	0.47	0.51	0.51	0.52
0.1	0.15	5.0	0.0	9.0	0.41	0.44	0.44	0.45
0.1	0.20	6.8	0.0	9.3	0.37	0.40	0.40	0.41
0.19	0.01	-1.1	0.0	9.9	1.01	0.74	0.74	1.35
0.19	0.05	-1.9	0.0	18.2	0.59	0.61	0.61	0.70
0.19	0.10	-0.3	0.0	20.5	0.47	0.50	0.50	0.54
0.19	0.15	1.4	0.0	22.9	0.41	0.44	0.44	0.47
0.19	0.20	2.5	0.0	23.5	0.37	0.40	0.40	0.42

Note: $\theta_{fiber} = 97°$, $\theta_{flat} = 115°$

Appendix 8. ΔG and ΔP of EG on a Teflon® flat surface and PP fiber tip or body.

Fiber radius r_f (mm)	Liquid volume V_0 (μL)	Free energy, $J\times10^{-9}$			Laplace pressure, mN/mm^2			
		$\Delta G_{T\text{-}Flat}$	$\Delta G_{T\&F\text{-}T}$	$\Delta G_{F\text{-}T\&F}$	ΔP_{Flat}	ΔP_T	$\Delta P_{T\&F}$	ΔP_F
0.1	0.01	0.9	0.0	1.4	0.54	0.69	0.69	0.65
0.1	0.05	5.6	0.0	0.1	0.32	0.42	0.42	0.39
0.1	0.10	10.1	-0.6	-0.7	0.25	0.33	0.31	0.31
0.1	0.15	13.6	-1.3	-0.9	0.22	0.29	0.27	0.27
0.1	0.20	17.1	-2.0	-0.7	0.20	0.26	0.25	0.25
0.19	0.01	-1.5	0.0	5.2	0.54	0.48	0.48	0.67
0.19	0.05	1.3	0.0	6.0	0.32	0.40	0.40	0.38
0.19	0.10	5.4	0.0	4.2	0.25	0.33	0.33	0.30
0.19	0.15	9.1	0.0	3.5	0.22	0.29	0.29	0.26
0.19	0.20	12.1	0.0	1.9	0.20	0.26	0.26	0.24

Note: $\theta_{fiber} = 69°$, $\theta_{flat} = 85°$

Appendix 9. ΔG and ΔP of Kaydol on a Teflon® flat surface and PP fiber tip or body.

Fiber radius r_f (mm)	Liquid volume V_0 (μL)	Free energy, $J\times10^{-9}$			Laplace pressure, mN/mm^2			
		$\Delta G_{T\text{-}Flat}$	$\Delta G_{T\&F\text{-}T}$	$\Delta G_{F\text{-}T\&F}$	ΔP_{Flat}	ΔP_T	$\Delta P_{T\&F}$	ΔP_F
0.1	0.01	1.9	-1.3	-0.1	0.23	0.45	0.30	0.30
0.1	0.05	8.4	-4.8	0.0	0.14	0.27	0.21	0.21
0.1	0.10	14.4	-7.0	-0.2	0.11	0.22	0.18	0.18
0.1	0.15	19.3	-8.7	0.1	0.09	0.19	0.16	0.16
0.1	0.20	23.9	-10.1	0.0	0.09	0.17	0.15	0.15
0.19	0.01	-1.0	0.0	0.8	0.23	0.31	0.31	0.24
0.19	0.05	4.3	-3.3	-0.2	0.14	0.26	0.17	0.17
0.19	0.10	10.0	-6.8	-0.2	0.11	0.21	0.15	0.15
0.19	0.15	15.1	-9.8	-0.5	0.09	0.19	0.13	0.13
0.19	0.20	19.3	-12.4	0.0	0.09	0.17	0.13	0.13

Note: $\theta_{fiber} = 29°$, $\theta_{flat} = 56°$

Appendix 10. ΔG of water on a Teflon® flat surface and a nylon fiber.

Fiber radius r_f (mm)	Liquid volume V_0 (μL)	Free energy, $J\times10^{-9}$				
		$\Delta G_{Flat\&F\text{-}Flat}$	$\Delta G_{F\text{-}Flat\&F}$	$\Delta G_{T\&F\text{-}F}$	$\Delta G_{T\text{-}T\&F}$	$\Delta G_{T\&F\text{-}Flat\&F}$
0.143	0.1	-2.7	5.2	-2.9	0.0	2.3
0.143	0.5	-8.7	14.1	2.4	2.3	16.5
0.143	1.0	-12.8	22.4	2.3	7.4	24.7
0.143	2.0	-17.8	35.8	2.3	13.9	38.0
0.143	4.0	-24.3	57.5	3.1	21.6	60.6
0.19	0.1	-1.5	5.6	-8.6	0.0	-2.9
0.19	0.5	-8.9	14.5	-0.1	0.0	14.4
0.19	1.0	-14.0	22.4	4.3	2.2	26.7
0.19	2.0	-20.7	35.4	4.1	10.7	39.6
0.19	4.0	-29.2	56.8	3.5	22.3	60.3
0.229	0.1	-0.1	6.0	-14.1	0.0	-8.0
0.229	0.5	-8.2	14.9	-5.7	0.0	9.2
0.229	1.0	-14.2	22.7	0.3	1.1	23.1
0.229	2.0	-22.1	35.5	6.6	4.9	42.1
0.229	4.0	-32.3	56.3	8.1	16.2	64.5
0.288	0.1	2.4	6.7	-22.9	0.0	-16.3
0.288	0.5	-6.1	15.8	-16.7	0.0	-1.0
0.288	1.0	-13.1	23.7	-9.0	0.0	14.7
0.288	2.0	-22.5	36.2	0.3	2.2	36.5
0.288	4.0	-35.0	56.5	9.5	8.4	66.0

Note: $\theta_{fiber} = 72°$, $\theta_{flat} = 115°$

Appendix 11. ΔG of EG on a Teflon® flat surface and a nylon fiber.

Fiber radius r_f (mm)	Liquid volume V_0 (μL)	Free energy, $J\times10^{-9}$				
		$\Delta G_{Flat\&F\text{-}Flat}$	$\Delta G_{F\text{-}Flat\&F}$	$\Delta G_{T\&F\text{-}F}$	$\Delta G_{T\text{-}T\&F}$	$\Delta G_{T\&F\text{-}Flat\&F}$
0.143	0.1	-9.0	7.8	0.9	7.3	8.6
0.143	0.5	-17.8	25.2	0.7	21.9	25.9
0.143	1.0	-23.1	42.3	1.1	30.3	43.4
0.143	2.0	*-29.8*	*70.5*	*1.4*	*41.2*	71.9
0.143	4.0	-38.1	117.1	2.0	54.4	119.1
0.19	0.1	-10.6	7.7	1.0	5.2	8.7
0.19	0.5	-22.2	23.7	0.8	23.8	24.4
0.19	1.0	-29.5	39.5	0.5	36.0	40.0
0.19	2.0	-38.5	66.2	1.6	49.9	67.8
0.19	4.0	-49.7	110.7	2.2	68.1	112.9
0.229	0.1	-11.5	7.8	1.1	2.4	8.9
0.229	0.5	-25.3	22.8	2.0	22.5	24.8
0.229	1.0	-34.2	37.9	2.2	36.4	40.1
0.229	2.0	-45.1	63.3	1.1	55.8	64.4
0.229	4.0	-58.8	106.2	4.3	75.3	110.5
0.288	0.1	-12.4	8.1	-1.7	0.0	6.4
0.288	0.5	-29.2	22.4	1.6	19.9	23.9
0.288	1.0	-40.2	36.3	2.4	36.4	38.7
0.288	2.0	-54.1	60.1	2.4	59.1	62.5
0.288	4.0	-71.5	100.6	4.9	85.2	105.5

Note: $\theta_{fiber} = 42°$, $\theta_{flat} = 85°$

Appendix 12. ΔG of Kaydol on a Teflon® flat surface and a nylon fiber.

Fiber radius r_f (mm)	Liquid volume V_0 (μL)	Free energy, $J\times10^{-9}$				
		$\Delta G_{Flat\&F\text{-}Flat}$	$\Delta G_{F\text{-}Flat\&F}$	$\Delta G_{T\&F\text{-}F}$	$\Delta G_{T\text{-}T\&F}$	$\Delta G_{T\&F\text{-}Flat\&F}$
0.143	0.1	-7.2	9.8	0.0	9.8	9.8
0.143	0.5	-13.0	34.0	-0.1	22.5	33.9
0.143	1.0	-16.4	57.5	0.3	29.8	57.8
0.143	2.0	-20.7	96.3	-0.2	39.8	96.1
0.143	4.0	-25.9	159.7	0.8	50.6	160.5
0.19	0.1	-9.0	9.1	-0.2	9.8	8.9
0.19	0.5	-16.9	31.1	0.3	26.0	31.4
0.19	1.0	-21.7	53.1	0.7	36.1	53.8
0.19	2.0	-27.5	90.0	0.8	48.9	90.8
0.19	4.0	-34.6	151.1	-0.5	66.2	150.7
0.229	0.1	-10.3	8.9	0.2	8.3	9.0
0.229	0.5	-19.9	29.3	-0.2	28.4	29.1
0.229	1.0	-25.8	50.1	1.0	39.8	51.2
0.229	2.0	-33.0	85.4	1.4	55.4	86.8
0.229	4.0	-41.8	144.5	1.7	74.7	146.2
0.288	0.1	-11.8	8.9	-0.2	5.7	8.8
0.288	0.5	-24.0	27.8	-0.3	28.7	27.5
0.288	1.0	-31.6	46.8	1.1	43.4	47.9
0.288	2.0	-40.9	79.3	1.3	63.9	80.6
0.288	4.0	-52.2	135.6	1.1	88.9	136.7

Note: $\theta_{fiber} = 17°$, $\theta_{flat} = 56°$

Appendix 13. ΔG of water on a Teflon® flat surface and a glass fiber.

Fiber radius r_f (mm)	Liquid volume V_0 (μL)	Free energy, $J\times10^{-9}$				
		$\Delta G_{Flat\&F\text{-}Flat}$	$\Delta G_{F\text{-}Flat\&F}$	$\Delta G_{T\&F\text{-}F}$	$\Delta G_{T\text{-}T\&F}$	$\Delta G_{T\&F\text{-}Flat\&F}$
0.145	0.1	-19.7	1.0	0.5	15.3	1.4
0.145	0.5	-38.7	5.3	1.2	39.6	6.5
0.145	1.0	-50.3	10.8	1.5	54.6	12.3
0.145	2.0	-64.7	20.9	1.6	73.7	22.5
0.145	4.0	-82.6	38.7	3.3	95.6	42.1
0.191	0.1	-22.9	0.7	1.4	12.1	2.1
0.191	0.5	-48.1	3.8	1.2	44.3	4.9
0.191	1.0	-63.7	8.0	1.7	64.4	9.7
0.191	2.0	-83.0	16.3	0.6	91.3	16.9
0.191	4.0	-107.0	32.0	2.5	121.3	34.5
0.233	0.1	-24.9	0.6	1.2	8.2	1.8
0.233	0.5	-55.3	2.9	2.6	43.8	5.6
0.233	1.0	-74.5	6.2	2.9	68.7	9.1
0.233	2.0	-98.4	13.1	0.4	102.9	13.6
0.233	4.0	-128.1	26.9	5.2	137.6	32.0
0.271	0.1	-26.0	0.7	0.4	4.1	1.1
0.271	0.5	-60.7	2.4	2.1	42.9	4.5
0.271	1.0	-83.2	5.1	2.2	71.6	7.3
0.271	2.0	-111.3	10.8	5.1	105.6	15.9
0.271	4.0	-146.1	22.9	1.5	155.4	24.4

Note: $\theta_{fiber} = 35°$, $\theta_{flat} = 115°$

Appendix 14. ΔG of EG on a Teflon® flat surface and a glass fiber.

Fiber radius r_f (mm)	Liquid volume V_0 (μL)	Free energy, $J\times10^{-9}$				
		$\Delta G_{Flat\&F\text{-}Flat}$	$\Delta G_{F\text{-}Flat\&F}$	$\Delta G_{T\&F\text{-}F}$	$\Delta G_{T\text{-}T\&F}$	$\Delta G_{T\&F\text{-}Flat\&F}$
0.145	0.1	-14.8	3.8	-0.2	17.2	3.6
0.145	0.5	-27.3	18.5	0.7	37.0	19.2
0.145	1.0	-34.8	34.1	0.7	49.6	34.7
0.145	2.0	-44.1	60.5	-0.4	66.2	60.1
0.145	4.0	-55.5	104.8	1.4	83.6	106.2
0.191	0.1	-18.2	2.7	-0.5	17.7	2.2
0.191	0.5	-35.0	14.8	0.9	43.7	15.7
0.191	1.0	-45.1	28.5	0.9	60.7	29.5
0.191	2.0	-57.7	52.7	0.7	81.9	53.5
0.191	4.0	-73.1	94.2	-1.0	109.7	93.2
0.233	0.1	-20.7	2.0	0.1	15.8	2.1
0.233	0.5	-41.3	12.0	-0.5	49.1	11.5
0.233	1.0	-54.0	24.1	1.1	68.6	25.2
0.233	2.0	-69.5	46.3	0.3	95.5	46.6
0.233	4.0	-88.7	85.2	-1.2	129.2	84.0
0.271	0.1	-22.6	1.7	-0.6	14.3	1.1
0.271	0.5	-46.5	10.1	-1.1	51.5	9.0
0.271	1.0	-61.4	20.8	-0.1	75.0	20.8
0.271	2.0	-79.8	41.1	2.2	103.4	43.4
0.271	4.0	-102.5	77.7	-0.7	144.3	77.0

Note: $\theta_{fiber} = 0°$, $\theta_{flat} = 85°$

Appendix 15. ΔG of Kaydol on a Teflon® flat surface and a glass fiber.

Fiber radius r_f (mm)	Liquid volume V_0 (μL)	Free energy, $J\times10^{-9}$				
		$\Delta G_{Flat\&F\text{-}Flat}$	$\Delta G_{F\text{-}Flat\&F}$	$\Delta G_{T\&F\text{-}F}$	$\Delta G_{T\text{-}T\&F}$	$\Delta G_{T\&F\text{-}Flat\&F}$
0.145	0.1	-7.8	9.0	-0.1	11.1	8.9
0.145	0.5	-14.0	32.7	0.5	24.1	33.2
0.145	1.0	-17.7	56.0	0.4	32.2	56.4
0.145	2.0	-22.2	94.4	-0.2	43.1	94.2
0.145	4.0	-27.8	157.4	0.9	54.4	158.3
0.191	0.1	-9.8	8.0	-0.3	11.5	7.7
0.191	0.5	-18.2	29.5	0.6	28.4	30.1
0.191	1.0	-23.2	51.2	0.6	39.5	51.8
0.191	2.0	-29.4	87.7	0.5	53.2	88.2
0.191	4.0	-36.9	148.3	-0.7	71.3	147.7
0.233	0.1	-11.3	7.5	0.1	10.3	7.5
0.233	0.5	-21.7	27.1	-0.3	31.9	26.8
0.233	1.0	-28.0	47.4	0.7	44.6	48.1
0.233	2.0	-35.8	82.2	0.2	62.1	82.3
0.233	4.0	-45.2	140.5	-0.8	84.0	139.8
0.271	0.1	-12.2	7.0	-0.4	9.3	6.6
0.271	0.5	-24.7	25.4	-0.7	33.5	24.7
0.271	1.0	-32.2	44.5	0.0	48.8	44.5
0.271	2.0	-41.3	77.7	1.4	67.2	79.1
0.271	4.0	-52.5	134.0	-0.5	93.8	133.6

Note: $\theta_{fiber} = 0°$, $\theta_{flat} = 56°$

Appendix 16. ΔG of EG on a Teflon® flat surface and a PP fiber.

Fiber radius r_f (mm)	Liquid volume V_0 (μL)	Free energy, $J\times10^{-9}$				
		$\Delta G_{Flat\&F\text{-}Flat}$	$\Delta G_{F\text{-}Flat\&F}$	$\Delta G_{T\&F\text{-}F}$	$\Delta G_{T\text{-}T\&F}$	$\Delta G_{T\&F\text{-}Flat\&F}$
0.1	0.1	-2.4	11.2	0.7	0.6	11.9
0.1	0.5	-5.1	32.6	0.7	5.0	33.3
0.1	1.0	-6.8	52.2	1.3	7.2	53.5
0.1	2.0	-9.0	83.6	0.6	11.3	84.2
0.1	4.0	-11.6	134.0	1.3	14.9	135.3
0.15	0.1	-2.6	11.7	-1.4	0.0	10.3
0.15	0.5	-6.6	32.5	1.7	3.0	34.3
0.15	1.0	-9.2	51.6	1.8	7.1	53.4
0.15	2.0	-12.4	82.4	3.1	11.0	85.4
0.15	4.0	-16.4	131.7	2.7	18.0	134.4
0.19	0.1	-2.5	12.2	-4.5	0.0	7.8
0.19	0.5	-7.3	32.9	1.7	0.7	34.6
0.19	1.0	-10.5	51.7	2.8	4.7	54.4
0.19	2.0	-14.6	81.9	3.9	10.1	85.8
0.19	4.0	-19.7	130.6	4.2	18.4	134.8

Note: $\theta_{fiber} = 69°$, $\theta_{flat} = 85°$

Appendix 17. ΔG of Kaydol on a Teflon® flat surface and a PP fiber.

Fiber radius r_f (mm)	Liquid volume V_0 (μL)	Free energy, $J\times10^{-9}$				
		$\Delta G_{Flat\&F\text{-}Flat}$	$\Delta G_{F\text{-}Flat\&F}$	$\Delta G_{T\&F\text{-}F}$	$\Delta G_{T\text{-}T\&F}$	$\Delta G_{T\&F\text{-}Flat\&F}$
0.1	0.1	-4.6	11.8	0.3	7.0	12.1
0.1	0.5	-8.1	38.6	1.3	13.7	39.9
0.1	1.0	-10.2	63.7	0.0	19.8	63.7
0.1	2.0	-12.8	104.5	0.0	25.7	104.4
0.1	4.0	-16.0	170.4	0.1	32.7	170.5
0.15	0.1	-6.5	10.9	0.2	7.6	11.1
0.15	0.5	-12.0	35.4	0.0	19.8	35.4
0.15	1.0	-15.3	59.1	0.0	27.1	59.1
0.15	2.0	-19.3	98.2	0.6	35.6	98.7
0.15	4.0	-24.3	161.9	1.3	46.0	163.2
0.19	0.1	-7.8	10.6	0.4	6.7	11.0
0.19	0.5	-14.8	33.6	0.5	21.5	34.2
0.19	1.0	-19.1	56.2	0.3	31.2	56.5
0.19	2.0	-24.4	93.8	0.5	42.6	94.3
0.19	4.0	-30.9	155.7	0.4	57.4	156.1

Note: $\theta_{fiber} = 29°$, $\theta_{flat} = 56°$

Appendix 18. ΔG of water on a PET flat surface and a nylon fiber.

Fiber radius r_f (mm)	Liquid volume V_0 (μL)	Free energy, $J\times10^{-9}$				
		$\Delta G_{Flat\&F\text{-}Flat}$	$\Delta G_{F\text{-}Flat\&F}$	$\Delta G_{T\&F\text{-}F}$	$\Delta G_{T\text{-}T\&F}$	$\Delta G_{T\&F\text{-}Flat\&F}$
0.143	0.1	-3.0	26.5	-2.9	0.0	23.7
0.143	0.5	-7.4	74.2	2.4	2.3	76.6
0.143	1.0	-10.2	117.3	2.3	7.4	119.6
0.143	2.0	-13.8	186.4	2.3	13.9	188.6
0.143	4.0	-18.2	297.0	3.1	21.6	300.1
0.19	0.1	-2.8	28.0	-8.6	0.0	19.4
0.19	0.5	-8.4	75.4	-0.1	0.0	75.3
0.19	1.0	-12.1	117.9	4.3	2.2	122.2
0.19	2.0	-16.8	186.2	4.1	10.7	190.3
0.19	4.0	-22.8	295.8	3.5	22.3	299.4
0.229	0.1	-2.4	29.4	-14.1	0.0	15.3
0.229	0.5	-8.8	76.9	-5.7	0.0	71.2
0.229	1.0	-13.1	119.1	0.3	1.1	119.5
0.229	2.0	-18.8	186.9	6.6	4.9	193.5
0.229	4.0	-26.0	295.5	8.1	16.2	303.6
0.288	0.1	-1.4	31.5	-23.5	0.6	8.0
0.288	0.5	-8.7	79.7	-16.6	-0.1	63.1
0.288	1.0	-13.9	122.0	-7.0	-1.9	114.9
0.288	2.0	-20.9	189.2	0.3	2.2	189.6
0.288	4.0	-29.8	296.8	9.5	8.4	306.3

Note: $\theta_{fiber} = 72°$, $\theta_{flat} = 72°$

Appendix 19. ΔG of EG on a PET flat surface and a nylon fiber.

Fiber radius r_f (mm)	Liquid volume V_0 (μL)	Free energy, $J\times10^{-9}$				
		$\Delta G_{Flat\&F\text{-}Flat}$	$\Delta G_{F\text{-}Flat\&F}$	$\Delta G_{T\&F\text{-}F}$	$\Delta G_{T\text{-}T\&F}$	$\Delta G_{T\&F\text{-}Flat\&F}$
0.143	0.1	-7.1	23.2	0.9	7.3	24.1
0.143	0.5	-13.1	71.3	0.7	21.9	72.0
0.143	1.0	-16.6	116.4	1.1	30.3	117.6
0.143	2.0	-21.0	189.8	1.4	41.2	191.2
0.143	4.0	-26.4	308.8	2.0	54.4	310.7
0.19	0.1	-8.8	23.3	1.0	5.2	24.3
0.19	0.5	-16.9	69.1	0.8	23.8	69.9
0.19	1.0	-21.8	112.5	0.5	36.0	113.0
0.19	2.0	-27.8	183.6	1.6	49.9	185.2
0.19	4.0	-35.2	299.5	2.2	68.1	301.8
0.229	0.1	-10.0	23.6	1.1	2.4	24.7
0.229	0.5	-19.8	68.1	2.0	22.5	70.0
0.229	1.0	-25.8	110.2	2.2	36.4	112.4
0.229	2.0	-33.2	179.4	1.1	55.8	180.6
0.229	4.0	-42.3	293.0	4.3	75.3	297.3
0.288	0.1	-11.4	24.5	-1.7	0.0	22.8
0.288	0.5	-23.6	67.7	1.6	19.9	69.2
0.288	1.0	-31.3	108.1	2.4	36.4	110.5
0.288	2.0	-40.8	174.8	2.4	59.1	177.3
0.288	4.0	-52.6	284.9	4.9	85.2	289.8

Note: $\theta_{fiber} = 42°$, $\theta_{flat} = 47°$

Appendix 20. ΔG of water on a PET flat surface and a glass fiber.

Fiber radius r_f (mm)	Liquid volume V_0 (μL)	Free energy, $J\times10^{-9}$				
		$\Delta G_{T\&F\text{-}T}$	$\Delta G_{F\text{-}T\&F}$	$\Delta G_{Flat\&F\text{-}F}$	$\Delta G_{T\&F\text{-}Flat\&F}$	$\Delta G_{Flat\&F\text{-}Flat}$
0.145	0.1	-15.0	17.3	0.5	15.3	17.8
0.145	0.5	-28.5	56.5	1.2	39.6	57.7
0.145	1.0	-36.7	94.6	1.5	54.6	96.2
0.145	2.0	-46.8	157.7	1.6	73.7	159.3
0.145	4.0	-59.4	261.1	3.3	95.6	264.4
0.191	0.1	-18.0	16.8	1.4	12.1	18.2
0.191	0.5	-36.0	53.0	1.2	44.3	54.2
0.191	1.0	-47.0	88.8	1.7	64.4	90.5
0.191	2.0	-60.7	148.6	0.6	91.3	149.2
0.191	4.0	-77.6	248.1	2.5	121.3	250.6
0.233	0.1	-20.1	16.8	1.2	8.2	18.0
0.233	0.5	-41.9	50.9	2.6	43.8	53.5
0.233	1.0	-55.6	84.7	2.9	68.7	87.6
0.233	2.0	-72.6	141.9	0.4	102.9	142.3
0.233	4.0	-93.5	237.8	5.2	137.6	242.9
0.271	0.1	-21.6	17.2	0.4	5.7	17.6
0.271	0.5	-46.7	49.8	2.1	42.9	51.9
0.271	1.0	-62.6	82.0	2.2	71.6	84.2
0.271	2.0	-82.6	136.9	5.1	105.6	141.9
0.271	4.0	-107.3	229.6	1.5	155.4	231.1

Note: $\theta_{fiber} = 35°$, $\theta_{flat} = 72°$

Appendix 21. ΔG of EG on a PET flat surface and a glass fiber.

Fiber radius r_f (mm)	Liquid volume V_0 (μL)	Free energy, $J\times10^{-9}$				
		$\Delta G_{T\&F\text{-}T}$	$\Delta G_{F\text{-}T\&F}$	$\Delta G_{Flat\&F\text{-}F}$	$\Delta G_{T\&F\text{-}Flat\&F}$	$\Delta G_{Flat\&F\text{-}Flat}$
0.145	0.1	-11.2	17.6	-0.2	17.2	17.4
0.145	0.5	-19.8	61.9	0.7	37.0	62.6
0.145	1.0	-24.9	104.8	0.7	49.6	105.5
0.145	2.0	-31.1	175.6	-0.4	66.2	175.2
0.145	4.0	-38.7	291.3	1.4	83.6	292.7
0.191	0.1	-14.1	16.0	-0.5	17.7	15.5
0.191	0.5	-25.9	56.5	0.9	43.7	57.4
0.191	1.0	-32.9	96.9	0.9	60.7	97.9
0.191	2.0	-41.4	164.5	0.7	81.9	165.3
0.191	4.0	-51.7	276.2	-1.0	109.7	275.2
0.233	0.1	-15.4	14.1	0.1	15.8	14.2
0.233	0.5	-31.1	52.6	-0.5	49.1	52.1
0.233	1.0	-39.9	90.7	1.1	68.6	91.8
0.233	2.0	-50.6	155.4	0.3	95.5	155.7
0.233	4.0	-63.5	263.3	-1.2	129.2	262.2
0.271	0.1	-13.7	10.2	-0.6	14.3	9.6
0.271	0.5	-35.5	49.8	-1.1	51.5	48.8
0.271	1.0	-45.9	86.0	-0.1	75.0	85.9
0.271	2.0	-58.6	148.0	2.2	103.4	150.2
0.271	4.0	-74.1	252.7	-0.7	144.3	251.9

Note: $\theta_{fiber} = 0°$, $\theta_{flat} = 47°$

Appendix 22. ΔG of EG on a PET flat surface and a PP fiber.

Fiber radius r_f (mm)	Liquid volume V_0 (μL)	Free energy, $J\times10^{-9}$				
		$\Delta G_{T\&F\text{-}T}$	$\Delta G_{F\text{-}T\&F}$	$\Delta G_{Flat\&F\text{-}F}$	$\Delta G_{T\&F\text{-}Flat\&F}$	$\Delta G_{Flat\&F\text{-}Flat}$
0.1	0.1	-2.0	28.2	0.7	0.6	28.9
0.1	0.5	-3.8	82.1	0.7	5.0	82.8
0.1	1.0	-4.9	131.0	1.3	7.2	132.2
0.1	2.0	-6.3	209.0	0.6	11.3	209.6
0.1	4.0	-7.9	333.6	1.3	14.9	334.9
0.15	0.1	-2.6	29.0	-1.4	0.0	27.7
0.15	0.5	-5.3	82.1	1.7	3.0	83.8
0.15	1.0	-7.0	130.1	1.8	7.1	131.9
0.15	2.0	-9.1	207.1	3.1	11.0	210.2
0.15	4.0	-11.7	330.3	2.7	18.0	333.0
0.19	0.1	-2.9	30.1	-4.5	0.0	25.6
0.19	0.5	-6.3	82.7	1.7	0.7	84.5
0.19	1.0	-8.5	130.3	2.8	4.7	133.1
0.19	2.0	-11.2	206.6	3.9	10.1	210.5
0.19	4.0	-14.5	328.7	4.2	18.4	332.9

Note: $\theta_{fiber} = 69°$, $\theta_{flat} = 47°$